# Changes in Lateral Stress During Slurry Trench Wall Installation.

Page, Jonathan

# Changes in Lateral Stress During Slurry Trench Wall Installation

by
Jonathan Page

A dissertation submitted for the
degree of Doctor of Philosophy
at
the University of London

Department of Civil Engineering
Queen Mary and Westfield College
September 1995

The thesis is concerned with the effects of slurry trenching (diaphragm wall installation) in an overconsolidated clay, with particular emphasis on the changes in lateral stress which occur.

A review of the literature on diaphragm wall installation in stiff overconsolidated clay was carried out, with particular reference to the measurement of changes in stress and the application of finite element analyses. The problem was investigated by means of centrifuge model tests and finite element analyses.

The main body of the thesis details the development and results of a series of centrifuge tests. A model at 1 to 100 scale was tested at 100 gravities, enabling both the long and short term effects of slurry trench walling to be investigated. The technique adopted used a fluid-filled neoprene rubber bag in the place of the trench that was drained to ground level to simulate excavation under bentonite slurry. A mixture of plaster of Paris, iron-filings, fine sand and cement powder was then deposited into the bag to simulate wall placement.

By using different fluid heights of different densities in the rubber bag, a series of initial earth pressure coefficients were modelled. The effects of both a stress and strain controlled boundary at the remote end of the model were also investigated. Finally, simulated concretes of different densities were adopted to see what effect this would have on placement stresses.

A technique was developed to enable the measurement of changes in total lateral stress changes at up to 10 locations within the model. Pore water pressures were measured at the same positions, and ground settlements were measured at the surface of the model.

A series of finite element analyses was carried out to extend the scope of the centrifuge model results by varying further the initial in situ conditions. The conclusions and suggestions for further work are presented at the end of the thesis.

I am extremely grateful to my supervisor, William Powrie, for his seemingly limitless help, encouragement and patience throughout this period of research. His considerable intellect and ability to communicate effectively have been truly inspirational.

I would also like to thank Roger Nelson, Michael Collins, Brian Nicholson and Harvey Skinner for their technical expertise, unstinting generosity and good humour. Without them none of the centrifuge tests would have been possible.

My thanks further extends to a great many others who have, in various ways and at various times, helped me over the last four years at QMW, in particular Gary Holmes, Mark Daly, David Richards, Roger Chandler, Christina Kantartzi, Ken Critolph, Jim Bowles and my parents.

Finally, I owe an enormous debt of gratitude to Jacqui Bowles whose love and support has kept me going throughout.

| | |
|---|---|
| $A_s$ | pore pressure coefficient |
| $c_v$ | consolidation coefficient |
| $D_{10}$ | diameter of the finest 10% of soil particles |
| $\Delta\sigma_h$ | change in horizontal stress etc. |
| $E$ | (usually with subscript) Young's modulus |
| $e_{cs}$ | void ratio on critical state line at $p'$=1 kPa $e$-ln$p'$ space |
| $\phi'$ | effective angle of shearing resistance |
| $\phi'_{crit}$ | effective angle of shearing resistance at critical state |
| $g$ | gravity |
| $G$ | shear modulus |
| $G$ | (usually with subscript) specific gravity |
| $\Gamma$ | specific volume on critical state line at $p'$= 1 kPa $v$-ln$p'$ space |
| $\gamma_b$ | unit weight of bentonite |
| $\gamma_c$ | unit weight of concrete |
| $\gamma_s$ | unit weight of soil |
| $\gamma_w$ | unit weight of water |
| $h$ | excess height above the surface of the model |
| $H$ | height above the trench |
| $i$ | hydraulic gradient |
| $k$ | permeability |
| $\kappa$ | slope of unload-reload line in $v$-ln$p'$ space |
| $K_o$ | earth pressure coefficient |
| $K_{onc}$ | earth pressure coefficient under normally consolidating conditions |
| $K_{ou}$ | earth pressure coefficient during initial unloading |
| $K_c$ | coefficient applied to consolidating concrete |
| $K_p$ | coefficient of passive earth pressure |
| $\lambda$ | slope of one dimensional compression line $v$-ln$p'$ space |
| LVDT | linear variable displacement transducer |
| $m$ | mass |
| $M$ | slope of critical state line in $q$-$p'$ space |
| $\nu$ | Poisson's ratio |

| | |
|---|---|
| $\eta$ | porosity |
| $n$ | scaling constant |
| OCR | over consolidation ratio |
| $p'$ | mean normal effective stress |
| $p_k$ | capillary pressure |
| PPT | pore pressure transducer |
| $q$ | deviatoric stress |
| $\sigma'_h$ | effective lateral stress |
| $\sigma'_v$ | effective vertical stress |
| $\sigma_h$ | total lateral stress |
| $\sigma_v$ | total vertical stress |
| $t$ | elaspsed time |
| $\tau$ | shear stress |
| TST | total stress transducer |
| $T_v$ | consolidation time factor |
| $\overline{u}$ | excess pore water pressure |
| $u$ | pore water pressure |
| $v$ | flow velocity |
| $z$ | depth under consideration |

# *Chapter 1*

# *Introduction*

## *1.1 Introduction*

The high premium placed on urban land and the likely proximity of adjacent buildings has led to the increased adoption in built-up areas of construction techniques that have a minimum impact on the surrounding environment. This thesis is principally concerned with the increasingly common technique of slurry or diaphragm walling and examines the behaviour of the surrounding soil during the installation process.

## *1.2 Retaining walls*

Retaining walls are now used extensively and are often found in road improvement schemes, cut and cover tunnels, major buildings and industrial facilities in general. It is often necessary to take account in design of prescribed limits on ground movements or stress relief, particularly in built up areas.

Broadly, there are two methods of retaining wall construction;

1) Backfilled (after wall construction the retained soil is compacted into place)
2) Placed in situ.

Placed in situ walls take three forms:

a) Driven (sheet pile walls provide the most common example)
b) Bored pile walls (either secant or contiguous)
c) Slurry trench or diaphragm walls

The slurry trench walling technique has minimum impact on the surrounding environment, with lower noise levels than driven pile walls and less disturbance to the surrounding ground than the backfilled method. A typical construction sequence involves first the excavation of a trench under bentonite slurry (which provides a support as well as forming a seal on the sides of the trench).

The use of bentonite is economical as the screening plants installed on site permit its reuse once cleaned, and also facilitates fast-track construction methods. However, during excavation the lateral pressures on the sides of the trench are reduced to the bentonite pressure. This may result in a softening of the clay and a reduction in shear strength around the trench, particularly in the longer term when full pore water pressures are re-established. In low permeability clays, the initial unloading may result in the clay drawing in water and this can also have a significant impact on the subsequent behaviour of the finished wall. After excavation has been completed the reinforcement cage is lowered into the trench and concrete is tremie-piped into the bottom of the trench.

A general understanding of retaining wall behaviour can be obtained from back analysis of existing walls, as well as from constant monitoring, during and after an installation. The effects of the installation on the in situ stresses have been given increased attention and the errors and approximations inherent in traditional methods that assume ground

conditions are unaffected by wall installation have been recognised. The resulting empirical methods that have been developed for both soil and retaining wall design now recognise the need for accurate input data as well as a reliance on many assumptions. Soil by its nature is inhomogeneous and often very complex on both a micro and macro scale. Similarly, retaining walls are often constructed from complex materials, and are capable of unpredictable behaviour.

In certain circumstances the stress state in the ground may change substantially during diaphragm wall installation and have a significant effect on the behaviour of the wall in service. Field measurements, particularly in overconsolidated clays, have shown a significant range of earth pressure coefficients for different soils at different depths. High initial, in situ, lateral stresses associated with these clays may be greatly reduced depending on the wall construction method employed.

Although a number of mathematical models have been developed that can be used in an attempt to predict soil behaviour (Roscoe, 1957; Schofield, 1980; Stallebrasse, 1990; Simpson, 1992) very few physical measurements of the reductions in lateral stress that actually occur have been made at either prototype or model scale. This thesis is concerned primarily with the changes in lateral stress that occur during installation, and their implications for the subsequent behaviour of the wall.

## *1.3 Modelling techniques*

In order to investigate the stress reduction due to wall installation two techniques have been used,

1) centrifuge modelling
2) finite element analyses

### *1.3.1 Centrifuge modelling*

Centrifuge modelling is now a widely accepted technique in geotechnical engineering research and has been shown to give an accurate indication of the mechanisms that operate in many geotechnical situations. Centrifuge tests are carried out at a small scale, in a fraction of the time and at a fraction of the cost of full scale tests.

In the model tests described in this dissertation, a specimen of overconsolidated speswhite kaolin was cut to the required size and geometry and instrumented so that pore water pressures, lateral stresses and ground movements could be recorded during

the simulated excavation of a diaphragm wall panel. The model developed for this purpose by Kantartzi (1994) was further adapted to extend the range of earth pressure coefficients that could be modelled and also to record in situ lateral stresses.

The trench excavation was modelled at one end of the sample and then concrete placement was simulated. The resulting changes in lateral stress, porewater pressure and surface movements were recorded and these results have been analysed. The results are presented for the short and long term, to investigate whether stress reductions that have occurred during excavation were re-established during concreting.

### *1.3.2 Finite element analyses*

Advances in computer technology have led to the increasing use of complex mathematical models to investigate geotechnical problems. Finite element analyses have been developed extensively and many different soil models have been implemented. The analyses presented were used as a comparison with the centrifuge data and to develop the understanding of the stress changes occurring during diaphragm wall installation.

# *Chapter 2*

# *Slurry trenching techniques*

## *2.1 Introduction*

The principle behind the slurry trenching technique originated in the oil well industry, where fluid mud was used as a well support during drilling. Colloidal suspensions like bentonite were also employed to provide relatively impermeable boundaries to prevent the migration of leachate or groundwater. Further developments led to the use of concrete and bentonite mixes to provide permanent cut-offs and reinforced concrete to provide structural, diaphragm retaining walls.

### *2.1.1 Slurry trenching in overconsolidated soil*

The demand for space in urban areas and the obvious financial benefits of top-down construction have led to the adoption of diaphragm type retaining walls in many civil engineering projects. Also, increased litigation has prompted an awareness of the importance of careful and diligent construction in order to minimise the movement of adjacent facilities. Contractors attempt to minimise extensive temporary works (such as shuttering) as this reduces cost considerably (Clough and O'Rourke 1990).

In the construction of in situ diaphragm walls, bentonite slurry is used to provide stability during excavation as the bentonite slurry compensates in part for the loss in total lateral stress due to excavation. Also, the bentonite balances the head of water in the soil and in high permeability soils attenuates groundwater seepage by forming an impermeable filter cake at the edges of the trench.

Diaphragm walls will often be required to carry high horizontal soil pressures (particularly in overconsolidated clay soils) and vertical loads, and to act as an impermeable barrier to groundwater. The cast in-situ method of construction provides a cost-effective technique that satisfies the necessary strength and permeability criteria.

First this chapter presents existing research on the formulation of the earth pressure coefficient (the ratio of horizontal to vertical effective stress for different soil depths). The chapter then examines the use of bentonite slurries used to support the trench during excavation and discusses methods of cleaning and the problems associated with contamination. Finally, the effects of concrete placement are looked at and a consolidation mechanism is proposed for the accurate prediction of the lateral stresses applied by the fresh wet concrete during and after placement.

## *2.2 Overconsolidated clay deposits*

Overconsolidated clay will tend to exhibit high in situ lateral stresses due to deposition and subsequent erosion of overlying material over a geological timescale. The earth pressure coefficient, $K_o$, defines the in situ ratio of horizontal effective stress to vertical effective stress at different depths. Relationships were first proposed to predict values of $K_o$ for soils in virgin compression. These relationships have since been extended to predict $K_o$ values at any point on a stress path.

### *2.2.1 Virgin compression relationships*

Jaky (1944) proposed that

$$K_o = 1 - \sin\phi' \qquad (2.1)$$

from experimental results which provided the basic equation for normally consolidated soils. Brooker and Ireland (1965) used a one dimensional compression cell which measured radial pressures under a condition of zero lateral strain to investigate earth pressure coefficients experimentally. They proposed for clay a correction to the relationship proposed by Jaky (1944) from the data for five different soils of varying plasticity index:

$$K_o = 0.95 - \sin\phi' \qquad (2.2)$$

concluding that Jaky's (1944) original equation was more representative of sands. Conversely, Mayne and Kulhawy (1982) after examining data from over 170 samples concluded that the relationship proposed by Jaky (1944) for $K_{onc}$ for normally consolidated soil was valid for clays and moderately valid for sands. Minor adjustments to the original Jaky (1944) relationship have little effect in the context of design, and it is generally accepted as satisfactory for most situations.

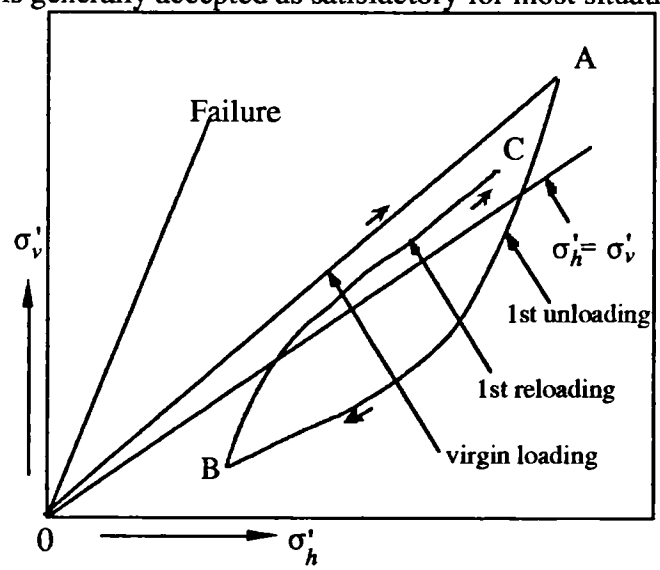


Figure 2.1 *Simplified stress history of soil under $K_o$ conditions*

Initial, normal consolidation is indicated in figure 2.1 by OA (the virgin loading line). Overconsolidation occurs after point A, following unloading from the point at which the maximum pre-consolidation stress has been applied. The figure also demonstrates that overconsolidated clays are at a position on a stress path that must be defined by a different relationship, where the criterion $\sigma_h' > \sigma_v'$ can be satisfied at high overconsolidation ratios.

### *2.2.2 $K_o$ for an overconsolidated clay*

Brooker and Ireland (1965) suggested that the stress history of the soil governed the value of the coefficient of earth pressure during unloading and presented data as a function of internal friction and plasticity index. Schmidt (1966) used the same data and represented the relationship as

$$\frac{K_{ou}}{K_{onc}} = OCR^{\alpha} \qquad (2.3)$$

where $K_{onc}$ is the at-rest coefficient during normal compression, $K_{ou}$ is the coefficient during unloading, OCR is the overconsolidation ratio, and $\alpha = \sin(1.2\phi')$.

Having adjusted the Brooker and Ireland (1965) equation to

$$K_{onc} = 1 - 1.2\sin\phi' \qquad (2.4)$$

Schmidt (1966) concluded that the earth pressure coefficient relationship during initial unloading was best defined by

$$K_{ou} = (1 - \sin 1.2\phi').OCR^{\sin 1.2\phi'} \qquad (2.5)$$

Mayne and Kulhawy (1982) simplified the above to give a better approximation to the data from different samples to

$$K_{ou} = (1 - \sin\phi').OCR^{\sin\phi'} \qquad (2.6)$$

$K_o$ cannot, in any case, exceed the Rankine passive pressure coefficient

$$K_p = \frac{1 + \sin\phi'}{1 - \sin\phi'} \qquad (2.7)$$

Using equations 2.6 and 2.7 an overconsolidation limit (above which the relationship defined by Mayne and Kulhawy (1982) does not apply) may be calculated from

$$OCR_{lim} = \left[\frac{(1+\sin\phi')}{(1-\sin\phi')^2}\right]^{(1/\sin\phi')} \tag{2.8}$$

If $\phi' = 30°$, $OCR_{lim}$ may be as high as 36. Mayne and Kulhawy (1982) proposed an $OCR_{lim}$ of approximately 25 for design purposes.

During reloading (path BC on figure 2.1) Wroth (1972) proposed the linear relationship

$$\sigma'_h - \sigma'_{h\,min} = m_r(\sigma'_v - \sigma'_{v\,min}) \tag{2.9}$$

where $m_r$ is the reload coefficient. The minimum values of horizontal and vertical effective stress refer to point B on figure 2.1. Using these definitions of minimum effective stresses a new parameter, $OCR_{max}$ may be defined as

$$OCR_{max} = \frac{\sigma'_{v\,max}}{\sigma'_{v\,min}} \tag{2.10}$$

From empirical data Wroth (1972) defined the reload coefficient as

$$m_r = \left(\frac{3}{4}\right)(1-\sin\phi') = \left(\frac{3}{4}\right)K_{onc} \tag{2.11}$$

One equation can be used to approximate the earth pressure coefficient at any point along a load-unload-reload path. The basis of this relationship is essentially empirical and dependent on the relationships proposed by Jaky (1944), Mayne and Kulhuwy (1982) and Wroth (1972).

$$K_o = (1-\sin\phi')\left[\left(\frac{OCR}{OCR_{max}^{(1-\sin\phi')}}\right) + \frac{3}{4}\left(1-\frac{OCR}{OCR_{max}}\right)\right] \tag{2.12}$$

Using a different approach, Skempton (1961) defined a relationship between earth pressure coefficient and depth in an overconsolidated clay using the measured capillary suction, $p_k$, such that

$$p_k = p[K_o - A_s(K_o - 1)] \qquad (2.13)$$

where p is the overburden pressure and $A_s$ is the relevant pore pressure coefficient. Skempton (1961) adopted four different methods to obtain values for the swelling pressure (capillary pressure) and found acceptable agreement between them. $A_s$ was taken as 0.3 for the case discussed.

As explained in chapter 3, in the present work a Speswhite kaolin sample was loaded and unloaded in an attempt to simulate the stress state found in a typical overconsolidated clay. Further horizontal pressures were applied to the sample that were consistent with extreme values of earth pressure coefficients from field data, in an attempt to simulate overconsolidated clay behaviour.

## *2.3 Installation of diaphragm walls*

### *2.3.1 Introduction*

Research into the design of in situ retaining walls has paid considerable attention to the depth of embedment and/or the prop systems required to maintain wall stability (Tedd et al, 1984; Powrie, 1986; Bolton and Powrie, 1988; Fourie and Potts, 1989; Higgins et al, 1989; Powrie and Li, 1991; Symons and Carder, 1989, 1992). Less attention has been paid to the effects of wall installation. Numerical modellers, for example, will often assume the in situ stresses at the start of the main excavation, and neglect the problem of wall installation effects (Higgins et al., 1989).

Recently, researchers have paid more attention to ground movements and stress changes resulting from wall installation (Kutmen, 1986; Gunn and Clayton, 1987; Powrie and Kantartzi, 1993; Kantartzi, 1994; Ng, 1993; Lings et al, 1993). The three different installation methods commonly used will have an effect on the degree of stress relief that occurs. These are considered below:

a) contiguous bored pile walls
b) secant bored pile walls, and
c) panel construction diaphragm walls

### *2.3.2 Contiguous bored pile walls.*

Pile diameters may vary from 0.25m to 1.5m with independent piles spaced at a minimum of 1.1 pile diameters to allow for construction tolerance. Piles are drilled with or without the support of temporary casings (depending on the soil strata), but adjacent piles are not necessarily touching. The vertical gaps between vertical piles are sometimes infilled with piles of a smaller diameter.

Construction in stiff or hard strata will often require a 'mudding up' technique. (Thompson, 1990). This involves boring the hole with an auger before mixing the loosened soil with bentonite and water. A temporary casing is then inserted and the loosened soil is removed before the concreting proceeds.

### *2.3.3 Secant bored pile walls*

Primary piles are constructed in a similar way to the first stage of a contiguous pile wall. These piles are usually cast using a soft concrete. After pour but before the concrete has fully set, intermediate (secondary) piles are constructed from a stronger concrete. Adjacent piles interlock to form a wall. The required speed of construction necessitates the construction of guide walls so that accurate placement is achieved.

This method has become increasingly popular and the construction of one such wall at Bell Common was discussed by Symons and Carder (1992). The wall consisted of a line of cast in situ bored piles, reinforced with I-section steel universal beams. Throughout installation (and later during propping prior to the main excavation) the wall was extensively instrumented to monitor stresses and porewater pressures in the adjoining ground. The data provided firm evidence of the substantial ground movements and stress changes that occur during the installation stage of an embedded retaining wall.

### *2.3.4 Panel construction diaphragm walls*

A third construction method uses a series of panels to form the diaphragm wall. Current 'fast track' construction approaches have led to the increasing use of tight critical path programming schedules, with non-adjacent panels excavated and filled simultaneously optimising the use of expensive grab equipment and batching plants. Once the concrete has reached sufficient strength the remaining intermediate panels are constructed.

Typically, excavation is performed using a cable-controlled grab or rotary-percussive drill bits with the minimum width of the trench limited to the width of the grab. The excavator is aligned with guide walls that are cast at the edges of the proposed trench prior to excavation. Bentonite slurry is pumped into the excavation as it progresses to apply hydrostatic pressure to the sides of the trench.

Panels will be in the range 0.6 m to 1.2 m thick and up to 6 m in length. It is generally advantageous to use longer rather than shorter units. This reduces the number of vertical construction joints, provides fewer problems with the alignment of the wall and reduces the risk of water seepage through the wall. However three dimensional effects (which are beneficial in reducing ground movements during the installation of individual panels) are more significant when shorter panel lengths are adopted (Kantartzi, 1994).

One technique of linking consecutive panels uses a stop-end pipe, where single-length, smooth tubes are bedded into the ground at both ends of the first panel, similar to the bored pile methods (Boyes, 1975). These are removed when the concrete has reached near-set. Adjacent panels are then excavated and a single stop-end tube is placed at the remote end of each successive trench before a prefabricated reinforcing cage is lowered in place.

The stop-end pipe is not an essential requirement for diaphragm wall construction. In many situations where the soil or bedrock is sufficiently stiff it is not necessary to provide additional support to the ends of the trench. Dibiagio and Roti (1972), Burland and Hancock (1977) and Ng (1993) make no reference to the use of the stop end tubes in panel type constructions.

The most common concrete placement technique uses a tremie pipe that is inserted into the trench (often through the reinforcement mesh). Concrete is pumped into the trench either in a series of lifts or at a constant rate, filling the trench from the bottom up as the bentonite is displaced and returned to agitators.

## *2.4 The use of bentonite in slurry trenches*

In the construction industry, the term 'bentonite' refers to sodium bentonite which is either mined as naturally occurring sodium bentonite (from Wyoming, for example) or as calcium bentonite and subjected to cation exchange.

The bentonite has two principal functions; first to provide lateral support to the sides of the trench and secondly to prevent the migration of ground water by forming an impermeable layer around the edge of the excavation. Bentonite is susceptible to contamination and this may compromise the stability of the trench and hence a knowledge of the chemical characteristics of bentonite is essential if it is to be employed in diaphragm wall construction.

### *2.4.1 The structure of bentonite*

The primary structure of all clay minerals is the silicon-oxygen tetrahedron $SiO_4^{4-}$.

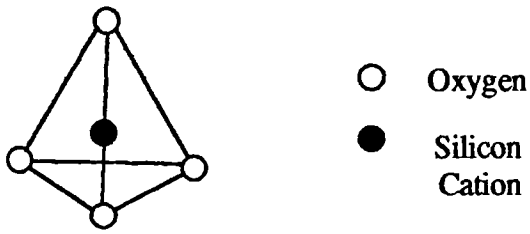


Figure 2.2 *The basic tetrahedron particle*

Montmorillionite clays (which include bentonite) form a 'sandwich' structure with sheet layers of tetrahedrons joined 'point-in' by a shared oxygen atom, forming octahedral spaces within the structure. An additional cation (usually $Al^{3+}$ or $Fe^{3+}$) is 'sandwiched' between the two layers of tetrahedrons. The cation configuration of the clay particles is therefore a single layer of octahedral cations sandwiched between two layers of tetrahedral cations ($Si^{4+}$). This group of clays is said to have a 2:1 layer configuration.

Within the structure cation substitution occurs. Substitution of ions of a lesser charge ($Si^{4+}$ by $Al^{3+}$ in tetrahedral positions and $Al^{3+}$ or $Fe^{3+}$ by $Mg^{2+}$ or $Fe^{2+}$ in octahedral position) produces resultant negative charges on the particle edges.

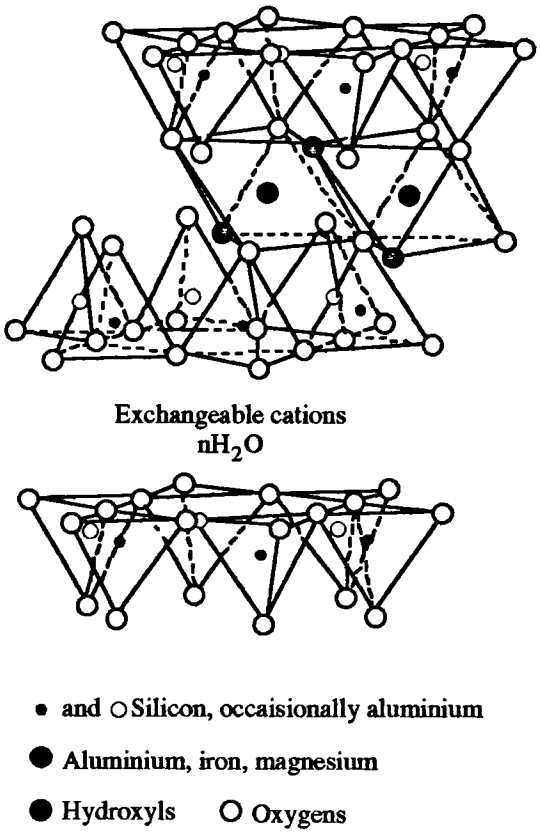


Figure 2.3 *Cross-section of a bentonite particle. 2:1 configuration*

The negative edge charges are balanced by exchangeable cations (commonly $Na^+$, $Ca^{2+}$ or $Mg^{2+}$) that exist as a cloud around the clay particles (Jefferis, 1992) and it is the charge of the exchangeable cation that controls the adsorption of water. The bonds that hold the octohedrons and tetrahedrons together are strong compared with the bonds that exist between the exchangeable cations and the particle edges.

In solution water is ionised to form hydrogen and hydroxyl ions and as sodium has more strongly positive charge than calcium (as only one valence electron must be removed from the outer shell for the atom to reach an ideal configuration) it will attract more hydroxyl ions and therefore more water. As the water is absorbed the bentonite disperses and particles of dimensions 0.1μm x 0.1μm x 0.001μm are colloidally suspended.

### *2.4.2 Thixotropy*

The montmorillonite group of clays have considerable thixotropic strength because the water that is adsorbed is oriented around the particle surfaces. At low bentonite

concentrations (normally in the region of 4.5 - 5% for slurry trench walling), where the exchangeable cation is sodium, water will be oriented more quickly than when the exchangeable cation is calcium. Once oriented, the water molecules will give the bentonite thixotropic strength and a 'gel-like' consistency. If the bentonite is reworked the orientation of the molecules is destroyed, but when allowed to stand the water orientation gradually redevelops and the thixotropic strength is regained (Grim, 1962).

The relationship between shear stress and rate of shear for a simple (Newtonian) fluid will be linear and can be described by a single parameter, the viscosity. However, colloidal suspensions (like bentonite slurry) show a more complex, thixotropic, relationship. Figure 2.4 indicates how slurries will behave as solids at low shear stresses (at any point along OB) and how a shear rate (hence flow) only occurs at a threshold value of shear stress.

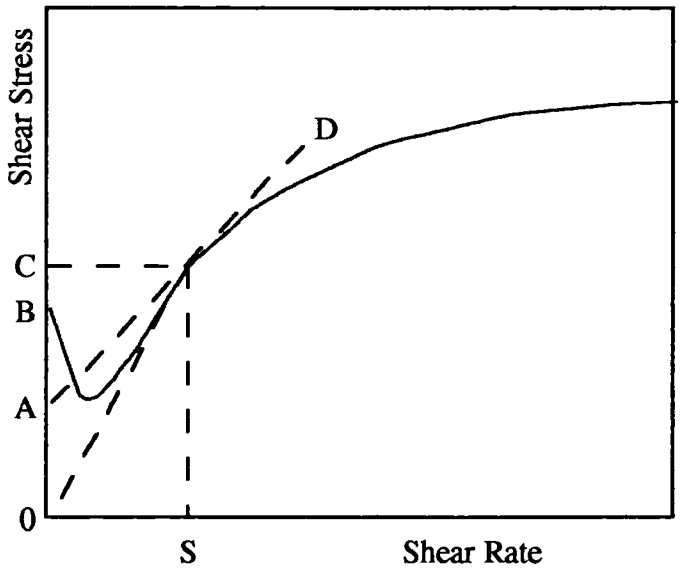


Figure 2.4 *Shear stress against shear rate for a non-Newtonian fluid*

Figure 2.4 above defines OB as the gel strength of the slurry at rest. At any point along the curve the plastic viscosity = CA/OS, the apparent viscosity = OC/OS and the yield value = OA. For any shear rate the tangent to the curve gives the plastic viscosity and the extrapolation of this tangent to the shear stress axis gives the yield value. The slope of the line from the origin to any point on the curve will give a value for the apparent viscosity - the equivalent Newtonian viscosity.

The shear rate at which sodium bentonite flows is greater at all levels of concentration than calcium bentonite. Sodium bentonite is therefore better suited to slurry trench stabilisation as it develops stronger thixotropic gel strengths more quickly.

### *2.4.3 Slurry contamination*

The structure of bentonite is such that larger exchangeable cations are more readily adsorbed onto the particle edges. Calcium ions are larger than sodium ions and are therefore exchanged for sodium ions in situations where both exist in the interlayer cloud. This can have a considerable impact in a civil engineering environment where calcium is released in solution during the primary stages of cement hydration and the bentonite is recycled for further use.

During initial hydration, free lime ($Ca(OH)_2$) is released as $Ca^{2+}$ and $OH^-$ ions in solution. The calcium ions are exchanged for sodium ions whilst the hydroxyl ions are adsorbed, changing the properties of the slurry. The effect of increasing the concentration of calcium salt in sodium bentonite on the gel strength is shown in figure 2.5.

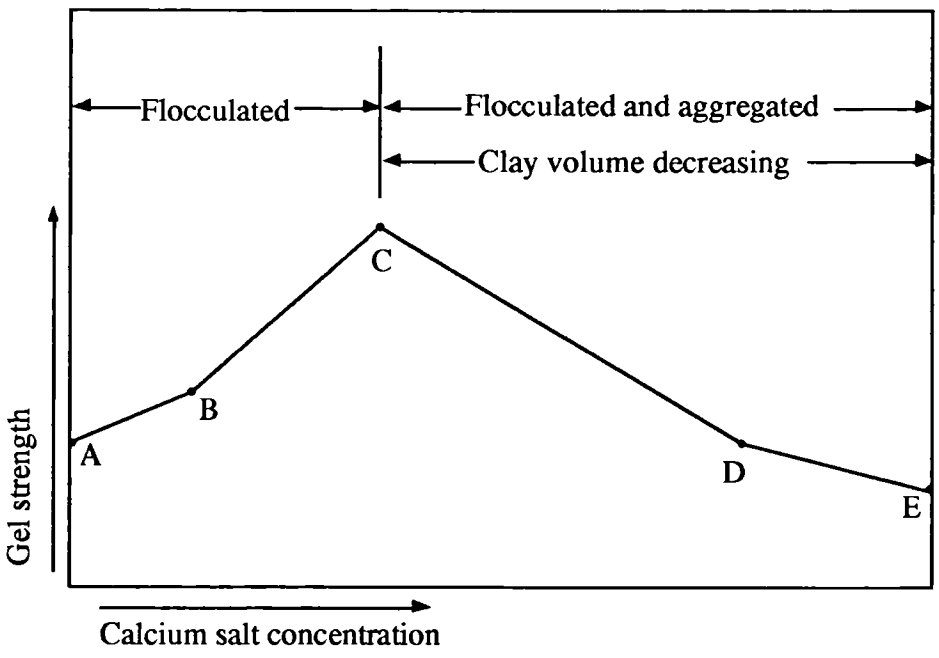


Figure 2.5 *The effects of calcium salts on sodium bentonite*

Initial calcium contamination (A to C) will result in an increase in gel strength as calcium bentonite particles flocculate (i.e. form edge to face particle bonds) but remain in suspension. Further addition of calcium salt to the bentonite (C to E in

figure 2.5) causes more of the sodium ions on the particle surfaces to be displaced by calcium ions. This reduces the negative repulsive forces and allows intense flocculation and aggregation (i.e. the formation of face to face particle bonds). As aggregation continues, water appears at the surface and flocculated and aggregated calcium bentonite particles sink.

High levels of contamination will result in a severe reduction in viscosity and thixotropic gel strength of the slurry. Diminishing thixotropic strength may lead to a dangerous loss of trench stability. The low concentration of sodium bentonite that remains suspended in the trench will result in a reduction of lateral hydrostatic pressures on the sides of the trench and increased fluid loss to the surrounding strata. Although fluid loss into the sides of a trench is of less significance in a stiff impermeable clay, the loss in stability due to the reduction in lateral pressure may have a considerable effect. Further some softening of the sides of the trench may occur leading to reduced trench stability (Harrison and Clear, 1985). Clearly, there is a considerable need for cleaning and anti-contamination measures on site.

### *2.4.4 Slurry cleaning and thinning*

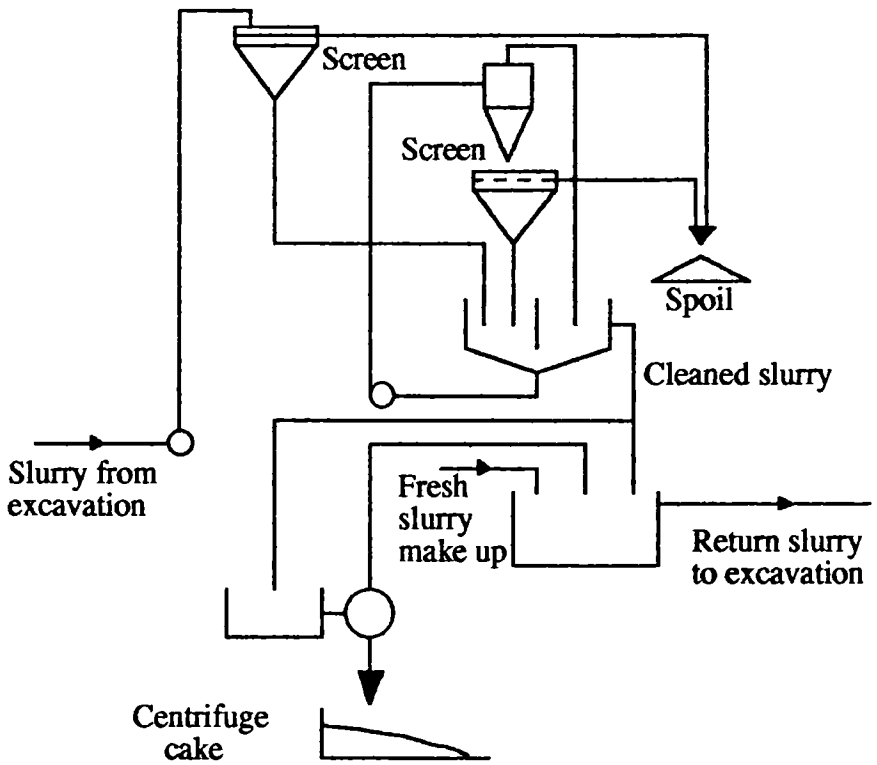


Figure 2.6 *Slurry cleaning apparatus (Jefferis, 1992)*

Figure 2.6 shows a schematic diagram of a typical bentonite slurry cleaning apparatus. The cleaning procedure will usually start by screening the slurry using sieves ranging from 100μm to 10mm. Hydrocyclones are essentially centrifuges in which coarse particles migrate more quickly than fine particles towards the walls during spinning. A tapping is then used to siphon off the unwanted spoil. The grade of particles that are removed by a cyclone may be as fine as 20 microns but the process at this level of purity becomes slow as only a small amount of slurry may be spun at any one time.

The need for effective treatment of cement contaminated slurries has led to the adoption of chemical additives after the slurry has been removed from the trench so that the slurry may be re-used. The most common types of additives for slurry treatment:

1. Dehydrated phosphates
2. Polyphosphates
3. Plant extracts (Quebracho)
4. Lignosulphates
5. Mineral lignins

The slurry cleaning additives are designed principally as slurry thinners and are used to re-suspend flocculated and aggregated bentonite particles. Three methods of thinning are adopted; the precipitation of $Ca^{2+}$ ions; the neutralisation of $OH^-$ ions, or; the formation of a protective coating around the clay particles. Quebracho (complex compounds such as gallic and ellagic acids obtained from the Quebracho tree in Argentina) is the most effective thinner for low levels of contamination and works by latching onto the edges of the clay particles as a protective coating. Similarly, Ferrochrome Lignosulphate (FCL) uses hydrogen bonds to form a sheath around the surface of the clay particles.

The slurry is pumped from the trench during concrete placement and initially screened and filtered several times. The addition of a thinning treatment increases the gel strength as flocculated calcium particles are resuspended increasing the concentration of bentonite particles in suspension. However, it has been shown that the addition of a thinning agent to the bentonite prior to the use of the slurry does not have as significant an effect as the post treatment methods conventionally employed (Kim, 1988). If pre-treatment is adopted, flocculation will continue to occur and further post treatment will be necessary if the slurry is to be reused.

In practice, slurries cannot be re-used indefinitely. Where reflocculating treatment of calcium bentonite is adopted repeatedly gel strength decrease considerably. Upon further addition of the thinner, clay particles increase in size as further coatings bond to the particles, producing unworkable slurries requiring exceptionally high shear stresses to induce flow.

## *2.5 Bentonite in construction*

The fundamental requirements of the bentonite for construction expediency are blocking mechanisms and the provision of lateral support to the sides of the trench. There are two types of blocking mechanism and these are considered below.

### *2.5.1 Rheological blocking*

The pressure within the trench will cause individual particles to agglomerate at the edges of the trench where the shear stresses are smaller than those required for flow (less than OA on figure 2.5). As the bentonite is recirculated, a cake will develop at the sides of the trench providing the sodium bentonite suspension is of sufficient concentration (4 - 4.5%) and the soil is of low permeability (Kim, 1988).

The formation of a groundwater barrier is of less importance in impermeable clay than in coarse sand as fluid loss to the surrounding soil is unlikely to be significant. In a relatively impermeable clay the build up of a cake at the edges of the trench will make little difference to the rate of fluid loss into the surrounding soil.

However, rheological blocking in a fissured clay will help to reduce fluid loss into the fissures at the sides of the trench. The Bingham rheological model was extended by Van Olphan (1962) to calculate the length of slurry penetration into the soil or fissures. He proposed the relationship:

$$L = \frac{P}{\tau_o} . f . \frac{n}{n-1} . D_{10} \qquad (2.14)$$

where $L$ = penetrated distance, $P$ = driving pressure
$\tau_o$ = slurry yield value, $n$ = porosity
$f$ = tortuosity, $D_{10}$ = diameter of the finest 10% of the soil particles

The tortuosity of the flow path is quantified by $f$ and will be in the region of 0.3 for a coarse sand. Jefferis (1992) suggests that the above represents (at best) a coarse over-simplification but will give results that could be considered accurate in certain circumstances.

Fleming and Sliwinski (1977) proposed that the rate of fluid loss to the surrounding soil decreases with time according to the relationship

$$V = mT^{1/2} \qquad (2.15)$$

where $V$ = total loss of fluid
$m$ = constant dependant on particle size and bentonite concentration
$T$ = time for filter cake formation

The membrane formed by rheological blocking will depend on the shear rate at the sides of the trench. Larger pores or fissures will become rheologically blocked as rates of shear in these zones areas will be slower than in the rest of the trench.

### *2.5.2 Mechanical blocking*

The excavation techniques employed commonly will allow most of the bentonite to drain freely from the excavator grab back into the trench. The slurry that returns to the trench will be contaminated with spoil from the excavated soil. Mechanical blocking is the formation of blockages in fissures in the side of the trench by the spoil suspended in the slurry. If the fines in suspension are not sufficiently large to limit slurry penetration into the fissures, polymers are added (for example carboxymethyl cellulose) to promote particle flocculation around the contaminants.

## *2.6 Lateral stress changes during wall installation*

The effect of wall installation on the lateral stresses in a stiff clay has been the subject of several investigations (Dibiagio and Roti, 1972; Burland & Hancock, 1977; Clayton & Milititsky, 1983; Gunn & Clayton, 1987; Symons & Carder, 1989, 1992; Lings, Ng and Nash, 1993; Kantartzi, 1994; Ng, 1993 etc.). The principal factors that will affect the lateral stress changes are the stress relief due to excavation under bentonite and the reapplication of stress during concrete placement.

### *2.6.1 Stress relief due to excavation under bentonite slurry.*

Excavation under bentonite slurry will result in stress relief as soil is removed and the trench is filled with bentonite. The degree of lateral stress relief in an overconsolidated clay will depend on the in situ, initial earth pressures which may be high and the unit weight of the bentonite which, ideally, will be in the range of 10.14 and 12.26 kN/m$^3$ (Jefferis, 1992). This is shown in figure 2.7 below:

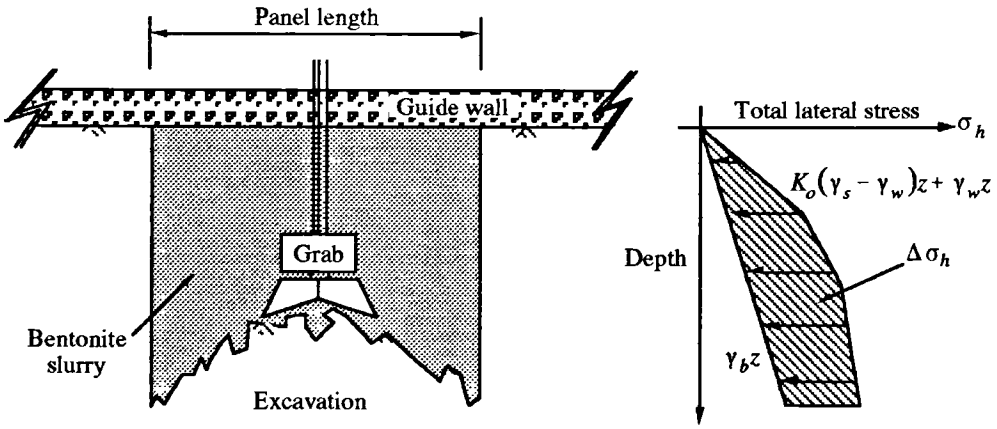


Figure 2.7 *Stress relief due to excavation*

This relationship, $\Delta\sigma_h$ may be defined as the difference between

$$\sigma_h = K_o(\gamma_s z - \gamma_w z) + \gamma_w z = z(\gamma_s K_o + (1 - K_o)\gamma_w) \quad (2.16)$$

and

$$\sigma_h = \gamma_b z \quad (2.17)$$

after excavation. Therefore

$$\Delta\sigma_h = [\gamma_s K_o o + (1 - K_o)\gamma_w - \gamma_b]z \quad (2.18)$$

The changes that occur further back from the trench are of a smaller magnitude than those that occur at the face. Kantartzi (1994) proposed that in plane strain conditions, settlements would occur at up to 1 trench depth back from the trench. Further, she proposed a zone, existing between the trench and a line at 45° from the toe of the trench to the surface of the model, inside which lateral stress changes would be significant.

Terzaghi (1943) suggested that horizontal stress relief at the face of the trench will induce horizontal stress increases in the soil below the toe. Pressure is transferred from a yielding mass of soil onto adjoining soil as the excavated face of the trench arches vertically over the natural prop at the bottom where comparatively firm support is provided. Ng (1993) experienced *horizontal* arching where panels of a finite length were excavated. He presented field data in which the horizontal stresses at the *sides* of the panel during placement increase to levels that are considerably larger than the initial in situ horizontal stresses.

### *2.6.2 Lateral pressure changes due to cement placement*

Two main theories have been proposed for the lateral stress profile imposed during concrete placement. The most simple method was adopted in numerical models by Higgins et al (1989) and Kutmen (1986). Both assumed that concrete pressure during placement was applied at the full hydrostatic value for the entire depth of the trench. In both cases a plane strain mesh was assumed, with pressures applied that corresponded to concrete unit weights of 24 kN/m$^3$ and 23 kN/m$^3$ respectively, increasing linearly over the depth of the trench.

The pressure applied to the bottom of the trench after concrete placement was taken as approximately 384 kPa for a 16m deep trench (Higgins et al., 1989) and 460 kPa for a 20m deep trench (Kutmen, 1986). The distributions of lateral pressure with depth in an analysis of this type is shown in figure 2.8.

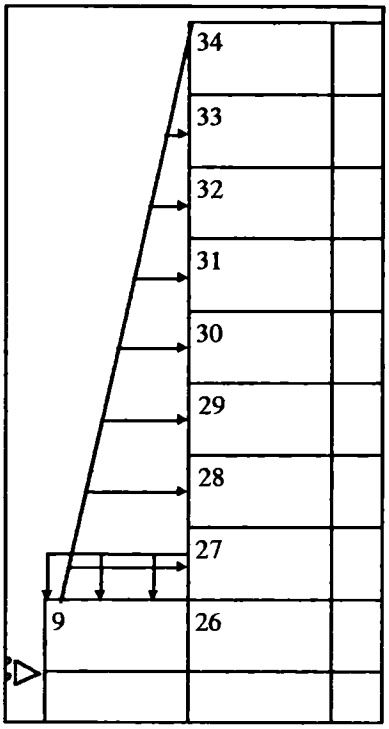


| Element number | Confining pressure kPa |
|---|---|
| 34 | 0.0 |
| 33 | 57.5 |
| 32 | 115.0 |
| 31 | 172.5 |
| 30 | 230.0 |
| 29 | 287.5 |
| 28 | 345.0 |
| 27 | 402.5 |
| 26 | 460.0 |
| 9 | 460.0 |

Figure 2.8 *Total pressure applied by concrete (Kutmen, 1986)*

Observations made during field monitoring of different sites would tend to refute this assumption and more complex, bilinear methods have been proposed. Dibiaggio and Roti (1972) proposed that full hydrostatic pressure of the fresh concrete would be exerted on the sides of the trench during concreting only as long the column of overlying concrete did not exceed some limiting value, a critical depth.

The formulation of a critical depth of hydrostatic concrete pressure was explored further by others, notably, Gardner and Ho (1979), Harrison, (1983); Harrison and Clear (1985), and Ng (1993). Clayton and Milititsky (1983) measured hydrostatic concrete pressures at shallow depths but found that at deeper depths pressures did not increase as fast.

Gardner and Ho (1979) concluded that the most significant factors affecting the maximum lateral pressure exerted by freshly poured concrete on formwork were the rate of pour and the slump of the concrete. A fifteen foot form was erected and instrumented to measure lateral pressure as the concrete was poured. Soon after the form was filled, the front face was moved outwards and another set of load readings was taken. The readings indicated that the initial lateral stresses diminished substantially very soon after pour. This work has been discredited and other suggestions have been made.

From 350 sets of data, Harrison and Clear (1985) produced CIRIA report 108 which examined the pressures exerted on the sides of formwork. The relationship they derived to find the pressure, $P_{max}$, at critical depth is empirical and errs towards an overestimation of the worst case investigated. The code proposed that the concrete exerts full hydraulic pressure on the formwork while the aggregate and cement are suspended in water at a certain depth from the top of the trench. At deeper positions lateral pressures would not increase and it was suggested that the maximum value should be applied at all deeper positions.

A design formula was proposed:

$$P_{max} = D\left[C_1\sqrt{R} + C_2K\sqrt{H - C_1\sqrt{R}}\right] \text{ kN/m}^2 \qquad (2.19)$$

or

$$Dh \text{ kN/m}^2 \qquad (2.20)$$

which ever is the smaller

where $P_{max}$ = Maximum lateral pressure exerted by concrete
$C_1$ = Coefficient dependent on the size and shape of formwork
$C_2$ = Coefficient dependent on the constituents of concrete
$D$ = Density of the concrete
$H$ = vertical height of the form
$h$ = vertical pour height
$K$ = temperature coefficient = $\left(\frac{36}{T+16}\right)^2$
$R$ = rate at which the concrete rises vertically up the form
$T$ = concrete temperature at placement

Lings et al. (1993a) supported the design approach proposed, with a reservation that the approach will err towards under-prediction in some cases at greater depths. Ng (1993) measured lateral stresses over the depth of a diaphragm wall installed in Gault clay, in Cambridge. During construction the trench was supported by a bentonite slurry suspension. He proposed that once a critical depth of concrete had been poured, any further increase in lateral stress would equal the density of the bentonite multiplied by the increase in poured depth. This was because the bentonite acted as a surcharge that should be added to the lateral pressure at and below the critical depth. He proposed the relationship:

$$\begin{aligned} \sigma_h &= \gamma_c z && \text{for } z \le h_{crit} \\ \sigma_h &= \gamma_b z + (\gamma_c - \gamma_b) h_{crit} && \text{for } z > h_{crit} \end{aligned} \qquad (2.21)$$

This is shown in figure 2.9.

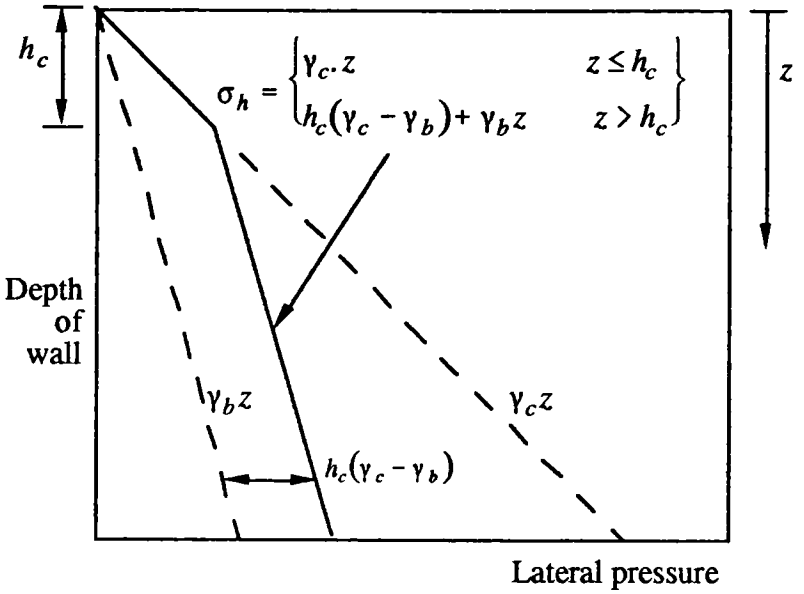


Figure 2.9 *Ng's bilinear distribution (Ng, 1993)*

The bilinear approach proposed by Ng (1993) supports the formulation of a critical depth below which the increase in lateral pressure is controlled by factors other than the unit weight of the fresh concrete. From data recorded in Cambridge and the data presented above (Uriel & Oteo, 1977; Dibiagio and Roti, 1972 etc) Ng (1993) proposed that, for design purposes the critical depth should be equal to one third of the depth of the trench.

### *2.6.3 Appropriate curve fitting*

Current methods of predicting the lateral stress imposed during concrete placement in a trench or diaphragm wall are essentially empirical. Whilst these relationships may provide an adequate basis for design, they leave many questions unanswered. Current proposals may lead to problems when design situations are encountered that are dissimilar to those previously investigated.

A more appropriate model for the lateral stress versus depth profile adopts the process of consolidation as a basis for understanding the mechanisms that control the lateral pressure distribution during and after concrete placement.

The concrete is tremie-piped to the bottom of the trench and bleed water is forced into the surrounding soil and up to the surface of the concrete, leading to a decrease in void volume in the concrete under load. If the concrete is treated as a saturated soil, the resulting change in void ratio over a period of time may be treated as a process of consolidation and as the void ratio decreases, the skeletal matrix of aggregate will provide support for the overlying mass of concrete.

Load is applied by the surcharge of bentonite and/or the weight of the overlying concrete, and the aggregate will form a skeletal matrix with hydrating cement-saturated pores. Excess pore pressure will dissipate from initial ($t = 0$) values equal to the full hydrostatic pressure of the concrete. In the analyses performed in this dissertation, the concrete is assumed to remain in a fluid state and the pores of the aggregates are assumed to remain saturated with cement paste. At $t = \infty$ the excess pore water pressure will have completely dissipated and the pore pressure on the sides of the trench will equal the hydrostatic pressure of the pore fluid. Therefore lateral effective stresses will have fallen to the active lateral pressure of the aggregate.

The conventional consolidation relationship proposed by Terzaghi (1943) takes no account of the changes in permeability or compressibility as a load increment is applied to the concrete. Gibson, England and Hussey (1967) proposed a correction to the relationship proposed by Terzaghi (1943) from which a series of isochrones can be formulated that define the profile of pore water pressure against depth at any time after the start of consolidation. They proposed that the average degree of consolidation is given by

$$\overline{U} = 1 - \frac{8}{\pi^2} \sum_{n=0}^{\infty} \frac{1}{(2n+1)^2} \exp\left[-(2n+1)^2 \pi^2 T_0\right] \tag{2.22}$$

where $$T_0 = \frac{C_T t}{h^2(0)} \tag{2.23}$$

and h = height of the increment of soil.

$C_F$ is a correction to the coefficient of consolidation, $c_v$, which was proposed by Gibson et al. (1967) to allow for a uniform change in void ratio that occurs whilst load is applied during the specified time increment. To account for changes in void ratio

$$C_F = \frac{(1+e_0)c_v}{(1+e)} \tag{2.24}$$

where $e_0$ is the void ratio at the start of consolidation, $e$ is the void ratio at a time $t$ thereafter

and $$c_v = \frac{k}{(\gamma_w . m_v)} \tag{2.25}$$

In equation 2.25 $k$ is the permeability of the fresh wet concrete, $\gamma_w$ is density of water

and $$m_v = \frac{\eta_0 - \eta_1}{p_1 - p_0} \tag{2.26}$$

In equation 2.26 $\eta_0$ is the initial porosity and $p_0$ is the initial applied stress and $\eta_1$ and $p_1$ are the porosity and applied stress at end of a time increment.

Diaphragm wall concretes must have a high plasticity and slump. This aids placement and minimises the risk of air pockets occurring in the trench. Typically, the concrete will have a water to cement ratio of 0.4 and a void ratio of approximately 0.4. Data from RMC (Ready Mix Concrete) are given in table 2.1 (Cook, 1994). During consolidation the cement powder was assumed to remain, unset, in solution, and was therefore treated as part of the liquid phase of the concrete.

C35, min 400, 20PC, 175 Slump

| | Sand | 10mm AGG | 20mm AGG | Cement | Water |
|---|---|---|---|---|---|
| mass (kg) | 650 | 330 | 765 | 405 | 166 |
| SG | 2.65 | 2.6 | 2.6 | 3.15 | 1 |

Super placticiser P4 (1134ml)

Permeability, $k = 2 \times 10^{-6}$ m/s (Neville, 1990)

Table 2.1. *Values used for consolidation analysis (Cook, 1994).*

The void ratio for the concrete was be defined for a particular load from

$$e_o = \frac{\frac{m_w}{G_w} + \frac{m_c}{G_c}}{\frac{m_s}{G_s} + \frac{m_{10A}}{G_{10A}} + \frac{m_{20A}}{G_{20A}}} = 0.4364 \qquad (2.27)$$

$$e = e_o - \lambda_o \ln(\sigma'_v) \qquad (2.28)$$

$\lambda_o$ may be calculated knowing that

$$\frac{K'}{p'} = \frac{v}{\lambda_o} \qquad (2.29)$$

in first compression and assuming $\frac{G}{p'} = 80$ and $\nu' = 0.2$ (Neville, 1990), from

$$K' = \frac{2G(1+\nu')}{3(1-2\nu')} \qquad (2.30)$$

$$G = \frac{3K'}{4} \rightarrow \frac{3K'}{4p'} = 80 \qquad (2.31)$$

$$\frac{K'}{p'} = \frac{v}{\lambda_o} = \frac{1+e}{\lambda_o} = \frac{320}{3} \qquad (2.32)$$

$$e_o = 0.4364 \; ; \; \lambda_o = 0.013466$$

These data are presented graphically in figure 2.10 below

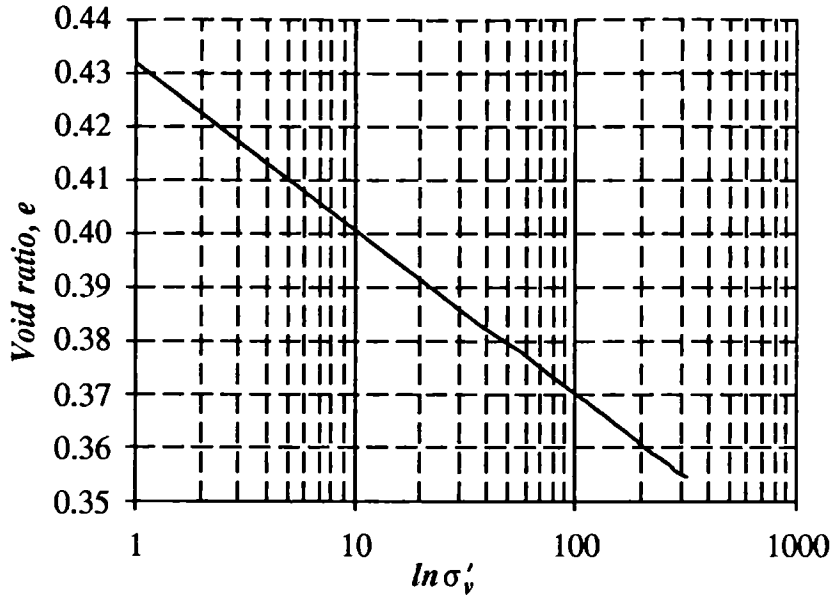


Figure 2.10 $e = e_o - \lambda_o \ln \sigma'_v$ *relationship for fresh-wet concrete*

Consolidation was considered for two cases. First, a worst case was considered where the concrete is poured infinitely quickly, in one pour. The second case adopts a series of pours that consolidated for a specified length of time to approximate actual site conditions.

### *2.6.4 One pour concrete placement*

Full hydrostatic pressures dissipate over time, with levels at a full depth of 18.5m changing from 444 kPa at $t = 0$ to 259 kPa at $t = 1000$ minutes.

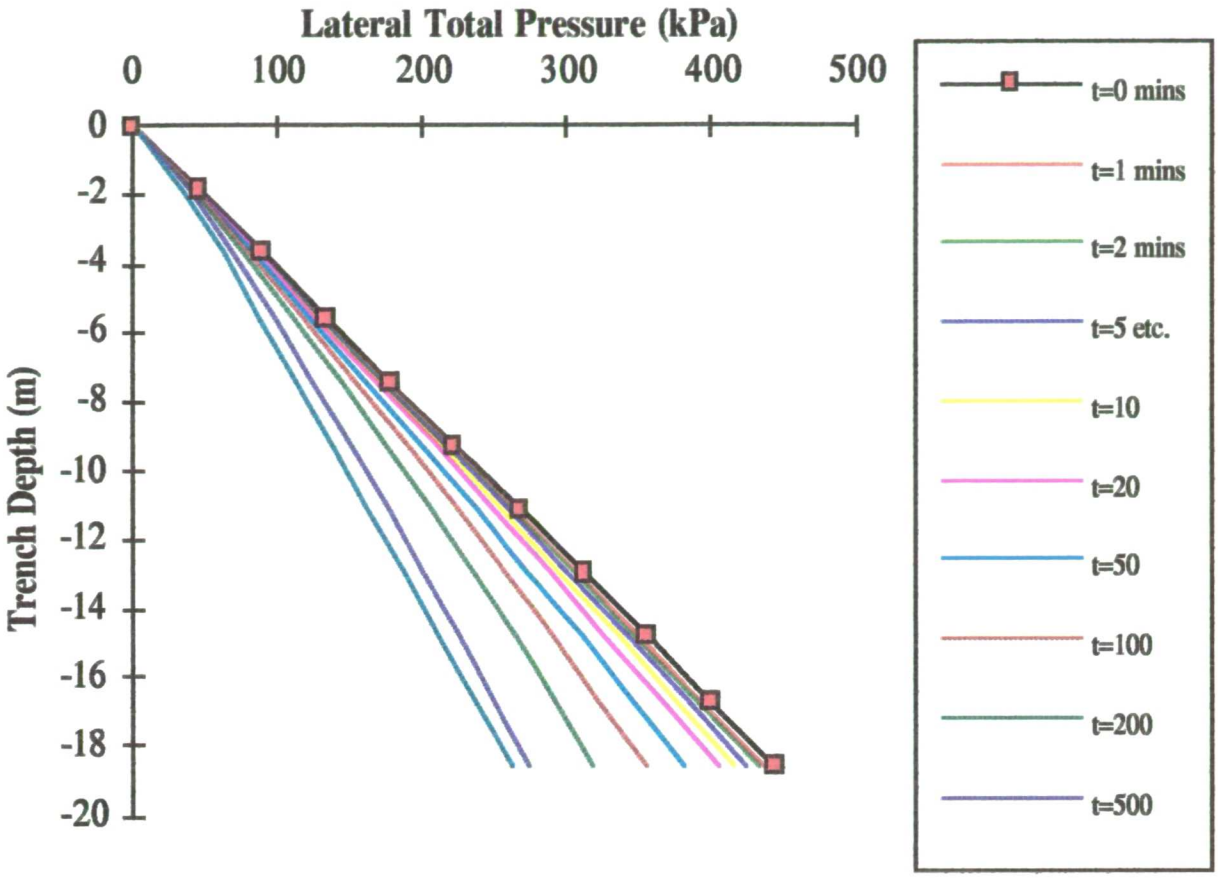


Figure 2.11 *One lift analysis. Worst case scenario (time in minutes).*

The cement paste was assumed to remain in a fluid state throughout the analysis so consolidation was due purely to the aggregate forming a consolidated matrix under load with a fraction, $K_a$, of the vertical load transmitted laterally. The excess pore water pressure dissipated from a maximum value of

$$\bar{u} = (\gamma_c - \gamma_w)z \quad \text{to} \quad 0. \tag{2.33}$$

From simple definitions

$$\sigma_v = \gamma_c z \tag{2.34}$$

$$u = \gamma_w z + \bar{u} \tag{2.35}$$

$$\sigma_v' = (\gamma_c z - \gamma_w z) - \bar{u} \tag{2.36}$$

$$\sigma_h' = K_a\left[(\gamma_c - \gamma_w)z - \bar{u}\right] \tag{2.37}$$

The total lateral pressure transmitted to the sides of the trench was

$$\sigma_h = K_a\left[(\gamma_c - \gamma_w)z - \bar{u}\right] + \gamma_w z + \bar{u} \qquad (2.38)$$

The gain in strength in the cement paste will accelerate the rate of reduction of total lateral stress. As the concrete sets the size of the cement particles increases and the skeletal matrix becomes stronger. Cement particles will absorb free water and will eventually exhibit negative pore pressures as the concrete hardens and an ever decreasing fraction of the vertical load is transmitted laterally. The full analysis, if cement hydration effects were considered, would be far more complicated than the analysis considered, applying smaller lateral pressure over time.

### *2.6.5 Multi pour case*

An ideal analysis would involve the consolidation of thin strips of concrete for short periods of time, representing the rate of fill of the trench. This ideal scenario is approximated by considering 10 equal pours each of 1.85m depth to give a total trench depth that was the same as was used in the centrifuge tests.

The analysis assumed that the deepest 1.85m segment was placed instantaneously at the start. A surcharge equal to 16.65m of bentonite was applied to the surface of this segment of the concrete which was then allowed to consolidate for 40 minutes. The second 1.85m segment was then placed. A reduced surcharge (equal to 14.8m of bentonite slurry) was applied to the concrete at the bentonite/concrete interface. The initial lateral pressure at the bottom of the trench (for this new segment) was the consolidated lateral pressure from the last increment plus the increase in pressure due to the difference between the self weight of 1.85m of concrete and 1.85m of bentonite. Consolidation for a further 40 minutes was then calculated before another segment of concrete was placed.

A total pour time of 400 minutes was adopted. This represented a rate of pour of approximately $14m^3$ per hour, which is well within realistic limits (Cook, 1994). The permeability of concrete immediately after pour for an Ordinary Portland Cement is given by Neville (1990) as approximately $10^{-6}$m/s. After 24 hours, permeability varies considerably depending on moisture content and the cement powder used. A value of between $10^{-9}$ and $10^{-11}$m/s has been suggested by Neville (1990).

At different times between pour and 24 hours the permeability of the concrete will vary considerably. For the purposes of the consolidation analysis constant a value of $10^{-7}$ m/s was adopted as a compromise between the initial and final values.

Initial set occurs in an ordinary Portland or rapid-hardening cement (BS 12) at least 45 minutes after the mix water is added. The placement time for each panel was assumed to be 40 minutes, slightly less than the time for initial set. Final set occurs at least 2 hours after initial set, Neville (1990). After final set the cement will start to harden i.e. gain strength, and permeability will be reduced further. The analysis assumes that permeability and gel strengths will remain constant for the entire 400 minutes, which will tend to over-estimate values of lateral earth pressure.

The analysis was based on ten equal pours of 1.85m to give a total trench height of 18.5 m - the same as the trench depth considered in the centrifuge tests.

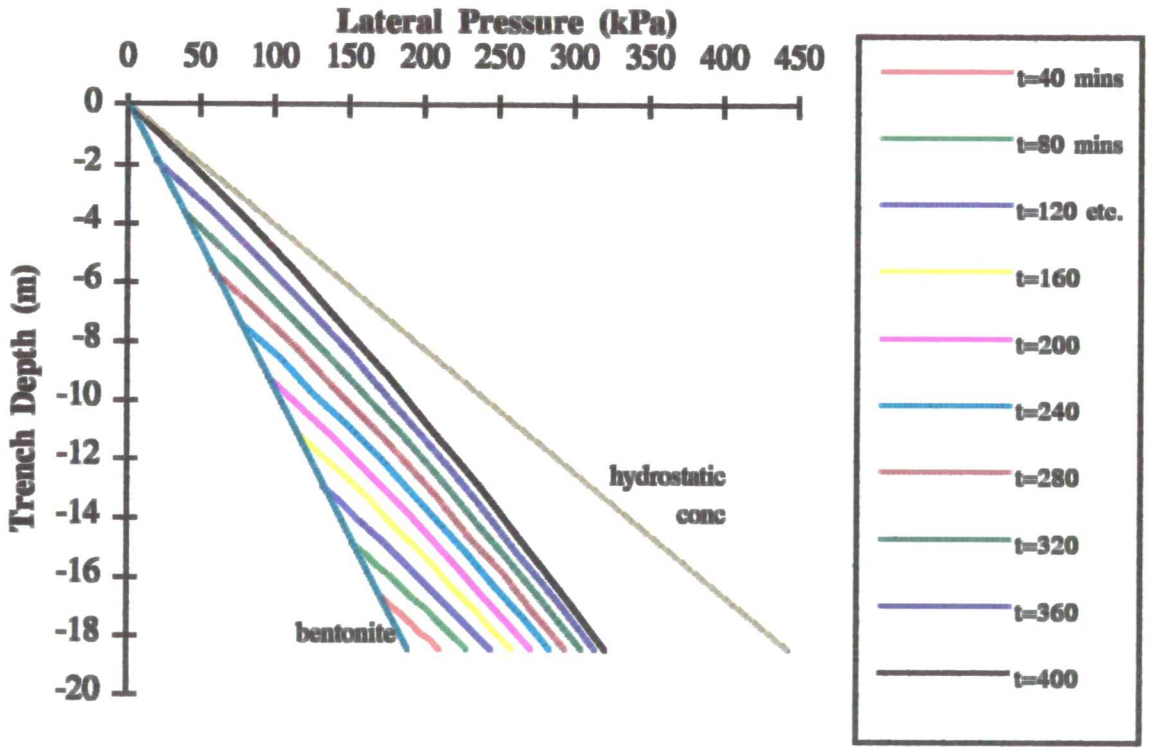


**Figure 2.12** ***Consolidation analysis considering 10 lifts of 1.85 m***

By comparing the two scenarios adopted, the rate of pour will have a very great effect in the lateral pressure applied to the sides of the trench.

Data from research by Dibiagio and Roti (1972) gives a comparison (in figure 2.13) with the results from the multi-pour consolidation analysis. The values recorded by Dibiagio and Roti at depths of 3 and 6m are greater than the hydrostatic pressure of fluid concrete, which would tend to suggest that some data recording errors have occurred. At greater depths, the concrete may have been poured very much more slowly than assumed in the consolidation analysis as the values presented by Dibiagio and Roti (1972) are generally smaller, suggesting that a greater degree of consolidation and/or set had occurred during pour.

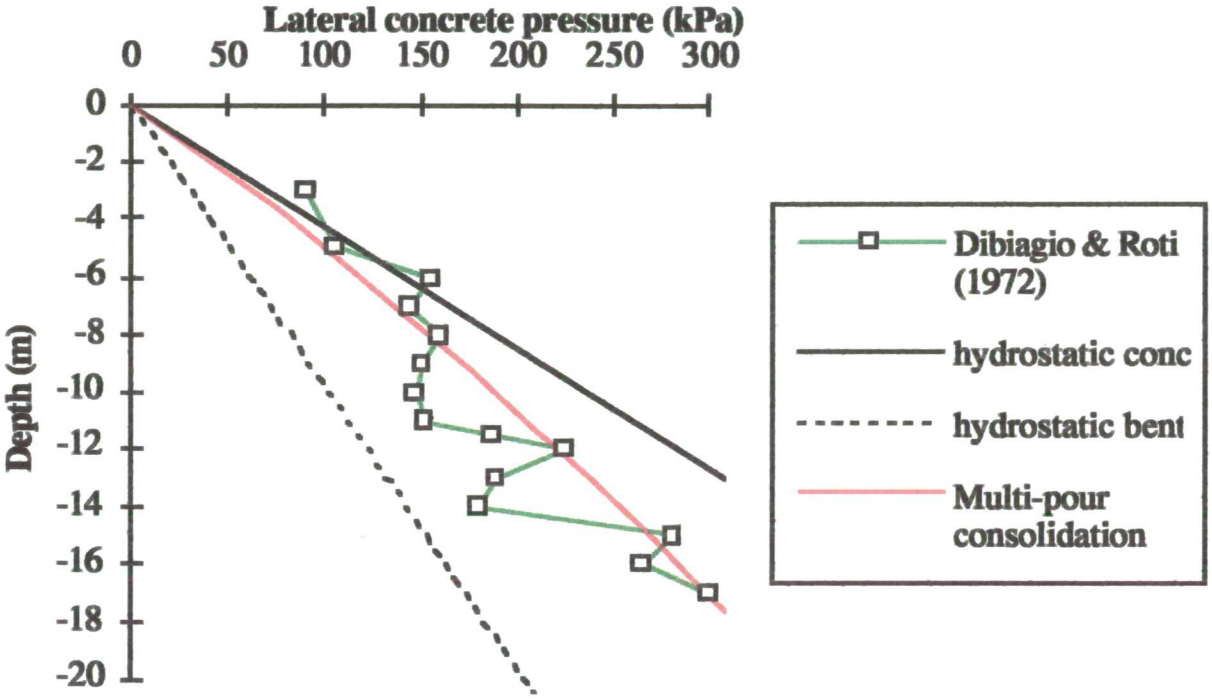


Figure 2.13 *Comparison of consolidation analysis with Dibiagio and Roti data (1972)*

Uriel and Oteo (1977) recorded values of lateral stress directly after and 24 hours after placement. Figure 2.14 shows a comparison between their data and the consolidation analysis. The consolidation curve for t=0 was generated using the multi-pour analysis described above and then consolidated for 24 hours to give the second curve. Ng's (1993) approximation was partly based on the Uriel & Oteo (1977) data and is also presented in figure 2.14. The full depth of the trench was 30m, and so Ng's suggested critical depth is presented at 10m.

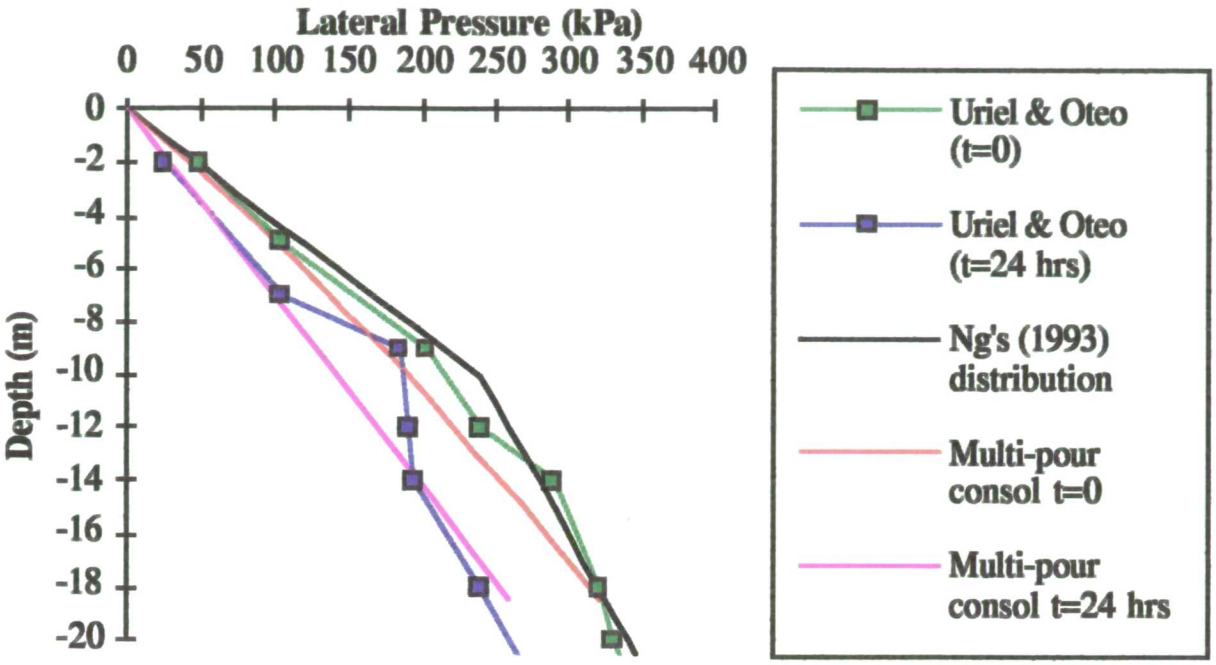


Figure 2.14 *Comparison with data by Uriel and Oteo (1977) and Ng (1993)*

Uriel and Oteo's results suggest that the concrete may have been placed more quickly than assumed in the consolidation analysis presented above, as the concrete pressures recorded at mid trench are generally slightly greater than the theoretical, calculated values. Overall, however, the consolidation analysis presents a remarkably close correlation with recorded values.

## *2.7 Conclusions*

The different methods of diaphragm wall installation will have a significant effect on the lateral stress in the soil during construction. Panel construction using slurry trench walls will cause significant reductions in lateral stress, which will be off set in part by bentonite slurry pumped into the trench during excavation.

Bentonite is a complex clay colloidally suspended but prone to calcium contamination which greatly reduces its thixotropic gel strengths and trench stabilising properties. Various treatment methods are available to enable the bentonite to be re-used.

The consolidation analysis offers a simple and accurate method for predicting not only the maximum lateral pressures exerted immediately after placement, but the pressures at times afterwards. The analysis represents the correct technique for

quantifying the lateral stresses applied to the sides of the trench, but a further understanding of the permeabilities of fresh wet concrete is necessary for the more accurate prediction of applied lateral stresses.

# *Chapter 3*

# *Design of the centrifuge model*

## *3.1 Introduction*

The earliest known geotechnical centrifuge was built by Pokrovsky over 50 years ago. The centrifuge modelling technique was slowly established over the next five decades with the most significant advances occuring in the last 15 years, particularly as centrifuges became more commonly available for research use and advances in computer logging enabled multi-channel data retrieval. The technique has been extensively developed all over the world and has been used to investigate both simple static consolidation problems and complex dynamic events such as earthquake loading and deep sea pile installations.

This thesis presents results from a 1:100 scale centrifuge model, spun at 100 gravities for approximately 2 hours prior to wall installation and for up to 17 hours afterwards. Total stresses, pore water pressures and ground settlements were recorded throughout each test, using three different types of transducer that were all pre-calibrated and installed in the required positions prior to starting of operation.

Complex apparatus was built to model the installation stages of the diaphragm wall. Much of this is discussed by Kantartzi (1994). However certain modifications were required for the current tests, in order to model different initial in situ earth pressure coefficients and different boundary conditions.

Chapter 3 is split into four further sections:

First, the preparation of the overconsolidated kaolin sample is presented in some detail, explaining any assumptions made.

In section 3.3, the centrifuge testing technique is examined. The relative merits of scale models are discussed and the scaling laws are presented.

In section 3.4 detailed drawings and photographs are used to illustrate the centrifuge strongbox arrangement and the modifications that were made for the different tests.

In the final section (3.5), the installation and calibration procedures of the different transducers used in the model are discussed.

## *3.2 Sample preparation.*

Speswhite kaolin was mixed from a powder under a partial vacuum, with de-aired, de-ionised water, to form a slurry of 95 % moisture content. Kaolin was chosen as it has (for a clay) a reasonably high permeablility (Al-Tabbaa, 1987), reducing equilibration time after spin-up in the centrifuge. Also it exhibits the features common to overconsolidated clays, ie. high small strain stiffness and high angles of shear resistance on initial monotonic swelling (Burland and Fourie, 1985).

Once mixed, the sample was placed into the strongbox where it was compressed using a jack and loading frame to a vertical effective stress of 1250 kPa over a period of about 10 days and then allowed to swell back to approximately 80 kPa over a period of about 2 weeks. Using values of $\phi'_{crit} = 22^{\circ}$, $\lambda = 0.187$ and $\kappa = 0.02$ (Al-Tabbaa, 1987) and assuming $K_{onc} = (1\text{-}\sin\phi')$ and $K_{ooc} = (1\text{-}\sin\phi')OCR^{\sin\phi'}$ (Mayne and Kulhawy, 1982) the state path in $v$ - $\ln p'$ space for the kaolin block during sample preparation is shown in figure 3.1 (as discussed in chapter 2).

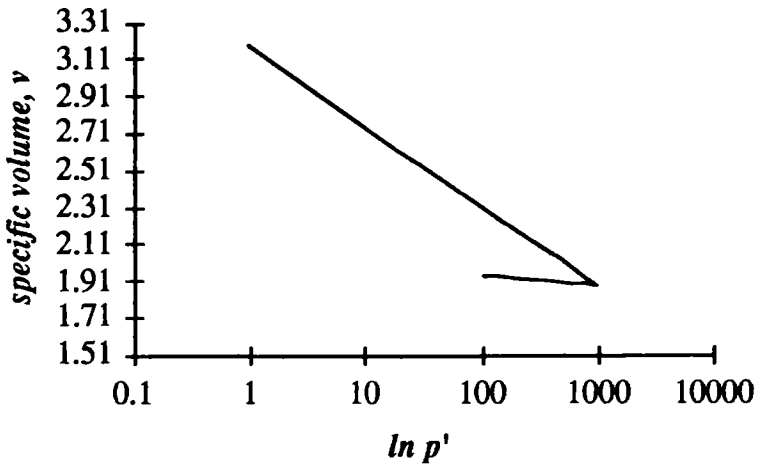


Figure 3.1 *v - lnp' graph for one-dimensional loading and unloading of kaolin prior to the use in the centrifuge model.*

Water was ejected from the sample during initial compression and absorbed during unloading, when care was taken to keep the top of the sample and the base drain fully saturated. The sample was then removed from the press, and one side of the strongbox was taken away so that the sample could be trimmed to the required size. The dimensions of the sample after it had been trimmed are shown in figure 3.2.

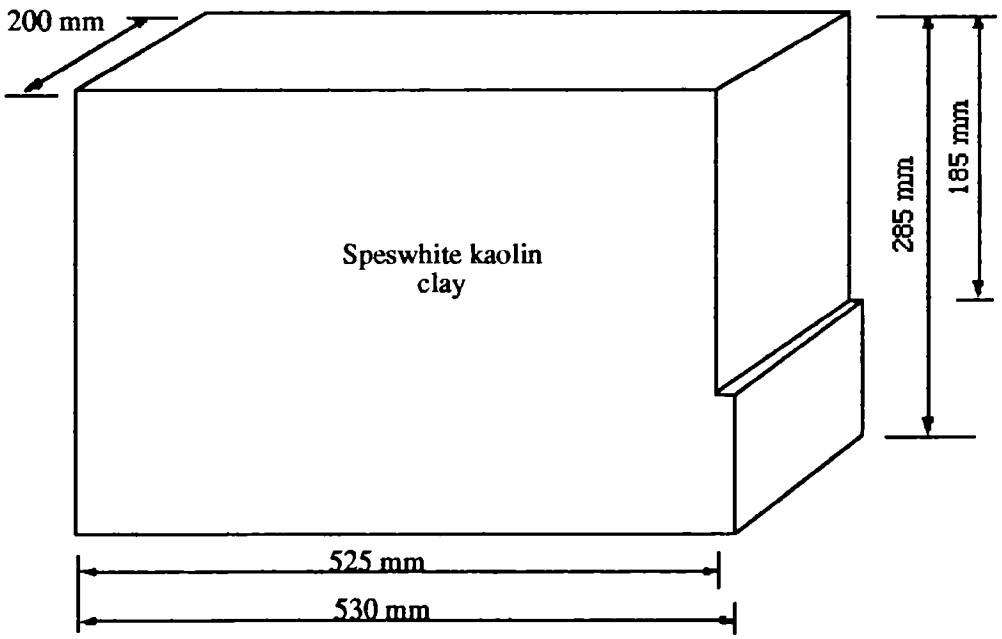


Figure 3.2 *Speswhite kaolin block*

A 5mm wide, 185mm deep, trench was cut from one end of the block where the installation of a diaphragm wall was to be simulated. A rubber bag filled to different heights above original ground level, with fluids of different densities, was used to simulate different in situ conditions prior to the start of excavation. During

excavation the fluid was drained down to ground level (to simulate excavation under bentonite slurry) before a quick setting plaster mixture was dumped into the trench, to form the diaphragm wall panel.

The model was assumed to be symmetrical about the trench centreline and therefore only half of the trench was modelled. The unit weight of the sample was found to be between 17.5 and 17.8 $kN/m^3$ for the seven tests presented in this dissertation.

## *3.3 Centrifuge testing techniques*

A centrifuge model at $1/n$ scale, tested at n gravities has two distinct advantages over prototype tests at Earth's gravity:

First, the tests may be constructed and modified relatively easily and inexpensively.

Secondly, consolidation effects due to the dissipation of transient porewater pressures are accelerated by $n^2$ (based on the assumptions enumerated in section 3.3.1). A large number of tests may therefore be carried out in a relatively short period of time.

Centrifuge testing is based on the premise that an increase in self-weight by a factor of $n$ (at $n$ gravities) will result in there being no material difference between the prototype and centrifuge model behaviour provided that a $1/n$ scale is adopted throughout the centrifuge model. This is not always the case and so compromises are sometimes made. For example, many soils behave consistently at 1 and $n$ gravities with differences such as grain size having very little effect. It is only in extreme cases (where, for example, the grain size is a significant proportion of the structure size) that abnormal behaviour occurs. However, if centrifuge tests are to realistically model prototype conditions then there are several scaling considerations to which attention must be given.

### *3.3.1 Scaling considerations for time dependent variables.*

a) Consolidation

$$\text{The time factor, } T_v = \frac{C_v t}{H^2} \qquad (3.1)$$

where $H$ = length of dissipation path

and $H_p = nH_m$,

Equation (3.1) defines the time nessesary for excess pore water pressures to dissipate for a soil with a particular dimensionless coefficient of consolidation, $C_v$. For similitude of modelling $T_{vp} = T_{vm}$ and therefore

$$\frac{C_{vp}t_p}{H_p^2} = \frac{C_{vm}t_m}{H_m^2} \qquad (3.2)$$

If prototype soil is used in the model then $C_{vp} = C_{vm}$ and it is possible to investigate any effects of consolidation $n^2$ times faster in the model than at prototype scale.

b) Seepage

The seepage velocity may be calculated using Darcy's Law,

$$v = ki \quad \text{where } i = \frac{\Delta h}{\Delta s} \qquad (3.3)$$

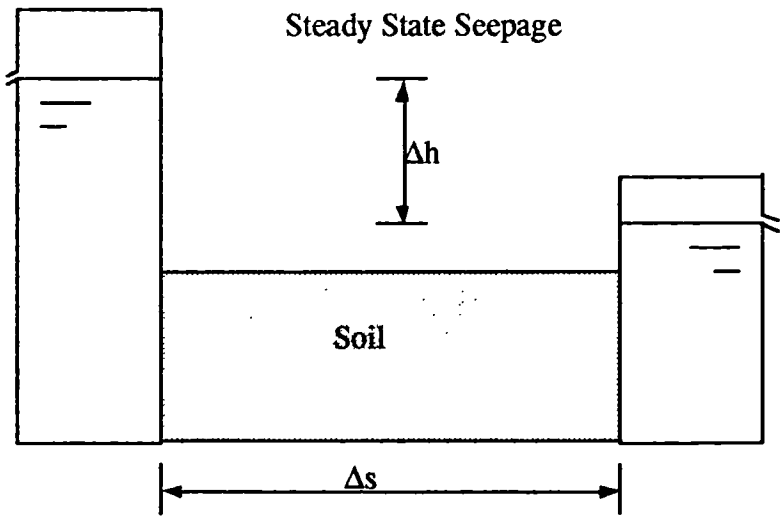


Figure 3.3 *Steady state seepage*

Although $s$ and $h$ are linear dimensions it is only convenience that standpipes are used. The head difference should not be treated as a linear dimension - the hydraulic gradient is a measure of pressure gradient it is just that the pressure loss is defined in terms of a linear dimension. Based on this assumption, if the acceleration field acting across the model increases, the measured pressure drop across the sample also increases and so the hydraulic gradient in the model becomes $n$ times that in the prototype:

$$i_m = ni_p \tag{3.4}$$

$$v_m = nv_p \text{ if } k_m = k_p \tag{3.5}$$

and as Time = distance/velocity (3.6)

$$t_m = \frac{L_m}{v_m} = \frac{L_p}{n.nv_p} \tag{3.7}$$

and so $$t_m = \frac{t_p}{n^2} \tag{3.8}$$

for the seepage velocity.

### *3.3.2 Effective radii*

The figure below demonstrates that different positions in the centrifuge model are at different radii.

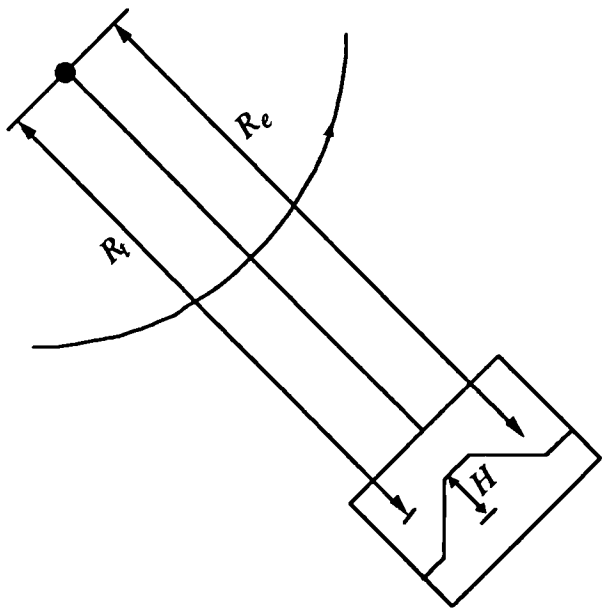


Figure 3.4 *Centrifuge model showing different radii*

$R_t$ = Radius at the top of the model

$R_e$ = Effective radius (at the centre of mass of the model)

$R\omega^2$ = Centrifugal acceleration

Across the sample the inertial acceleration changes because the gravity level throughout the sample is not constant. In order to minimise the error due to this variation it is necessary to determine the effective radius of the model. The inertial acceleration of the centrifuge gives a parabolic stress distribution in the model whilst at protype scale, the self weight stresses have a linear distribution as shown in figure 3.5.

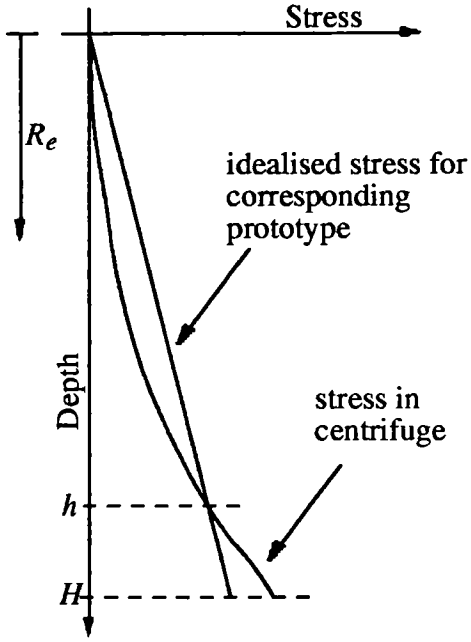


Figure 3.5 *Comparison of stress distributions*

A coincidence of stresses at a depth $h$ gives a similar understress at the surface of the model and an overstress at the base of the model. If $z$ is taken as the depth of a point below the surface of the model, at any depth, $z$

$$\sigma_{vm} = \int_0^z \rho\omega^2(R_t + z)dz \qquad (3.9)$$

$$\sigma_{vm} = \rho\omega^2 z\left(R_t + \frac{z}{2}\right) \qquad (3.10)$$

when $z = h$

$$\sigma_{vp} = nh\rho g = \rho\omega^2 h\left(R_t + \frac{h}{2}\right) \tag{3.11}$$

and for $n$ calculated at radius $R_e$

$$\omega^2 R_e = ng \tag{3.12}$$

$$R_e = R_t + \left(\frac{h}{2}\right) \tag{3.13}$$

which from the graph is halfway between the top and the depth $h$ at which the stresses coincide.

By looking at the ratios of understress at a depth $h/2$ (maximum understress) and overstress at a depth $H$ (maximum overstress) to the corresponding prototype stresses we can equate and calculate the optimum $R_e$.

$$1)\ R = \frac{\text{Understress at depth } h/2}{\text{Prototype stress at } h/2} = \frac{n\frac{h}{2}\rho g - \rho\omega^2\frac{h}{2}\left(R_e - \frac{h}{2} + \frac{h}{4}\right)}{n\frac{h}{2}\rho g} = \frac{h}{4R_e} \tag{3.14}$$

$$2)\ R = \frac{\text{Overstress at depth } H}{\text{Prototype stress at } H} = \frac{H-h}{2R_e} \tag{3.15}$$

Equating the ratios from equations 1 and 2 gives $h = (2/3)H$; that is $R_e$ should be at one third of the depth of the model. Using the value for $R_e$ it is now possible to calculate the angular velocity for a specific acceleration. The overstress error at a depth $H$ is $H/6R_e$ so that only tall models on shorter radius centrifuges will cause error readings of any significance. The maximum overstress/understress error in the model considered in this dissertation, with the effective centrifuge radius $R_e$ of approximately 1.6m and a model height $H$ of 300 mm, is less than 2%.

### *3.3.3 Coriolis error*

The Coriolis acceleration is defined as

$$a_c = 2\left(\frac{dr}{dt}\right)\left(\frac{d\theta}{dt}\right) \tag{3.16}$$

The Coriolis *error* is generally expressed as (Oveson, 1990),

$$\frac{a_c}{a} = \frac{2\left(\frac{dr}{dt}\right)\left(\frac{d\theta}{dt}\right)}{r\left(\frac{d\theta}{dt}\right)^2} = \frac{2\left(\frac{dr}{dt}\right)}{r\left(\frac{d\theta}{dt}\right)} \tag{3.17}$$

i.e. as a fraction or (more usually) a percentage of the centrifugal acceleration. The error due to the velocity of particles moving perpendicular to the axis of rotation is given as a fraction of angular velocity (as both the numerator and denominator are divided through by the angular velocity of the centrifuge). According to some researchers (Oveson, 1990; Kantartzi, 1994) the error is manifest by a slumping into the direction of rotation where the radius of the moving particles increases, and a rising away from the direction of rotation where the radius decreases, as shown in figure 3.6.

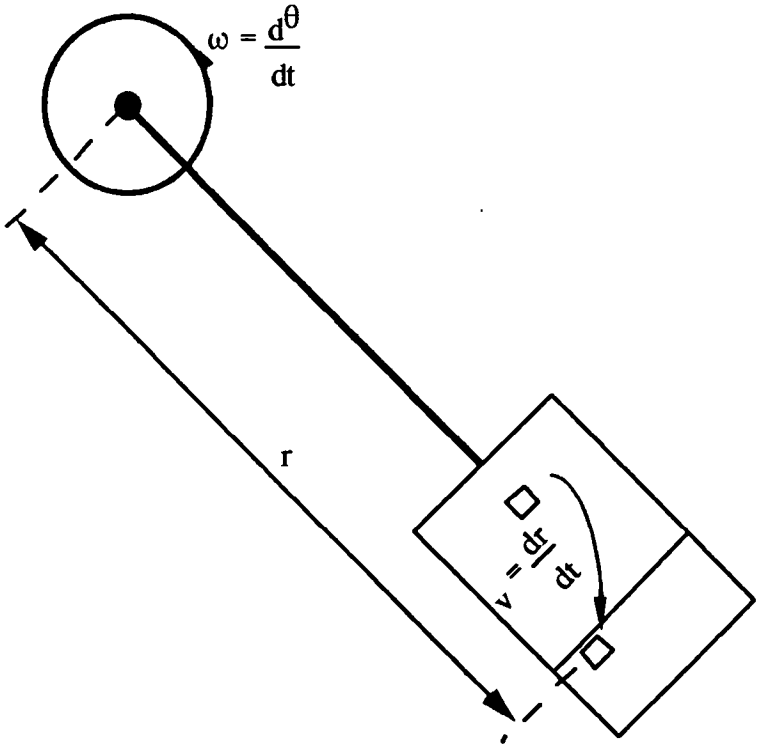


Figure 3.6 *Coriolis error terms*

From the term used to define the error, it is implied that the greatest errors occur where the moving particles are moving at higher speeds. However, the greatest movements into (or away from) the direction of rotation occur at *low* velocities perpendicular to the axis of rotation, as indicated below.

The in plane movements may also be defined using equations of motion to calculate the movement across the face of the model ($\Delta s$) as particles move in a direction perpendicular to the axis of rotation ($\Delta r$).

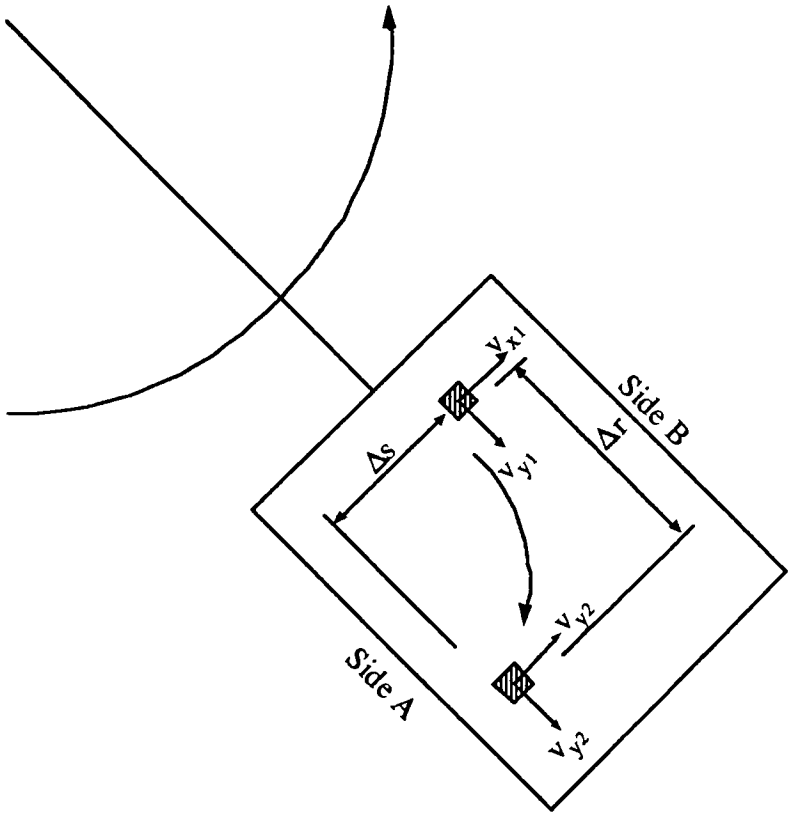


Figure 3.7 *Particle movement perpendicular to the axis of rotation.*

The closer particles are to the axis of rotation, the slower their tangential velocity and so at different depths in the model, particles will have different velocities, as shown in figure 3.7. As the particles with velocity $v_{x1}$ fall through a distance $\Delta r$ they will drift towards side A through a horizontal distance $\Delta s$ where the tangential velocity is greater. During the concreting phase in the centrifuge test, powder is dropped through a height of 200mm. The radius at ground level at the top of the model is 1.46m and at the bottom of the hopper it is 1.26m. The calculated difference in velocities ($\Delta v_x$) at the different model heights is 5.024m/s. After the hopper was opened the simulated concrete mixture fell into the trench in 0.2 seconds (reaching a terminal velocity, $v_{y2}$ = 19.8m/s).

The drift towards side A was found to be 100mm which was considered to be excessive (as it represented half of the width of the trench) 110mm baffles were therefore installed below the hopper to prevent drift during the first half of the fall as shown in figure 3.8.

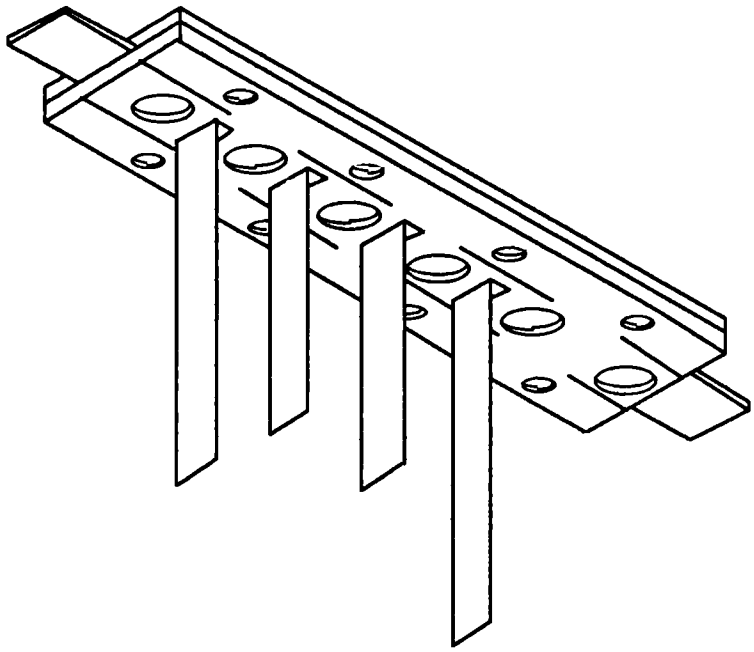

Figure 3.8 *Baffles arrangement viewed from underside.*

## *3.4 Centrifuge model layout and strongbox modifications.*

### *3.4.1 Centrifuge model layout.*

Figure 3.9 below shows a simple schematic diagram of the full width rubber bag installed in the trench. Two different bag lengths were used; a shorter bag (with an upstand level 90mm above the surface of the model) was used in test 1. The strongbox was then modified and a second, taller, bag was adopted (with an upstand of 200 mm). This second bag was used in tests 2, 3, 5, 6 and 7 where the level of fluid was either 140 or 180mm above the ground level of the model. In test 4, the bag was a quarter of the width of the trench, with two, 20mm thick wooden blocks positioned at either side so that the effective half width of the trench remained 5mm (0.5m at prototype scale).

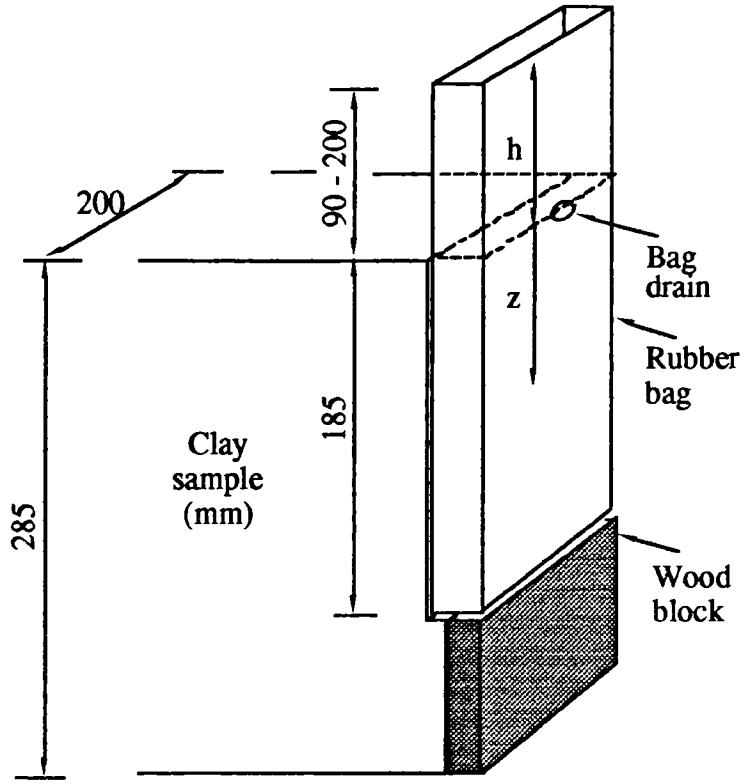


Figure 3.9 *Schematic diagram of the rubber bag in place in the trench*

A rubber bag was used for two principal reasons:

First, it was easier to drain the bag to ground level (thus reducing the stress on the side of the trench) in order to simulate the excavation than it would have been to excavate kaolin at the required position in a realistic time scale.

Secondly, by using different levels of fluid in the bag and by varying the fluid densities it was possible to simulate different initial in situ earth pressure coefficients. This may be explained as follows:

From figure 3.9, at any depth $z$

$$\sigma_h = (h + z)\gamma_b \tag{3.18}$$

$$\sigma'_h = \sigma_h - \gamma_w z = h\gamma_b + z(\gamma_b - \gamma_w) \tag{3.19}$$

$$\sigma_v = \gamma_s z \tag{3.20}$$

$$\sigma_v' = (\gamma_s - \gamma_w)z \tag{3.21}$$

and so $$K_o = \frac{\sigma_h'}{\sigma_v'} = \frac{h\gamma_b + z(\gamma_b - \gamma_w)}{(\gamma_s - \gamma_w)z} \tag{3.22}$$

Different values of $h$ (from 90 to 180mm) and $\gamma_b$ (9.81kN/m$^3$ to 11.5kN/m$^3$) produced different profiles of earth pressure coefficient against depth as shown in figure 3.10.

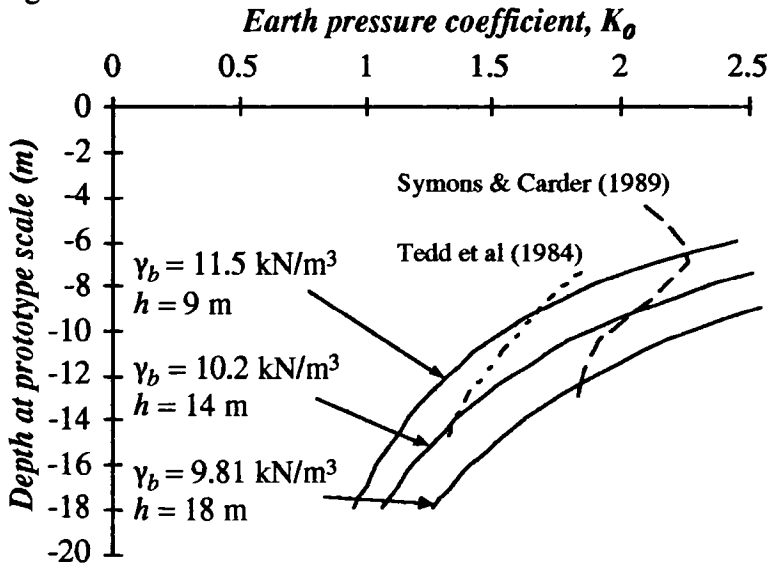


Figure 3.10 *Different earth pressure coefficient profiles*

In the model, values of total stress at the bottom of the rubber bag were approximately equal to the total stress in the soil at the same depth, i.e.

$$\frac{\sigma_{v,trench}}{\sigma_{v,bound}} = \frac{\gamma_b(H+h)}{\gamma_s H} \approx 1 \tag{3.23}$$

where H is the full depth of the diaphragm wall, $\sigma_{vtrench}$ is the total vertical stress at the bottom of the trench in the rubber bag and $\sigma_{vbound}$ is the total vertical stress at a level consistent with the bottom of the trench. In tests 5, 6, and 7 a second rubber bag was installed at the remote end of the strongbox to simulate a stress controlled boundary. The full excess fluid height of 180mm was adopted to give the maximum horizontal pressure on the excavated face furthest from the trench. The stress controlled boundary was installed to see what effect it would have on the wall installation process at the trench end in the strongbox.

### *3.4.2 Strongbox arrangement*

The general arrangement of the centrifuge strongbox and the kaolin sample is shown in figure 3.11. The transducer positions are also marked. A single rubber bag is shown at the trench end, with the wooden block indicated by the heavily shaded area beneath the base of the trench. The arrangement in figure 3.11 was used in the first test where the rubber bag had an upstand of 90mm (9m at prototype scale) above the original ground level of the model.

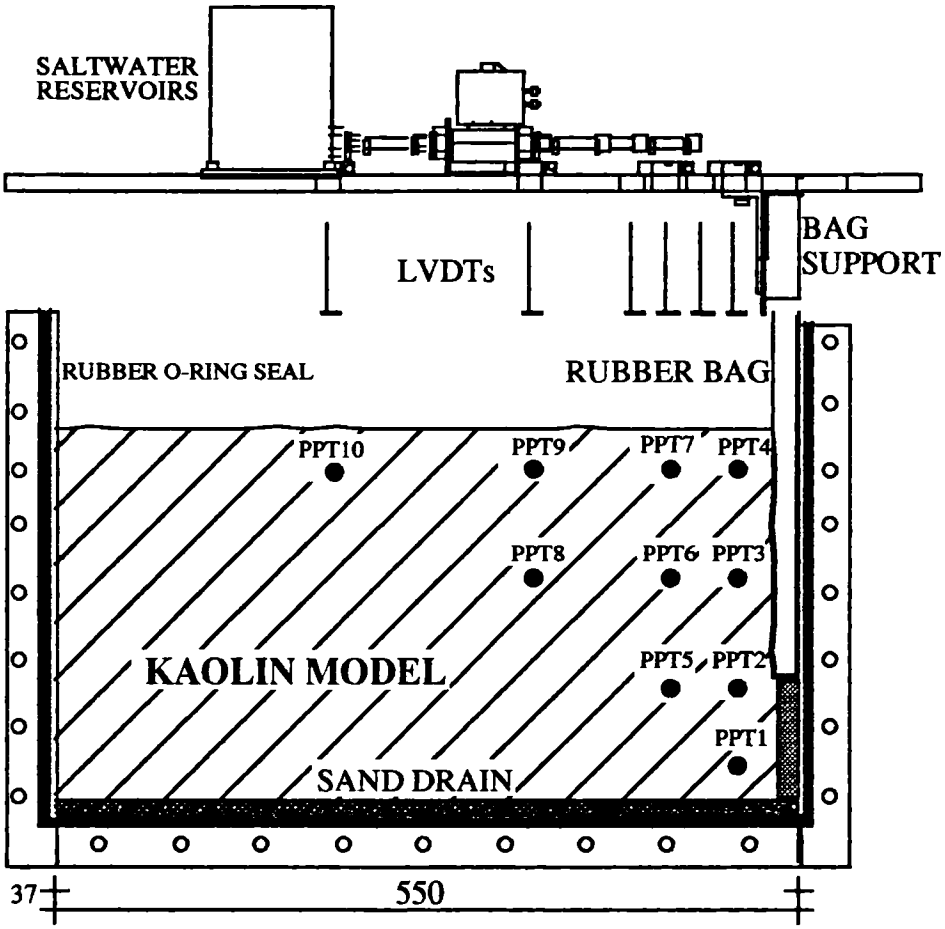


Figure 3.11 *Strongbox general arrangement*

Figure 3.11 shows the arrangement of the linear variable displacement transducers (LVDTs) on the surface of the model and the positions of the different pore water pressure transducers in the body of the model. A further pore water pressure transducer was placed in the bottom of the bag as this provided a measure of the level of fluid in the rubber bag at the different stages of the test. At the same cross-sectional postions as the pore water pressure transducers total stress transducers were also installed. All transducer calibration techniques and installation procedures are fully discussed in section 3.5 and in chapter 4.

The sand drain beneath the soil model and a water feed to the surface of the model maintained a hydrostatic equilibrium pore water profile throughout the depth of the model. A full height ground water level was maintained in all tests, with the sample fully saturated and prevented from drying out by a drip feed to the surface of the model via a standpipe. The drainage layout is shown in figure 3.12.

To prevent the bag from collapsing, a support plate was fixed to the underside of the strongbox lid. The support penetrated the top 5mm of soil to prevent collapse in this region, where horizontal lateral bag pressures were very much greater than horizontal lateral stresses in the soil. For all but test 5, soil collapse was prevented by the bag support to a depth of 5mm, and by the high strengths apparently mobilized by the soil in the region immediately below the bag support.

In other tests, the strongbox was extended to incorporate taller rubber bags. To this end, the upstand was extended by inserting 110mm spacers between the top of the strongbox and the lid. The LVDTs and the bag support plate were also extended.

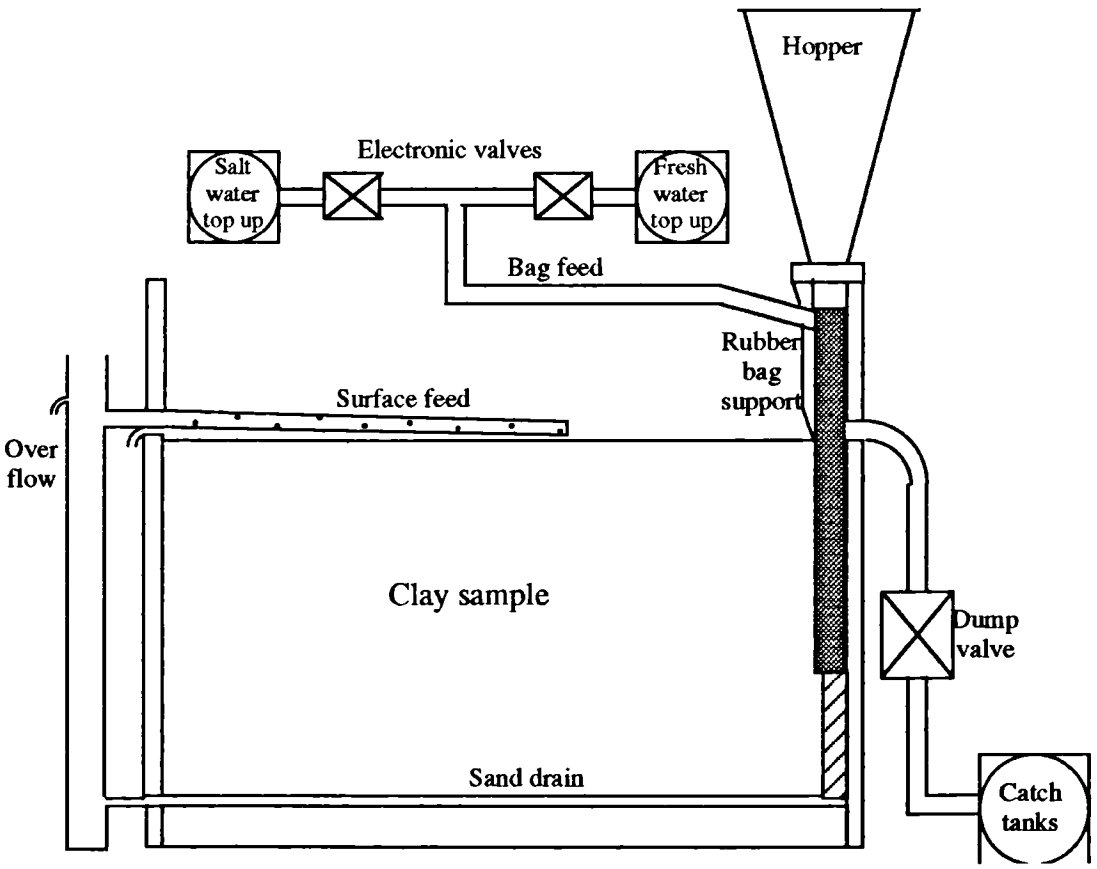


Figure 3.12 *Drainage layout*

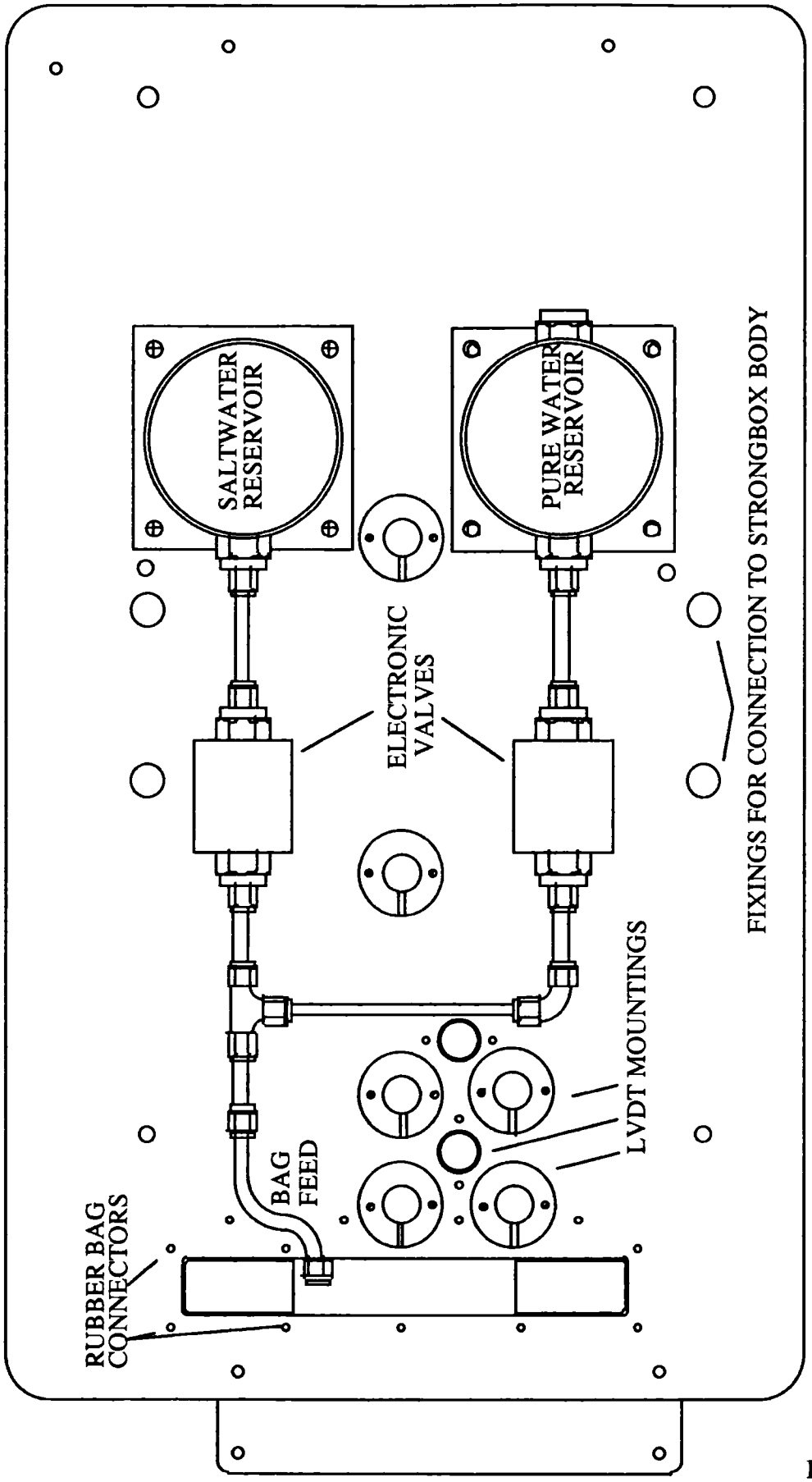
SALTWATER RESERVOIR
PURE WATER RESERVOIR
ELECTRONIC VALVES
FIXINGS FOR CONNECTION TO STRONGBOX BODY
LVDT MOUNTINGS
BAG FEED
RUBBER BAG CONNECTORS

Fig 3.13

Figure 3.13 above shows the lid of the strongbox indicating the two reservoirs. The saltwater reservoir was used to top up the bag prior to excavation. The fresh water reservoir was used to dilute the fluid in the rubber bag (after it had been drained down to ground level) to simulate the excavation stage of the installation process. In tests where a maximum upstand of 180mm of fluid in the rubber bag was adopted, freshwater was used in both reservoirs to compensate for any drop in fluid level during the re-consolidation stage of the test. Solenoid valves were used to control the flow of fluid into the bag.

After the excavation stage, a powdered plaster of Paris mixture was dumped into the trench to simulate the construction of the diaphragm wall. The powder was initially placed into a hopper attached to the strongbox lid above the bag support. Between the lid and the hopper a sliding shutter was used to control the flow of the plaster mixture into the trench. The hopper and dumping mechanism is shown in figure 3.14.

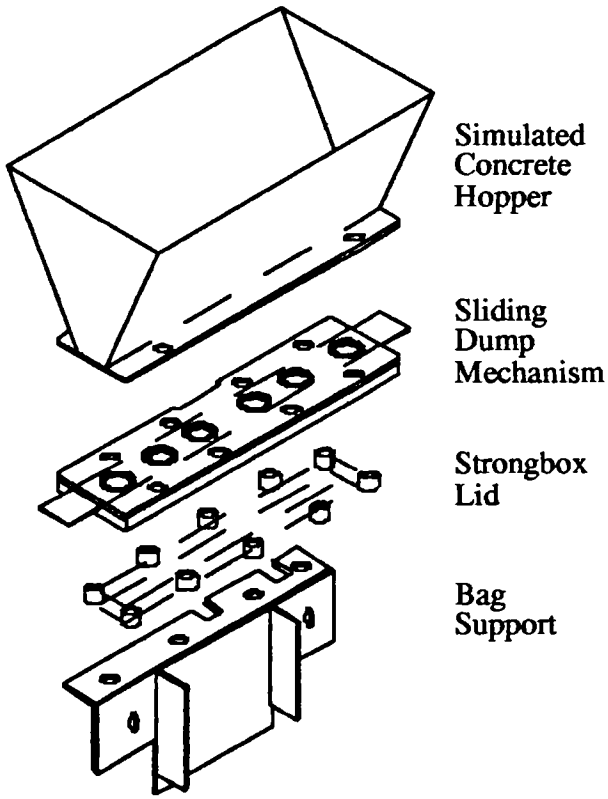


Figure 3.14 *Simulated concrete placement mechanism*

As already mentioned, baffles fitted to the underside of the sliding shutter prevented the concrete powder from drifting during placement. These are not shown in figure 3.14 in order to avoid confusion. The bag support shown in figure 3.14 is narrower

than the full width of the trench and is similar to the support used in test 4 where a quarter width bag was used.

The simulated concrete mixture used was adopted as it fulfilled three criteria:

First, the set unit weight was approximately 24 kN/m$^3$ - this is similar to the unit weight of reinforced concrete.

Secondly, full set should be achieved as quickly as concrete at full scale. Assuming concrete gains its full strength by 30 days, the simulated concrete mix should set in approximately 4.5 minutes. The mix did not fully satisfy this criterion, however, the actual setting time of between 7 and 9 minutes was felt to be acceptable.

Thirdly, the powder should mix with the fluid in the rubber bag quickly and thoroughly, so that a homogeneous mixture is produced. This was achieved as after the test was completed the wall was found to be cast in place and of a uniform appearance and strength.

The proportions of the mix are are shown in table 3.1. A less dense mix was used in test 7 where the effects of different mix densities were examined. The set unit weight of the mixture used in test 7 was approximately 16 kN/m$^3$

| Material | Tests 1-6 | Test 7 |
|---|---|---|
| OPC powder | 100g | 159.5g |
| Fine sand | 170g | 271.1g |
| Plaster of Paris | 900g | 1435.4g |
| Iron Powder | 696g | - |

Tables 3.1 *Simulated concrete mix constituents*

Figure 3.15 shows a photograph of a typical model ready for testing. Black marker beads were used to give an indication of the in-plane movements during testing and are most detailed around the trench where the wall was to be installed. At the remote end of the model the second rubber bag is visible at the edge of the perspex viewing screen. Around the base of the strongbox, three squat catch tanks can be seen, together with one tall standpipe that maintained the height of the fluid in the model at the ground surface. On the lid of the strongbox, the hopper is in position over the trench.

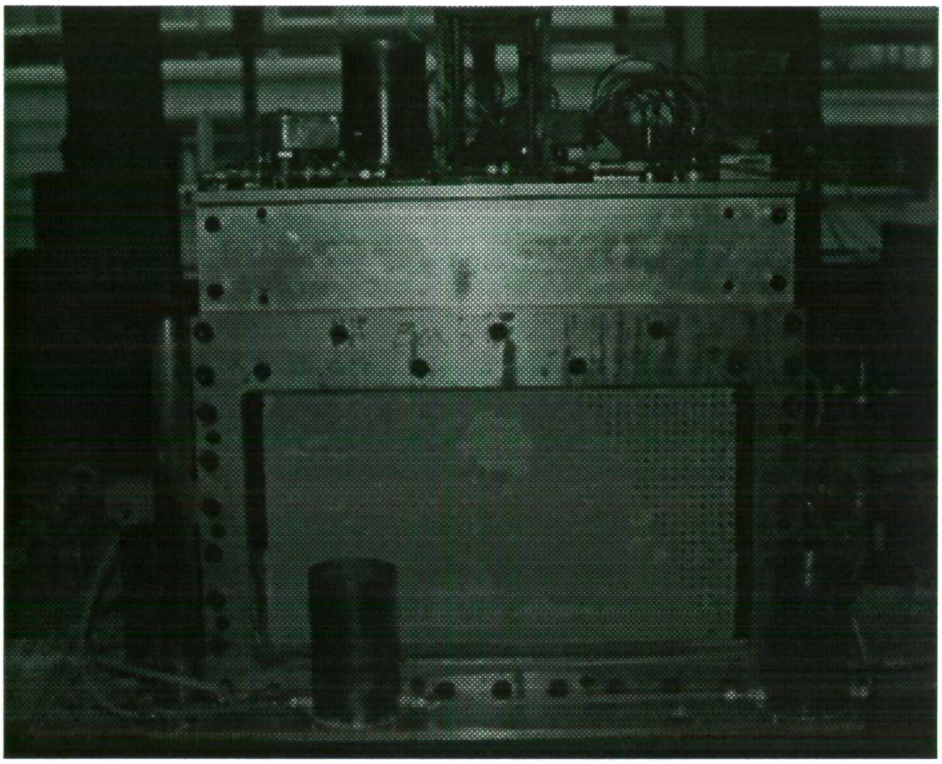

**Figure 3.15** ***Centrifuge model***

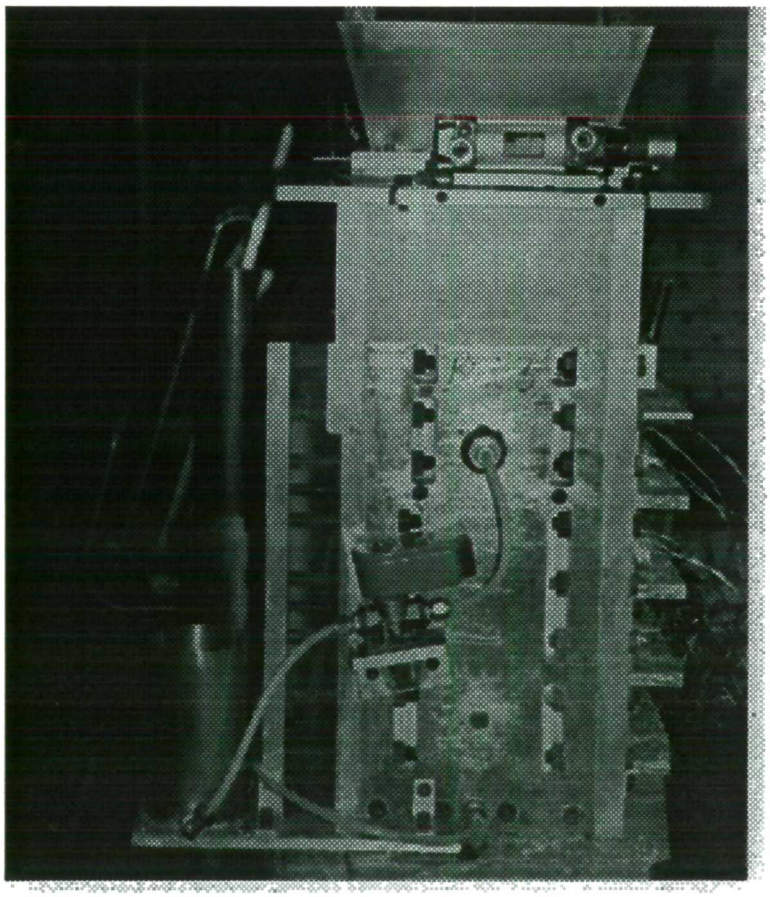

**Figure 3.16** ***Bag drainage arrangement***

Figure 3.16 gives an end-on view of the strongbox and shows the valve-operated waste pipe that drains the fluid in the rubber bag down to ground level and into the catch tanks at the base of the model. The feed to the sand drain at the bottom of the model is shown by the pipe that feeds into the centre at the bottom of the strongbox. The pneumatically driven slide is shown at the base of the hopper on the lid of the strongbox.

### *3.4.3 Boundary conditions*

Plane strain conditions were adopted in all but test 4. Plane strain conditions assume that the sides of the trench remain perpendicular to any movements that occur at the side boundaries of the model. This was achieved by applying silicone grease to the backplate of the strongbox and a mould release agent to the perspex viewing screen. The coefficients of friction between the kaolin and the strongbox were reduced to negligible levels. The boundaries at the sides of the model could therefore be reasonably considered to be rigid and frictionless. At the trench, the fluid pressure in the bag was sufficient to prevent surface water flowing into the trench.

## *3.5 Instrumentation of the model*

Three different transducer types were used to monitor the behaviour of the model during the wall installation phases and during pore water pressure equilibration both before and after wall installation. Surface movements were measured using LVDTs, positioned at the distances shown back from the trench along the centre line of the model, as shown in figure 3.17.

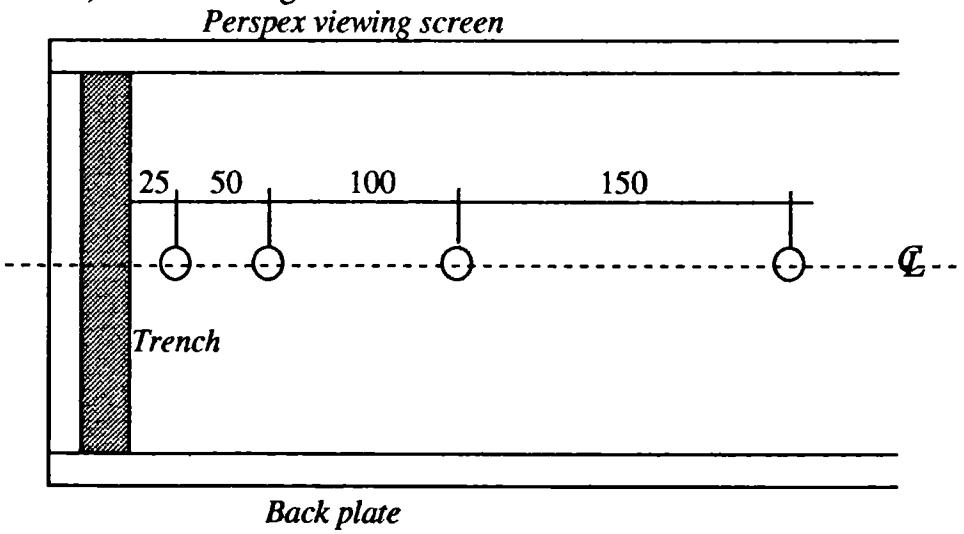


Figure 3.17 *Plan view of the LVDTs behind the trench. Dimensions in mm*

This dissertation is principally concerned with the measurement of total stress and pore water pressure during wall installation. At ten different positions in the model, (demonstrated in figures 3.11 and 5.1) DRUCK PDCR 81 pore water pressure transducers and Kyowa 5kA total stress transducers were installed. The total stress transducers were particularly sensitive to the installation procedure. Poor installation was found, after the first test, to have yielded unsatisfactory results. This is more fully discussed in chapter 5.

### *3.5.1 The installation technique.*

Once the model had been cut to the correct size, an 8 mm auger was used to drill holes horizontally through the model at the required positions. The correct positions were easily located as the back plate had been pre-drilled and plugged prior to the mixing of the kaolin slurry. A total stress transducer was first placed into a hole and rotated so that the sensitive face of the transducer was parallel with the excavated face of the trench, and hence measuring lateral stress changes. After alignment the transducer was gently pushed into the side of the hole, and then held in place with some of the kaolin that had been removed as the model was trimmed to size. The hole was then back-filled with slurry that was pumped both in front of and behind the transducer.

A pore water pressure transducer was then inserted behind the total stress transducer, taking care not to change its orientation. A plan section of a pair of transducers in the model is shown in figure 3.18.

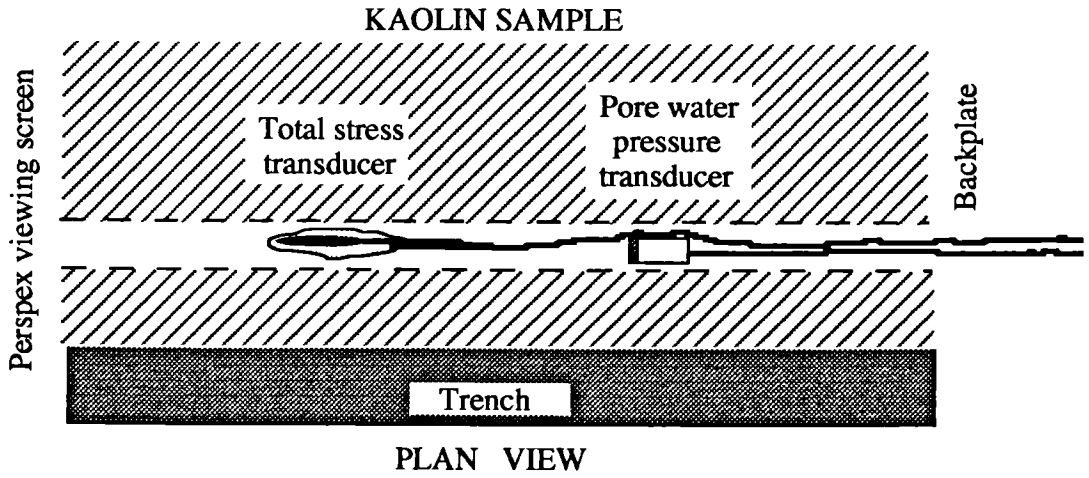


Figure 3.18 *Total stress and pore water pressure transducers in the trench*

After each test the transducers were carefully exhumed. Note was made of the actual positions of the total stress transducers, and if any rotation had occurred the results recorded by that transducer were disregarded. In the main, transducers did not rotate, and lateral stress changes was successfully measured.

### *3.5.2 Calibration procedures*

Total stress transducer calibration was found to be complex and not as easily repeatable as the calibration of the pore water transducers. Detailed consideration is given to the total stress transducer calibration techniques in chapter 4.

The pore water pressure transducers were calibrated relatively easily and repeatably. Similar electronic circuitry was used in the centrifuge tests and during calibration, producing calibration coefficients that were effectively identical. The transducers were fully de-aired prior to installation in the model. Known pressures up to a limit of 320 kPa were applied, and the resulting millivolt signals were recorded. Recently-highlighed problems regarding the clogging of porous stones (Bolton et al, 1994) are discussed with reference to the results from the centrifuge tests in chapter 5. An in-flight video camera was used to record images of the model during wall installation. Further details of the centrifuge tests are presented as appropriate in the forthcoming chapters.

# Chapter 4

# Embedded stress transducers

## 4.1 Introduction

The measurement of stress in soil using embedded gauges requires proper calibration and a knowledge of the performance of the gauges in soil (Selig, 1981). Total stress transducers positioned within or adjacent to a soil mass have been the subject of considerable research and discussion (Peattie and Sparrow, 1954; Tory and Sparrow, 1967; Fossberg, 1970; Brown, 1977; Hanna, 1985; Shad, 1989; Clayton and Bica, 1993 etc.). Whilst calibrations under fluid pressure will usually produce easily repeatable results, when the transducer is inserted into a soil mass the stress field in the vicinity of the cell is modified and this may lead to unrepresentative values being recorded.

In the centrifuge tests presented, up to 10 total stress transducers were adopted in each test each of which required calibration. Ideally, these calibrations should have been performed with the transducer embedded in a soil sample on each occasion. However, it was felt that once reliable calibration constants were obtained from the in sample tests, a correction could be applied to the fluid calibrations which could be more easily repeated prior to each test. The magnitude of this correction was found to be dependent on a number of factors. These are discussed below.

## *4.2 Transducer types*

The transducers that have been developed to measure total stresses in geotechnics have tended to be very much larger than would have been suitable for centrifuge testing (Uff, 1970; Tedd and Charles, 1985; Symons and Carder, 1992). For centrifuge testing, miniature transducers were adopted as they resulted in less disturbance to the small-scale model. In this thesis, two transducer types are considered and these are described below.

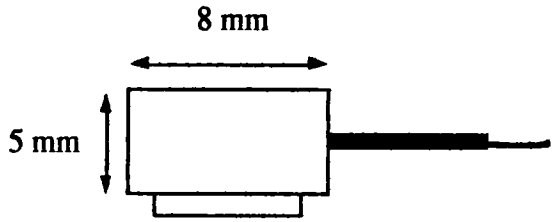


Figure 4.1 *The Entran pressure transducer*

The Entran cell (model: EPN-300IU-74-100A) was made from type 17-4PH-303 stainless steel with a fixed (5 mm) guard ring and a stiff diaphragm. The transducer was supplied at 10V and gave an output within the range 0 to 1V.

The Kyowa transducer was made from copper-berrilium and had a smaller aspect ratio (thickness/diameter) as it did not have a fixed diaphragm shell. The cell had a diameter, D, of approximately 6 mm and a maximum thickness, B, of 1mm (an aspect ratio B/D of 0.167). The transducer required a -3V supply and gave an output that was typically in the range -0.1V to 0V.

The cell and the wires were fragile and susceptible to corrosion and breakage and so a silicon dipping technique (using Dow Corning DW 3140 RTV adhesive silicon) was adopted to provide the cell with some protection and waterproofing, as shown in figure 4.2a).

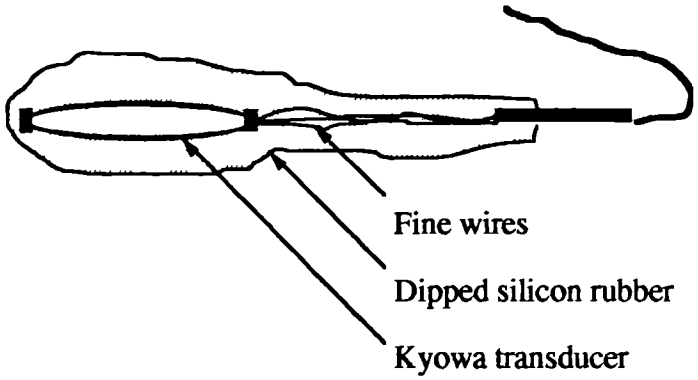


a) *Initial silicone rubber coating.*

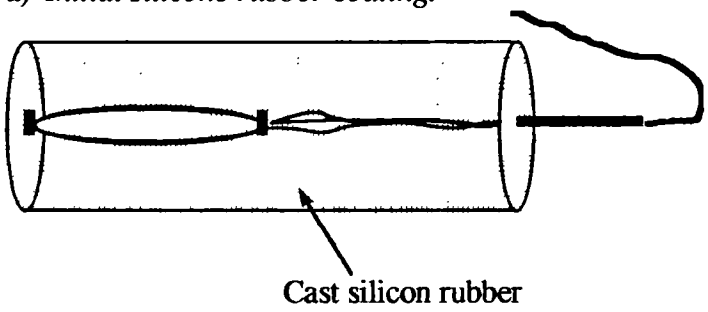


b) *Shaped silicone rubber coating.*

Figure 4.2 *Kyowa stress transducer with different silicone rubber coatings*

The initial dipping technique was modified as the fine wires were still prone to breakage due to the handling stresses experienced during centrifuge model making and testing. The transducer and fine wires were cast in silicon inside a split 6 mm diameter nylon tube which was carefully removed after casting and curing (figure 4.2b). The silicone rubber was felt to have had a much smaller effect on the in situ stress field than the stiff transducer, because the Young's Modulus for silicone rubber is considerably closer to that of Speswhite kaolin (over small strains) than Copper-Berillium, from which the transducer was made.

## *4.3 Calibration considerations*

Due to the modified stress field around a cell, a correction factor should be applied to the output from the cell, so that the value of total stress that would have existed in the model (in the absence of the cell) may be deduced. Many authors have tried to quantify the necessary correction factor for a number of different situations. From their work it becomes clear that the values recorded by the cell are dependent on a number of different factors.

The fundamental considerations are:-

- the relative stiffnesses of the soil and the transducer
- the dimensions of the cell and the sensitive diaphragm
- the void ratio and particle size of the soil
- the direction(s) of the applied stress, relative to the cell orientation

A further consideration for the purposes of centrifuge testing was found to be the effect of transducer installation. The programme of centrifuge tests was undertaken to measure *lateral* earth pressures and it was therefore necsessary to install the transducers at the correct orientation. This was performed by drilling 8mm holes into the model and carefully positioning the transducers before back-filling the holes with kaolin slurry.

It was felt that the installation procedure led to a degree of stress relief occurring around the transducers. Throughout the tests, it was found that whilst *changes* in lateral stress were measured reliably (using the adopted calibration coefficients) the *absolute values* were not representitive of the stresses in the sample. Therefore this thesis is only concerned with the *changes* in stress that occurred in the model during the diaphragm wall installation process.

Although revised installation techniques were adopted in later tests, and considered to give more representitive results, the absolute values indicated by the total stress transducers were not relied upon, and only the changes in total stress are presented.

## *4.4 Relative stiffnesses of the soil and the transducer.*

Taylor (1947) suggested that when a cell is introduced into the soil mass the stress field redistribution will result in an over-reading as demonstrated in figure 4.3.

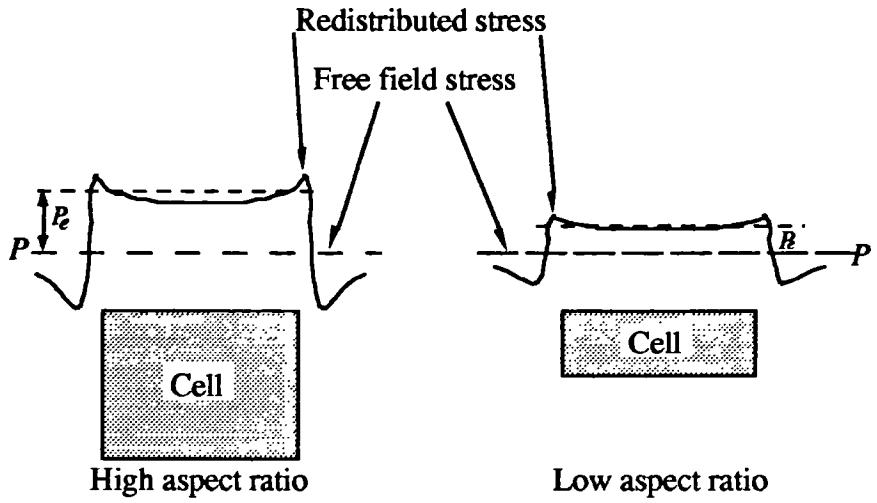


Figure 4.3 *Stress redistribution due to a relatively stiff cell in a soil mass (Brown, 1977).*

Taylor (1947) used the ratio $P_e/P$ to define the over-read, where $P_e$ is the average difference between the erronious stress value recorded due to the inclusion of the cell, and $P$ is the stress applied to the sample in which the transducer is embedded (the free-field stress). Peattie and Sparrow (1954) proposed that cell over-read could be estimated from a straight line relationship that was quantified by the ratio of the stiffness of the soil mass to that of the cell, plotted against the aspect ratio (the ratio of cell thickness to the cell diameter, $B/D$) as shown in figure 4.4.

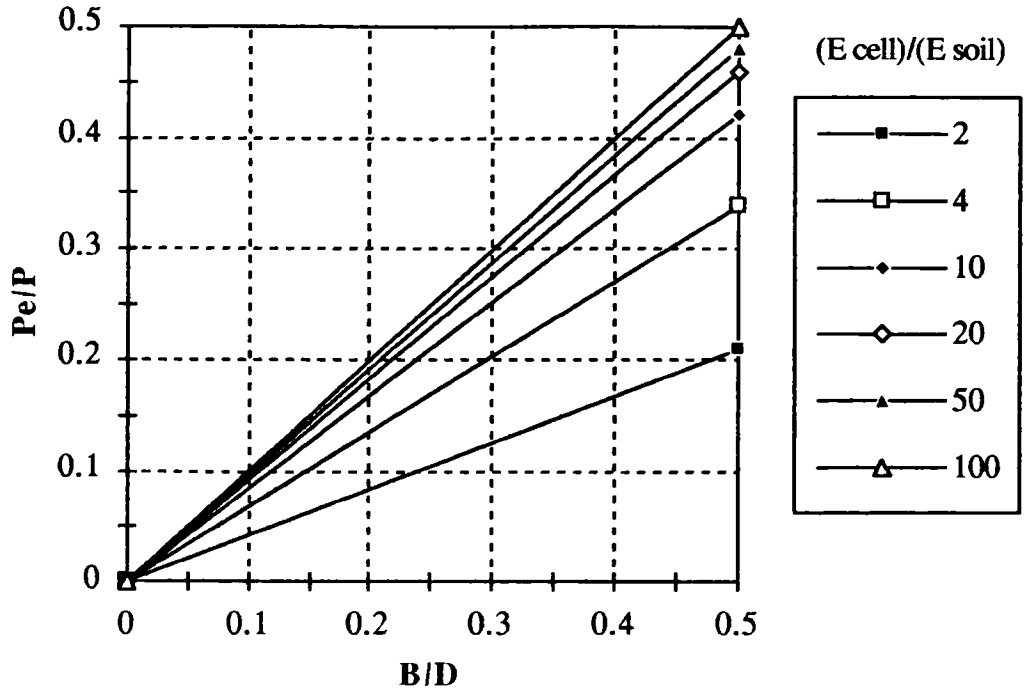


Figure 4.4 *Stress over-read (as a fraction of the applied stress) against aspect ratio plotted for different cell/soil stiffnesses (Peattie & Sparrow, 1954)*

## *4.5 Finite element analysis*

To model the stress redistribution due to the Entran and Kyowa transducers, finite element analyses were used. The analyses were carried out using CRISP90 (Britto and Gunn, 1987) for the two transducer types embedded in a soil sample. Figures 4.7 and 4.8 show the calculated redistributions due to the inclusion of a stiff body in a soil mass, and ignore other factors that might have an effect on the stress changes around a transducer. These are discussed below.

A soil sample 280mm in height and 56mm in width, with a centrally placed transducer (plane dimensions 5mm x 8mm) was considered. The dimensions of the sample were chosen to prevent stress changes at the edges of the mesh, with a width on either side of the transducer of three diameters, and a sample height of 55 transducer diameters. Collins, Lee, Lilly and Westmann (1977) concluded that mutual interference between closely spaced transducers would be negligible if the separation distance exceeded three diameters.

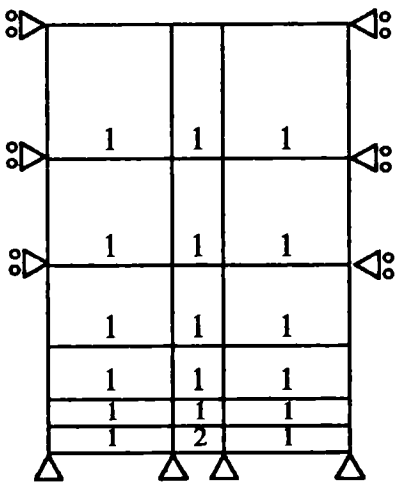


Figure 4.5 *Simplified mesh (not to scale)*

Figure 4.5 is a simplified version of the plane strain mesh which actually comprised 336 elements and represents the upper half of the symmetrical soil sample. For modelling purposes, the full mesh height was 140mm and the cell was modelled as a zone at the bottom, 2.5mm in height. In each analysis two material zones were specified, representing Speswhite kaolin (zone 1) and the transducers (zones 2a and 2b for the Entran and Kyowa transducers respectively). The material properties

assumed have been used in previous analyses with reasonable success (Powrie and Li, 1991) and are presented in table 4.1 below.

Material zone 1 modelled the kaolin sample using a soil behavioural model described by Schofield (1980). This is fully discussed in chapter 6, where finite element analyses of the centrifuge tests are presented. Material zone 2a modelled the Entran transducer in the first analysis before the mesh was adjusted to model the Kyowa transducer (figure 4.6). Material zone 2b was split into two material zones, with the central elements modelling the copper-berrillium (Kyowa) transducer, and the remaining, surrounding elements modelling silicone rubber.

| **Soil parameters: (Schofield model)** | **Value** |
|---|---|
| **Zone 1 - Speswhite kaolin** | |
| Slope of one-dimensional compression line in $v$ : ln $p'$ space | $\lambda = 0.25$ |
| Slope of unload/reload line in $v$ : ln $p'$ space | $\kappa = 0.035$ |
| Void ratio on critical state line at $p' = 1$ kPa in $v$ : ln $p'$ space | $e_o = 2.48$ |
| Slope of critical state line in $q : p'$ space | $M = 0.65$ |
| Poisson's ratio (for undrained case) | $\nu = 0.5$ |
| Unit weight of water | $\gamma_w = 9.81$ kN/m$^3$ |
| Bulk unit weight of soil | $\gamma = 17.34$ kN/m$^3$ |
| Bulk modulus of water (for undrained case) | $K_w = 5000$ kN/m$^2$ |
| Slope of no tension cut-off in $q : p'$ space | $s = 2.0$ |
| | |
| **Zone 2(a) - Stainless steel (Entran analysis)** | |
| Young's modulus | $E = 2 \times 10^8$ kN/m$^2$ |
| Poisson's ratio | $\nu = 0.3$ |
| Permeability | $k = 10^{-12}$ m/s |
| Shear modulus | $G = 0.72 \times 10^8$ kN/m$^2$ |
| **Zone 2(b) - Copper Berrillium (Kyowa analysis)** | |
| Young's modulus | $E = 1.44 \times 10^8$ kN/m$^2$ |
| Poisson's ratio | $\nu = 0.333$ |
| Permeability | $k = 10^{-12}$ m/s |
| Shear modulus | $G = 0.544 \times 10^8$ kN/m$^2$ |
| **Zone 2(b) - Silicone (DW 3140 RTV) (Kyowa analysis)** | |
| Young's modulus | $E = 5 \times 10^3$ kN/m$^2$ |
| Poisson's ratio | $\nu = 0.3$ |
| Permeability | $k = 10^{-12}$ m/s |
| Shear modulus | $G = 0.79 \times 10^3$ kN/m$^2$ |

Table 4.1 *Soil parameters used in the analyses (Powrie and Li, 1991), 2a) and 2b); Kaye and Laby, (1985)*

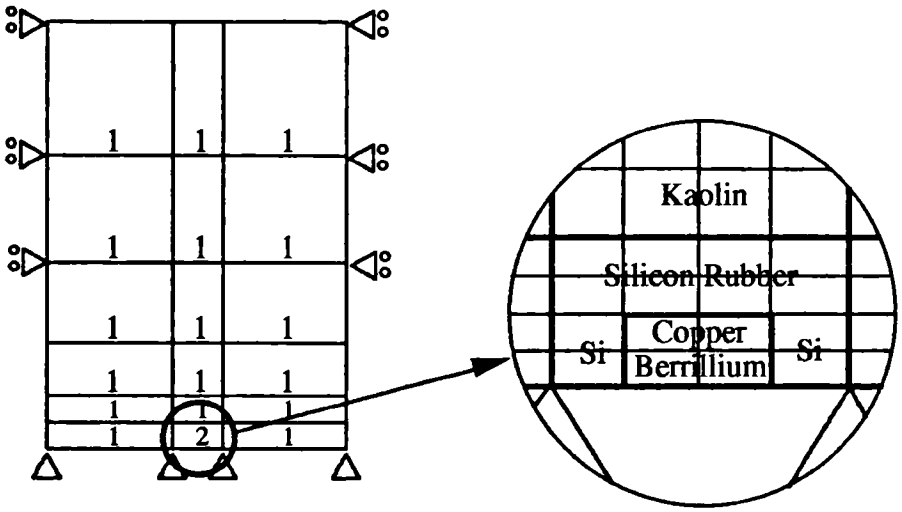


Figure 4.6 *Adjustment to the mesh to model zone 2b for the Kyowa cell*

The overall dimensions of material zone 2b remained the same as zone 2a, (i.e. 5 x 8mm). Therefore, the Kyowa transducer was modelled as 4mm x 2mm, and coated in silicone rubber, giving overall dimensions that were the same as the Entran cell. The same mesh was used in both analyses and only material zone properties were altered. For simplicity, two assumptions were made; first, a plane strain model was used, which was fixed at the bottom of the mesh and simply-supported along the sides, allowing in-plane deformations in a vertical direction only. Second, one dimensional loading conditions were adopted (rather than axi-symmetric, triaxial conditions) to isolate the effect of a stiff inclusion on *normally* applied loads. The normal load of 300 kPa was applied over 50 equal increments of 6 kPa.

### *4.5.1 Results*

For the Entran transducer analysis, the calculated stress redistribution is shown in figure 4.7. The position of the transducer extends to 4mm on either side of the y-axis and is marked by the significant changes in stress distribution that were calculated at the transducer edges.

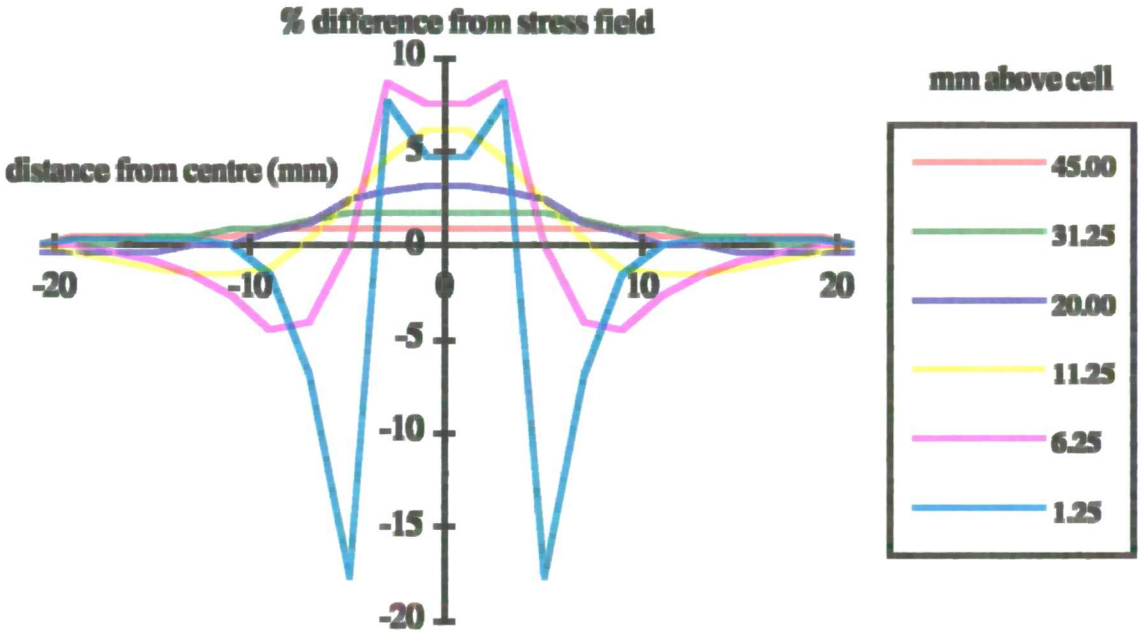


Figure 4.7 *Stress redistribution around the Entran transducer in Speswhite Kaolin*

The analysis results indicated that the maximum distribution would cause a 7.5% over read, assuming that the stress in the soil overlying the face of the cell was recorded.

Figure 4.8 shows the results of the Kyowa transducer analysis. The copper-berillium Kyowa transducer extends 2 mm either side of the y-axis where also significant changes in stress around the sample are also indicated. The pattern of stress is similar to the results of the Entran analysis. However, the disturbance to the stress field is not as great, with the redistribution at the sides of the transducer (5%) smaller than around the Entran cell.

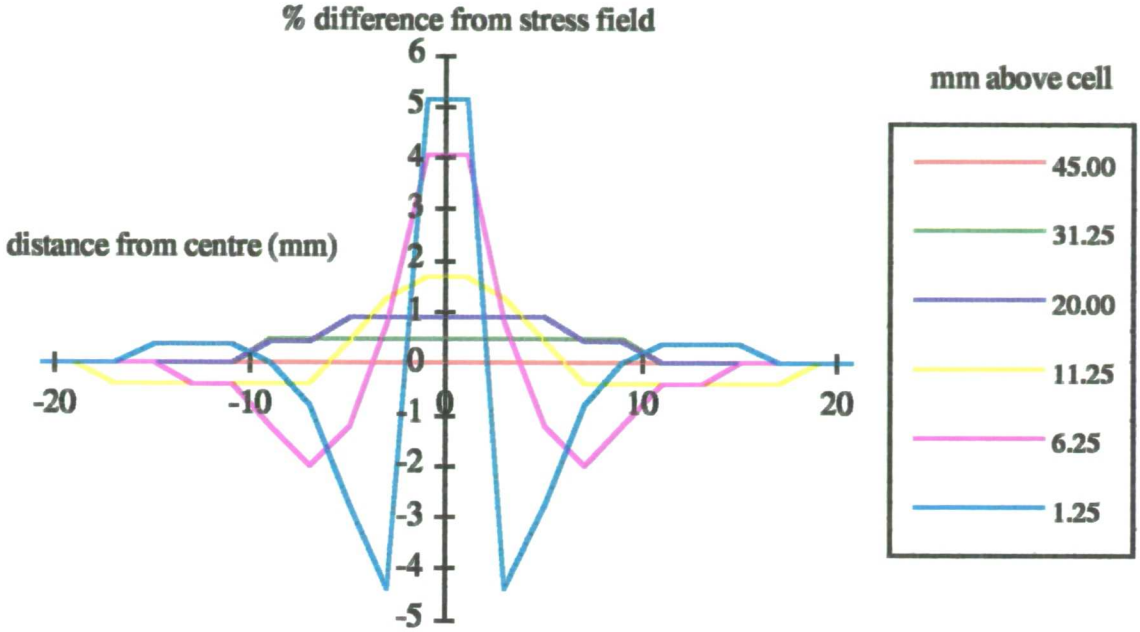


Figure 4.8 *Stress redistribution around a silicon coated Kyowa transducer*

Results from the two analyses show how the stress is increased around the stiff inclusion where a load is applied normal to the face of the transducer. The transducer would therefore give a higher millivolt signal than expected for the free-field stress, and therefore over-reads the stress in the adjacent soil. The increase in stress around the transducer would appear to depend on either material properties, and/or the dimensions of the cell. Previous work suggests that the aspect ratio of the cell is of fundemental importance.

The measured stress redistribution from the finite element analyses do not take account of the reduction in over read due to the flexibility of the diaphragm and this (as shown below) can have a considerable effect on the recorded results.

## 4.6 Diaphragm flexibility

Where a cell has been installed in a soil mass, a flexible diaphragm is generally employed to measure total stress and this can alter further the redistribution of stress around the cell. One simple method of estimating the reduction due to diaphragm flexibility assumes that when a diaphragm deflects an apparent strain may be calculated for the transducer, equal to the diaphragm deflection, δ, divided by the the cell thickness, B. For an applied stress, the apparent stiffness (applied stress/apparent strain) will vary across the face of the transducer as shown in figure 4.9.

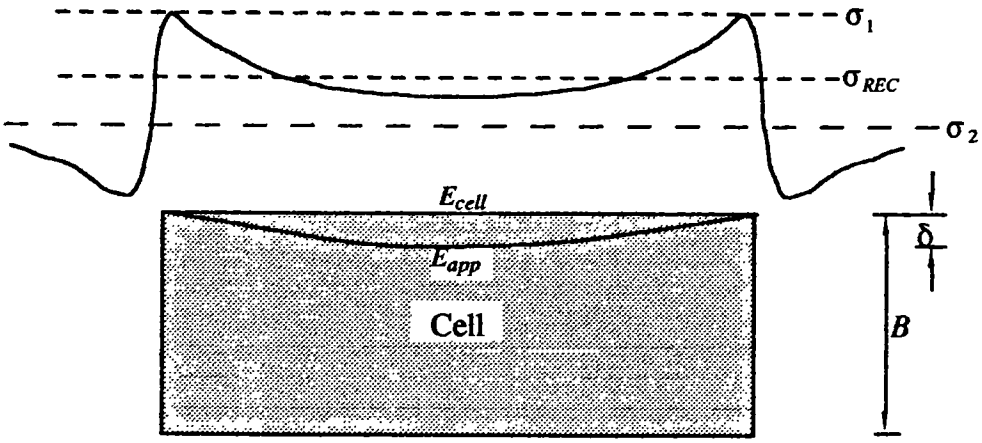


Figure 4.9 *Variation of stiffness and over read due to inclusion*

In figure 4.9, $\sigma_{REC}$ is the value recorded by the cell, $\sigma_1$ is the maximum stress due to the inclusion of a stiff body in a soil mass and $\sigma_2$ is the free-field stress. Therefore, at the centre of the diaphragm, $\sigma_{REC}$ may be calculated by adjusting the over-read in proportion to the ratio of the apparent stiffness of the cell to the stiffness of the soil at that point. Hence, when $E_{apparent} = E_{soil}$, $\sigma_{REC} = \sigma_2$ (the free-field stress)

$$\sigma_{REC} = \sigma_1 - \left( \frac{E_{Soil}}{E_{Apparent}} \right) \times (\sigma_1 - \sigma_2) \qquad (4.1)$$

And so where $E_{soil} > E_{apparent}$, $\sigma_{REC} < \sigma_2$ and vice versa.

Although this method gives some guide to diaphragm flexibility effects, it represents an over-simplification for two reasons. First, $\sigma_{REC}$ would not be recorded at one position at the centre of the diaphragm but across a considerable part of the face, requiring mathematical or numerical integration. Second, values of $E_{soil}$ will vary at different depths and at different positions across the diaphragm, presenting further practical estimating difficulties.

### *4.6.1 Flexibility factor method*

Tory and Sparrow (1967) extended the work of Peatie and Sparrow (1954) (see figure 4.4) by considering cells of varying diaphragm properties over a range of aspect ratios. They proposed a flexibility factor,

$$F = \frac{E_{soil} D^3}{E_{cell} t^3} \qquad (4.2)$$

where $D$ = cell diameter

$t$ = diaphragm thickness

Figure 4.10 shows that the values of stress at the diaphragm are still largely dependent on the geometry of the cell. The figure demonstrates that at low flexibility factors, the aspect ratio is the critical factor in determining the accuracy of the cell output, but as flexibility factor values increase the aspect ratio has a less significant effect.

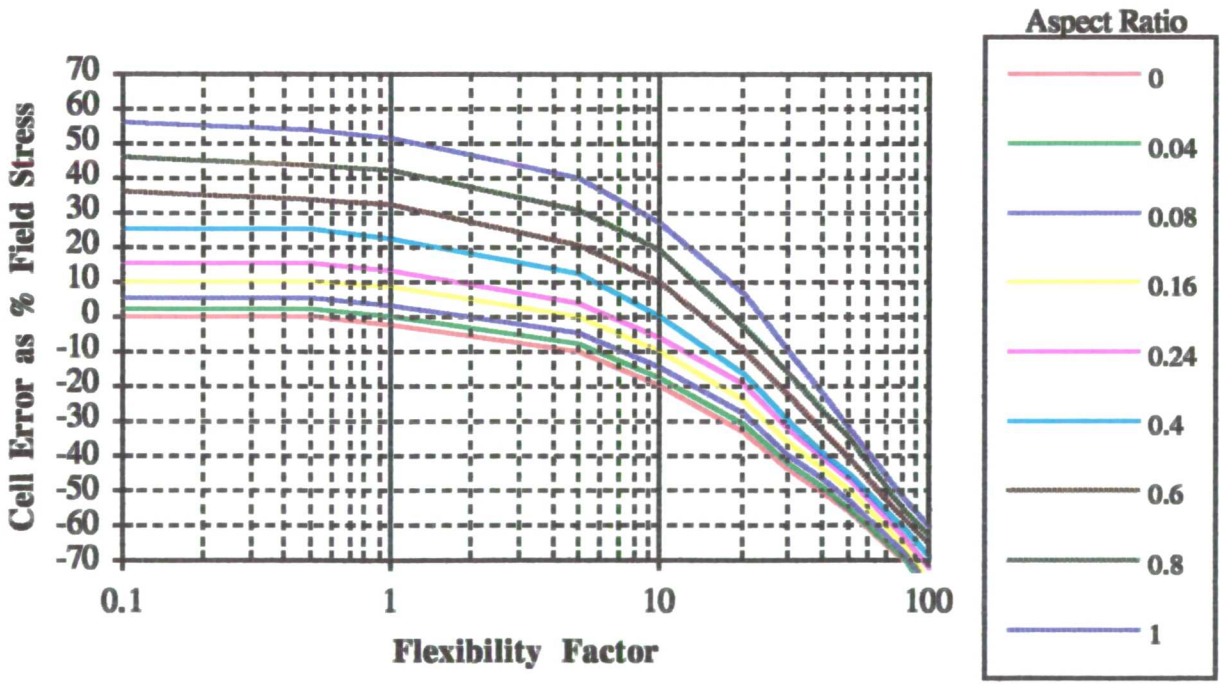


Figure 4.10 *Variation of cell error with flexibility factor and aspect ratio (Tory and Sparrow, 1967)*

The degree of redistribution relies on two primary considerations; the over-read due to the insertion of a relatively stiff body into a soil mass, and the stress relief caused by diaphragm deflection. Figure 4.10 presents curves that estimate the cell error as a percentage of the field stress and defines the flexibility factor (accounting for diaphragm flexibility) for a range of different aspect ratios (accounting for the insertion of a stiff body into a soil mass).

In order to calculate the flexibility factor the Young's modulus for the soil must be evaluated. If conditions of isotropic linear elasticity are assumed then $E_{soil}$ may be assigned one value for a particular clay. From triaxial testing a crude value for the secant stiffness could then be estimated from

$$\text{Young's Modulus } E_y = \frac{\text{uniaxial stress}}{\text{corresponding axial strain}}$$

(Bolton, 1979), with different normal stresses or confining cell pressures simulating different depths. However, soil stiffness changes with strain, and is conventionally high for small strains (for example, Wroth, 1971; Atkinson and Stallebrass, 1990; Al Tabbaa, 1987) and approaches a more constant value at large strains (Petley, 1966). The measurement of soil stiffness has become an important issue and different soil models have been formulated to predict the behaviour of soils particularly at small strains (Schofield, 1980; Atkinson and Stallebrass, 1990 and Simpson, 1992)

For undrained, over-consolidated samples, by assuming a value for the Poisson's ratio, $\nu_u = 0.5$ (Wroth, 1972), the relationship $E_u = 2G(1+\nu_u)$ (where G is the shear modulus) may be adopted once values of shear modulus have been calculated. The shear modulus depends on a number of different factors; principally:

- the type of soil
- the stress history of the soil (recent and general geological)
- the position of the soil element in the ground (stress state)
- the stress path to which the soil is subjected

A laboratory investigation into the variation with $p'$ (mean effective pressure) of the initial tangent shear modulus, $G$, obtained from undrained unloading/reloading cycles triaxial in shear tests on consolidated samples gave an approximately straight line relationship (Al-Tabbaa, 1987) with $G = 62\,p'$. This relationship was consistent with the expression

$$G = \frac{p'}{\kappa^*}\frac{3}{2}\frac{(1-2\nu')}{(1+\nu')} \tag{4.3}$$

in which $\nu' = \dfrac{\text{negative lateral strain}}{\text{axial strain}}$

and $\kappa^*$ is the slope of an intial unload/reload line following a change in direction of the stress path in ($\ln.v$ - $\ln.p'$) space. For a heavily overconsolidated Speswhite kaolin sample on an unload/reload ($\kappa^*$) line, this empirical relationship is appropriate. Values of mean effective stress for the soil at the same depths as the transducers are shown in table 4.2, below, for which

$$p' = \frac{(\sigma_v' + 2\sigma_h')}{3} \tag{4.4}$$

and $$1 < K_o = \left[\frac{\sigma_h'}{\sigma_v'}\right] < 2.56$$

| Depth (m) | $\sigma_v'$ (kPa) | $\sigma_h'$ (kPa) | $p'$ (kPa) | $G$ (kPa) | $E_{soil}$ (kPa) |
|---|---|---|---|---|---|
| 3.0 | 23.1 | 59.1 | 47.1 | 2917.9 | 8753.7 |
| 11.0 | 84.6 | 164.9 | 138.2 | 8565.1 | 25695.3 |
| 19.0 | 146.1 | 176.3 | 166.2 | 6305.4 | 30916.3 |
| 25.5 | 192.3 | 192.3 | 192.3 | 11919.5 | 35758.5 |

Table 4.2 *Young's modulus for overconsolidated Speswhite kaolin used in the centrifuge model tests*

The values of horizontal effective stress were calculated by considering a worst (maximum) case in which the earth pressure coefficient is at an estimated passive failure limit (2.56) up to a depth of 10m, reaching unity at a depth of 18.5m. The range of values of Young's Modulus is similar to the ranges of values given by other writers for other clays. Tests on heavily overconsolidated London Clay (tested consolidated undrained) yielded values of Young Moduli of 50000 kPa at 0.01% strain and 4000 kPa at 1% strain (Jardine, Symes and Burland, 1984). Powrie and Li

(1991) showed a range of values of $E_u$ between 4000 and 80000 kPa for a stiff overconsolidated boulder clay.

To calculate the flexibility factor, F, other properties must also be determined. The Kyowa cell is made of Copper Berillium which has a Young's modulus similar to Hidurax Special (a copper, berillium and nickel alloy), $E_y$ = 144.5 GPa. For the Entran cell the stiffness was taken as 215.3 GPa for stainless steel (Kaye and Laby, 1985) and the thickness of the diaphragm was taken as equal to 0.1mm. This gives the following correction factor for each cell at each depth, using figure 4.10.

| Depth (m) | $E_{soil}/E_{cell}$ | $(D/t)^3$ | $F$ | Aspect Ratio ($B/D$) | Tory and Spa % Correction |
|---|---|---|---|---|---|
| 3.0 | $4.06\times10^{-5}$ | 512000 | 20.817 | 0.625 | -11 |
| 11.0 | $11.93\times10^{-5}$ | 512000 | 61.105 | 0.625 | -48 |
| 19.0 | $14.36\times10^{-5}$ | 512000 | 73.521 | 0.625 | -56 |
| 25.5 | $16.61\times10^{-5}$ | 512000 | 85.036 | 0.625 | -61 |

*(a) Correction for the Entran cell.*

| Depth (m) | $E_{soil}/E_{cell}$ | $(D/t)^3$ (mm) | $F$ | Aspect Ratio ($B/D$) | Tory and Spa % Correction |
|---|---|---|---|---|---|
| 3 | $6.1\times10^{-5}$ | 125000 | 7.625 | 0.2 | 13 |
| 11 | $17.8\times10^{-5}$ | 125000 | 22.250 | 0.2 | -12 |
| 19 | $21.4\times10^{-5}$ | 125000 | 26.750 | 0.2 | -18 |
| 25.5 | $24.7\times10^{-5}$ | 125000 | 30.875 | 0.2 | -22 |

*(b) Correction for the Kyowa cell.*

Table 4.3 *Transducer corrections factors from Tory and Sparrow (1967)*

The values of correction factor for the Entran cell cover a wider range than for the Kyowa cell. However, for both transducers, the predicted error at the deepest position would be unacceptable and was found to be far greater than the actual range of errors measured in the triaxial calibrations, presented below.

The reason for this is that the data used to plot figure 4.10 were obtained from a transducer made of Dural (a relatively soft material with a smaller $E_{cell}$ than stainless steel or copper-berillium), with a diaphragm thickness 1/15th of the sensitive diaphragm diameter. In the miniature total stress cells, the diaphragm thickness to

cell diameter ratios were estimated to be 1/80 and 1/50 for the Entran and Kyowa cells respectively. Tory and Sparrow's correction is based on the idea of aspect ratio and diaphragm flexibility independently affecting the stress redistribution that occurs around a transducer. The percentage correction as calculated from equation 4.2 is outside the range of errors found when the miniature transducers were calibrated and this may be due to the significant differences in diaphragm geometry.

The flexibility factor was used by Askgaard (1961) in a slightly altered form that also took the Poisson's ratios of the soil and the transducer diaphragm into account. Askgaard (1961) presented the results from a finite difference analysis which showed close agreement with the results presented by Tory and Sparrow (1967), when similar cells were adopted.

Peattie and Sparrow (1954) suggested that only 45% of the total area of the transducer face should be a sensitive diaphragm, to reduce the variation in stress levels (see figure 4.3). They concluded that to reduce the error due to the flexibility of the diaphragm, a stiff guard ring should be employed, and the diaphragm should be very stiff relative to the soil, see figure 4.10. Hanna (1985) proposed that the cell should be as flat as possible, limiting the over-read due to the aspect ratio (figure 4.4) and that the ratio of diaphragm diameter to deflection should be greater than 2000 (Shad, 1989).

## *4.7 Soil void ratio and particle size*

The effect of soil void ratio and particle size was the subject of reports by the US Army Engineer Waterways Experiment Station, (Taylor, 1947) which concluded that soil void ratio and particle size were only important considerations in extreme circumstances. By comparing calibrations in fluid with calibrations in two grades of sand, it was shown that the fully saturated sands with the greatest void ratio yielded calibration constants that were closest to those carried out in fluid.

Clayton and Bica (1993) investigated the under-read due to diaphragm flexibility alone, by considering a boundary cell. They defined a cell action factor (CAF) as the ratio of measured stress to applied stress. For different soils they concluded that the CAF approached unity (ie. the stress measured by the cell was closest to the stress applied to the sample) where the void ratio was greatest. Similarly, the smaller the void ratio, the smaller the CAF at each stress level. It was also found that for each void ratio, at larger stresses the CAF was smaller. They concluded that saturated

fine-grained soils (with high void ratios) resulted in CAFs that were closest to unity at all stress levels.

It has been suggested also that the diaphragm dimensions should be a minimum of 50 times the largest particle size and individual large particles should be kept away from the diaphragm face (Shad, 1989; Clayton and Bica, 1993). With a particle size for Speswhite Kaolin of approximately $10^{-6}$m this criterion is easily achieved. Also Shad (1989) suggested that the transducer must have a sufficiently large soil/diaphragm contact area to prevent, first, individual particles and second, the formation of soil bridges, from having an effect.

## *4.8 The direction(s) of the applied stress*

Fossberg (1970) considered axisymmetric stress conditions for a range of cross sections and carried out a series of finite element analyses. His work showed that a known stress, applied normal to the face of the diaphragm, was consistently over-read, but by increasing the force that acted parallel to the diaphragm the over-read was reduced.

Collins, Lee, Lilly and Westmann (1977) looked at prolate and oblate spheroid shaped transducers of varying aspect ratios, and also at the effect different ratios of stress (acting parallel and perpendicular to the axis of symmetry) had on the recorded data. They defined calibration coefficients that corrected for each resolved component of stress, where $C_N$ was the coefficient for the normal stress, $\sigma_N$, and $C_T$ was the coefficient for the transverse stress, $\sigma_T$. According to their research, $C_N$ increased with aspect ratio, and the over-read could be reduced by up to 20% of the pressure applied laterally. Further tests were carried out with the transducer rotated at angles of 35° and 55° to the plane of maximum principal stress, from which the authors proposed:

$$\sigma_F = C_N.\sigma_N + C_T.\sigma_T \qquad (4.5)$$

where $\sigma_F$ = stress measured by the transducer

Theoretical methods were used to calculate values of $C_N$ = 1.18 to 1.25 and $C_T$= -0.065 to -0.20, and the test data showed close agreement with these values.

For the purposes of quantifying the effects of stresses applied in more than one direction, the stresses may be resolved into two componants. The more significant component is the one that acts in a direction normal to the diaphragm face. The second component may be considered to act as a shear force across the face of the diaphragm.

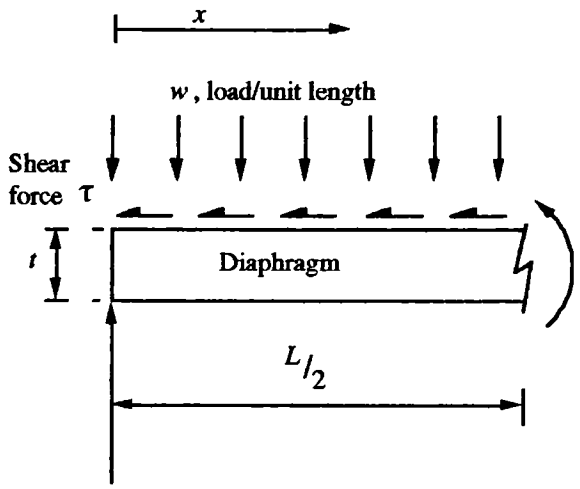


Figure 4.11 *Simple resolution of moments*

The supporting force moment and normal force moment is

$$= \frac{wLx}{2} - wx\frac{x}{2} = \frac{wx}{2}(L-x) \qquad (4.6)$$

The shear force moment (where t is the thickness of the diaphragm) is

$$= \frac{\tau xt}{2} \qquad (4.7)$$

The net moment is therefore

$$= \frac{wx}{2}(L-x) - \frac{\tau xt}{2} \qquad (4.8)$$

A simple resolution of moments (figure 4.11) shows that the shear effect will reduce the recorded level of stress (based on the diaphragm bending inwards) - thus counteracting, to some extent, the increase due to the inclusion of a stiff body in a soil mass. However, the bending moment due to the shear force will only be of significance when t approaches L, and then only at the edges of the face of the cell. Generally, miniature total stress cells have thin diaphragms and so diaphragm

value. The 20% recorded by Collins et al. was achieved for an oblate-shaped transducer to which high shear forces and small normal loads were applied.

## *4.9 Laboratory calibrations.*

Previous research has been based on data from specific transducers under specific conditions, from which calibration relationships have been calculated. In order to establish a reliable relationship for the transducers used in the centrifuge tests, calibrations were performed as described below. The use of stress cells to measure *lateral* stresses in a centrifuge model presents further difficulties of installation and orientation, because of the miniature scale of both the model and the transducer. Therefore, a triaxial cell was adapted so that the miniature transducers could be sealed inside and tested under pressures of up to 250 kPa, both in the fluid and embedded in a triaxial sample.

For both types of transducer, three methods of calibration were adopted:-

1. Calibration in fluid
Calibration embedded in a kaolin triaxial sample, varying
2. deviatoric pressure with constant confining pressure
3. confining pressure under zero deviatoric stress.

When calibrated in the fluid alone, the transducer measured the pressure that was applied; i.e. there were no effects due to inclusion, diaphragm flexibility or shear stresses. By understanding likely stress distributions around transducers embedded in soil a correction may be applied to fluid calibrations to obtain consistent calibrations for cells installed in the model. For fluid calibrations the transducers were simply positioned in the centre of the triaxial cell shown in figure 4.13. The transducers were sealed inside a triaxial cell with a rubber bung and silicone grease and the confining pressure was increased and decreased to give calibration constants. This was quicker to set up than an in-sample test and was found to yield more readily repeatable results.

### *4.9.1 In-sample calibrations*

Two different in-sample calibration stress combinations were adopted, modelling isotropic and shear stress changes to represent the stress conditions at different

positions in the centrifuge model. Some depths in the centrifuge tests will start from isotropic conditions whilst other depths will start with a deviator stress. This is demonstrated by figure 4.12.

For transducers positioned at depths in the model where $K_o$ was approximately equal to 1 initial isotropic stress conditions were appropriate during calibration. For transducers positioned at shallower depths (i.e. where initial $K_o>1$) applied deviatoric stress changes were appropriate during calibration. Excavation to a $K_o=1$ could then be modelled by reducing the deviatoric pressure and then concrete placement could be simulated be increasing it to the appropriate pressure. However, to simulate conditions where $K_o<1$ an extension cap would have been required.

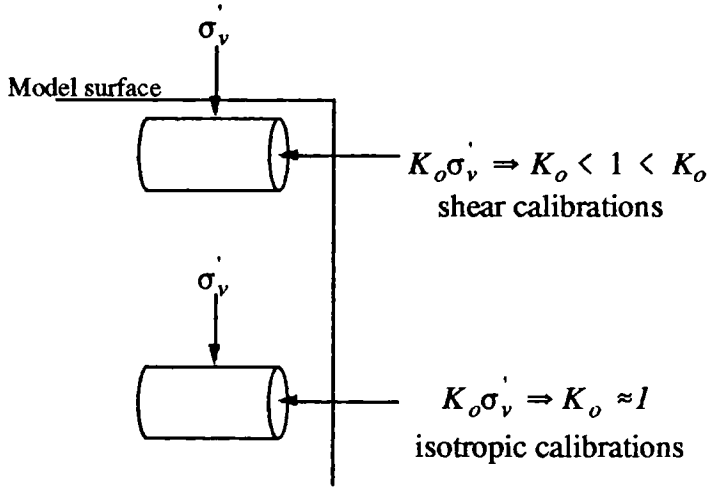


Figure 4.12 *In-sample calibration applicability*

Ultimately, in order to achieve a calibration over a wide range of applied pressures, deviatoric and isotropic calibrations were carried out over a wider range of cyclical variations than the centrifuge tests required. This was so that two possible extremes of behaviour could be investigated.

### *4.9.2 Transducer calibration apparatus*

The apparatus used for triaxial calibrations is shown in figure 4.13. The samples were cut into two halves and a cylindrical recess of the same diameter and thickness as the transducer was drilled into the lower half as a mounting. In all cases care was taken to fit the transducer as exactly as possible to prevent air from being trapped when the two halves of the sample were put back together and re-aligned. The full sample height was approximately 100 mm.

when the two halves of the sample were put back together and re-aligned. The full sample height was approximately 100 mm.

A small hole was cut into a thin rubber triaxial membrane through which the plug and transducer wires were passed after the membrane had been stretched and placed over the sample. The sample was then slid onto a de-aired and saturated porous stone and mounted onto a de-aired triaxial cell pedestal and sealed with two rubber O-rings. Similarly, a perspex top cap was slid onto the top of the sample and sealed with a further O-ring. Care was taken at all stages to prevent any damage to the sample and not to trap air. The transducer wire was sealed to the rubber membrane using a silicon-based mastic sealant and left to cure, wrapped in clingfilm, for 24 hours. The transducer plug was then fed through an orifice drilled into the top plate of the triaxial cell and sealed with a rubber bung and silicone grease. This system proved to be sufficient for triaxial cell pressures of up to 250 kPa.

To ensure accurate readings, the triaxial cell was filled with de-aired water pressurised via an air-water isolator (bladder interface), and measured using a Druck digital display pressure gauge (calibrated against a dead weight system). A pore pressure transducer (Druck - precalibrated against dead weight) and a Wykeham-Farrance proving ring (calibrated 04.09.93) were used to monitor pore pressures and deviator stress respectively, where relevant.

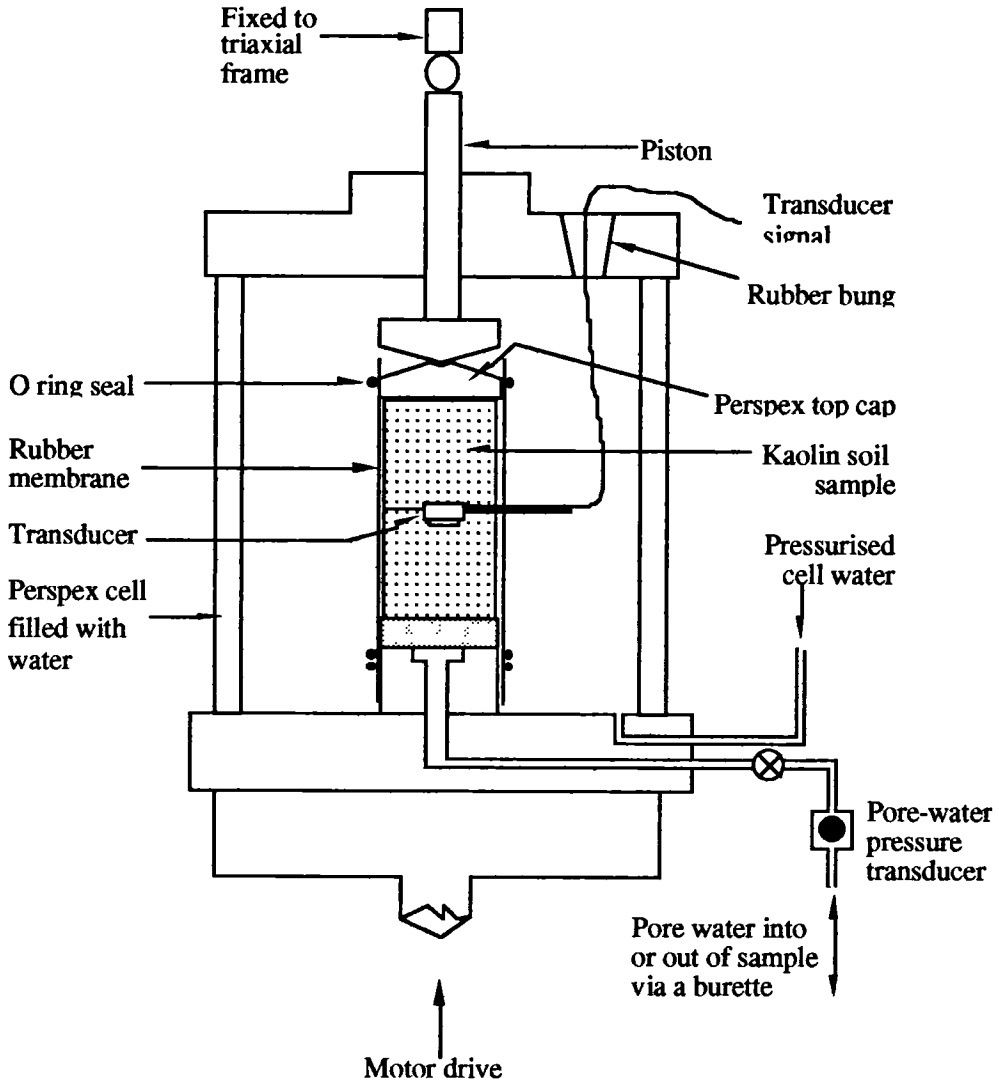


Figure 4.13 *Triaxial calibration apparatus*

The calibration tests were carried out consolidated-undrained on samples which had been left to reconsolidate until equilibrium conditions were achieved. A 'B' value test was carried out prior to the start of calibration to confirm that the sample was fully saturated and that there were no leaks or air pockets in either the sample, the water feed or the pore pressure measuring apparatus.

### *4.9.3 Isotropic stress calibrations*

The cell pressure was increased in steps of 2.5 kPa from an initial value of 50 kPa up to 250 kPa and then reduced in similar decrements from 250 kPa to 50 kPa. This cycle was usually repeated and pore pressures were recorded throughout.

The data are presented graphically in figures 4.14 and 4.15, which show the transducer output (mV) as a function of the cell pressure ($\sigma_3$ kPa) for the two different transducers. The loading portion of each cycle is shown in red with unloading in green. Each calibration graph shows a best fit line (the black line) and a fluid calibration line (the black dotted line). The two light brown lines represent variations on the best fit lines of ±15% and encompass most of the measured data. The best fit line was calculated using a method of least squares and the equations for these lines are given below in table 4.4. Also given is an $r^2$ term which gives a measure of the deviance of the plotted points from the calculated best fit line, and can be used as an indication of the reliability of the calibration gradient.

The fluid calibrations were carried out using the same apparatus as used in the in-sample calibrations with the transducers free and centrally positioned in the triaxial cell. In all cases the 'fluid calibration' fine dotted line was the average of at least four independent calibrations, showing very little variation, with (in all cases) $r^2$ = 1.0 +/- 0.05.

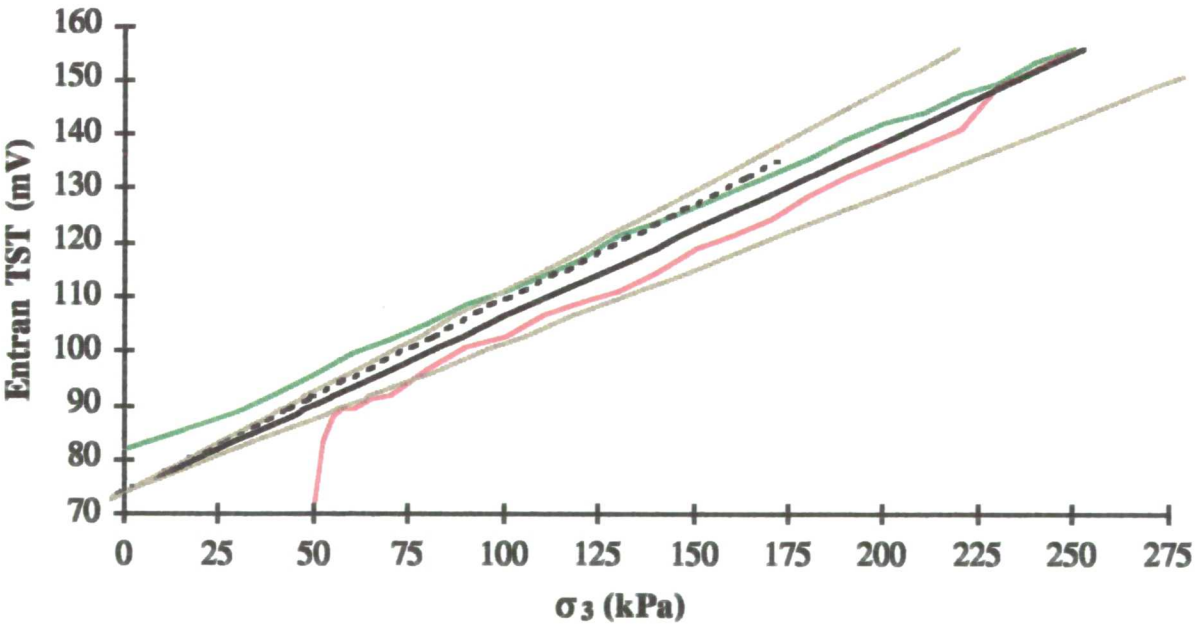


Figure 4.14 *Entran isotropic stress calibration with best fit (black) and ±15% (brown) lines with fluid calibration (dashed) line*

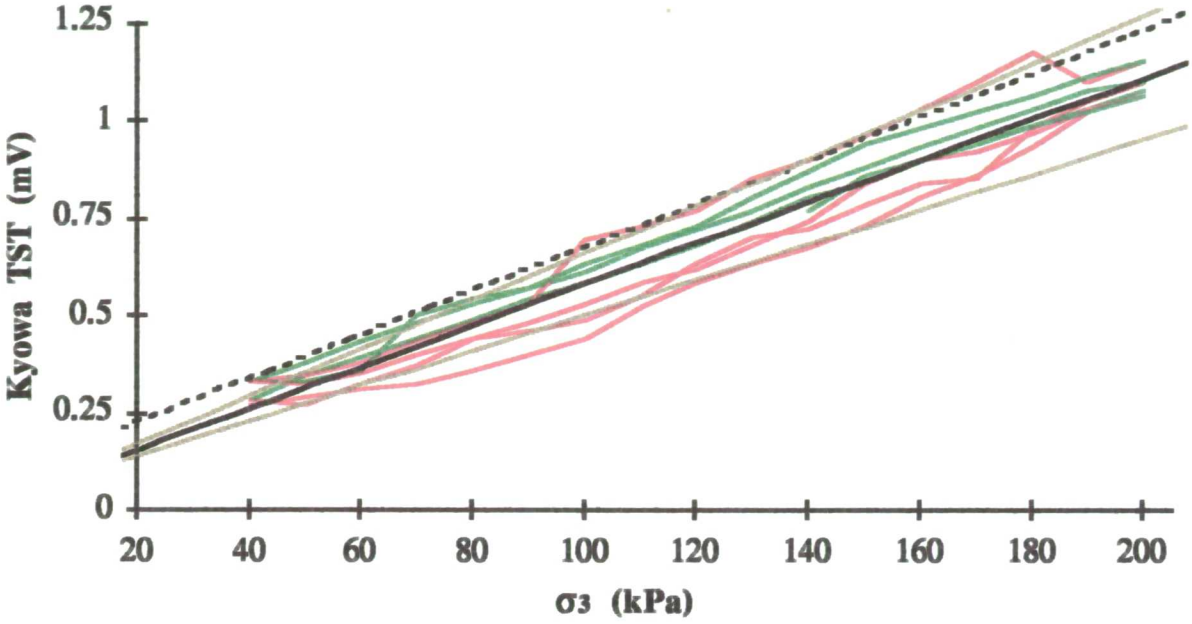


Figure 4.15 *Kyowa isotropic stress calibration with best fit (black) and ±15% (brown) lines with fluid calibration (dashed) line*

### *4.9.4 Shear stress calibrations*

The two transducer types were installed into Speswhite kaolin samples and placed into the triaxial apparatus as described earlier and shown in figure 4.13. The samples were then allowed to consolidate to equilibrium conditions under an intial cell pressure of approximately 50 kPa. A deviatoric stress was applied at a strain rate of 1 mm per hour (approximately 1% per hour) over a cycle that loaded for two hours and unloaded for one. This load cycle was repeated up to three times, so at the end of a calibration test the total strain had not exceeded 4%, with the sample exhibiting only a very slight ductile compression and no tendency to rupture.

The variations of the best fit line were found to be larger when the transducers were calibrated under isotropic conditions. A 25% margin of error was adopted in figure 4.16 for the Entran transducer, and 15% for the Kyowa transducer.

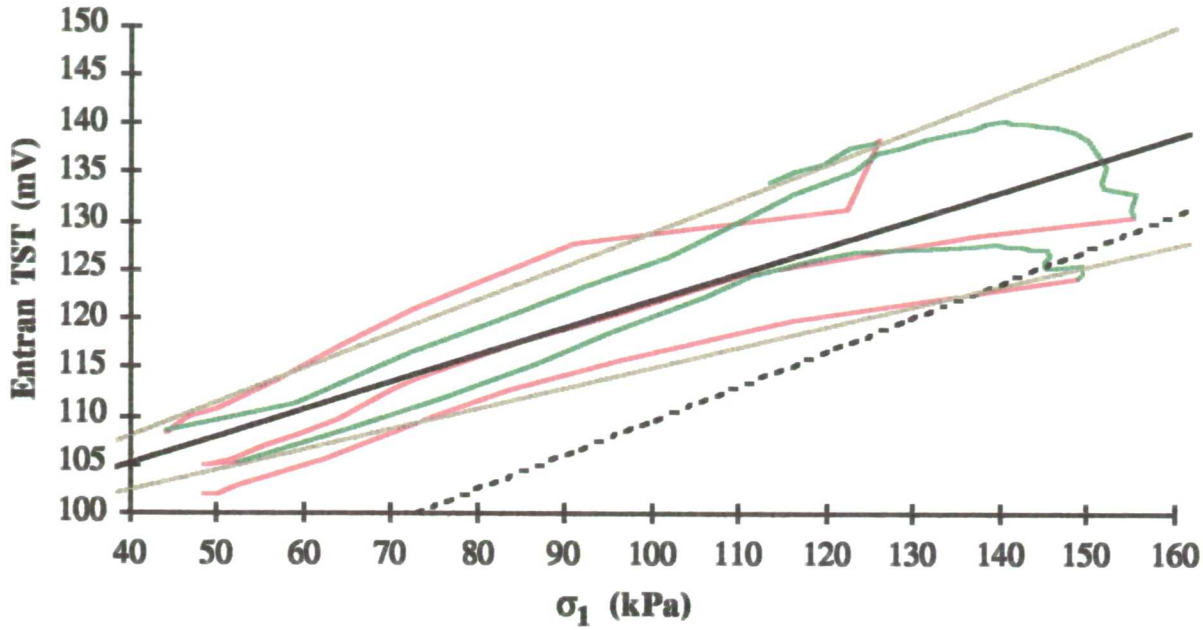


Figure 4.16 *Entran shear stress calibration with best fit (black) and ±25% (brown) lines with fluid calibration (dashed) line*

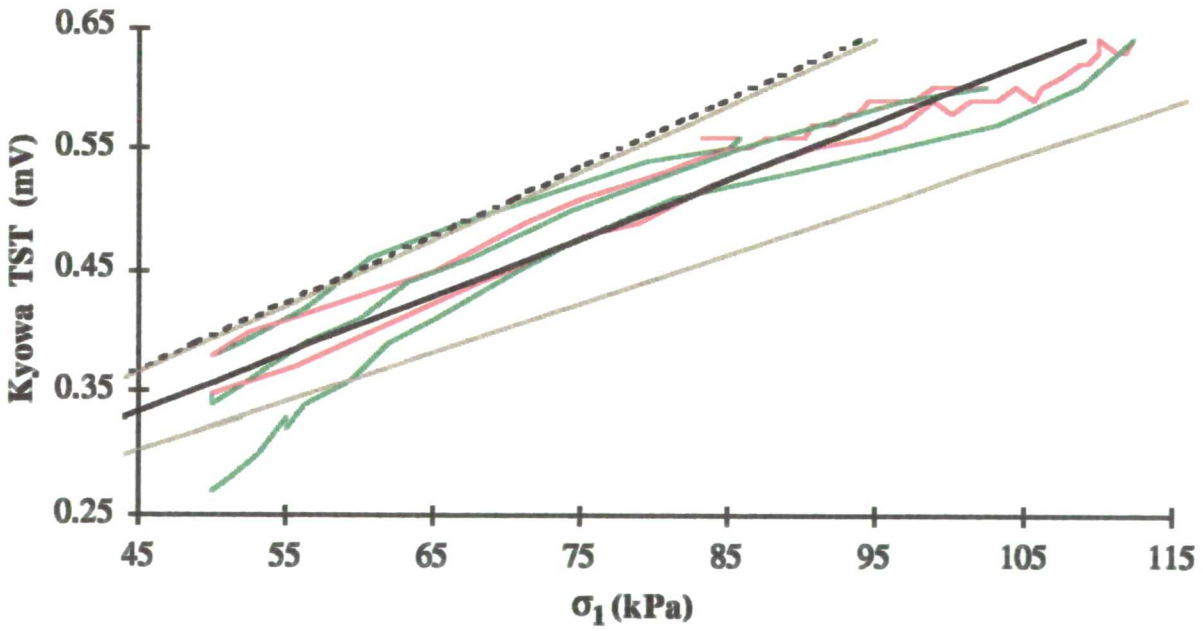


Figure 4.17 *Kyowa shear stress calibration with best fit (black) and ±15% (brown) lines with fluid calibration (dashed) line*

| Entran Transducer | | | |
|---|---|---|---|
| Calibration method | Offset (mV) | Gradient (mV/kPa) | Deviance ($r^2$) |
| Isotropic | 73.959 | 0.32365 | 0.950 |
| Shear | 93.310 | 0.27971 | 0.853 |
| Fluid | 74.116 | 0.35431 | 1.000 |

| Kyowa Transducer | | | |
|---|---|---|---|
| Calibration method | Offset (mV) | Gradient (mV/MPa) | Deviance ($r^2$) |
| Isotropic | -0.00978 | 0.52973 | 0.940 |
| Shear | 0.011975 | 0.47666 | 0.913 |
| Fluid | -0.011757 | 0.55723 | 1.000 |

Table 4.4 *Entran and Kyowa transducer results*

### *4.9.5 Variations from the best fit line.*

In each case the percentage variation line represents an estimation of the maximum likely error in the recorded results when the calibration constants from the best fit line are used. For the isotropic calibrations (figures 4.14 and 4.15) variations of 15 % are plotted for both transducers. For shear stress calibrations a variation of 15% was plotted for the Kyowa cell and a variation of 25% for the Entran cell which exhibited greater deviation from the best fit line during calibration. The $r^2$ term in table 4.4 above indicates that the greatest variance was experienced by the Entran transducer during both in-sample calibration methods.

Figures 4.14 and 4.15 presented the isotropic stress calibrations for both transducers. Generally, the deviation of isotropic calibrations from the best fit line was smaller than for shear stress calibration. This was due, in part, to greater hysteresis occurring in the shear stress calibrations where stress reversal led to increased soil stiffness around the transducer. This effect was most prominant around the Entran transducer with large loops occurring where the stress path changed direction.

### *4.9.6 Formulating a correction to fluid calibrations*

In comparison with fluid calibrations, after initial 'bedding-in' the in-sample calibrations yielded a gradient that was 9.5% less for the Entran transducer and 5.2% less for the Kyowa transducer. In figures 4.14 to 4.17, the results from the in-sample

calibrations were presented with the results from the calibrations in fluid. A comparison of the gradients in each figure gives an indication of the effect the cell has on the stress in the sample, from which a consistent relationship (i.e. a correction coefficient) may be calculated. This can be applied to a fluid calibration to allow for the differences due to calibrations in the two different media: as summarised in table 4.5 below.

| | Entran | | Kyowa | |
|---|---|---|---|---|
| Calibration method | Gradient (kPa/mV) | Percentage error | Gradient (kPa/mV) | Percentage error |
| Fluid | 2.822 | 0 | 1794.6 | 0 |
| Isotropic | 3.09 | -9.5 | 1887.8 | -5.2 |
| Shear | 3.575 | -26.7 | 2097.9 | -16.9 |

Table 4.5 *Comparison of laboratory calibrations*

The results indicated that the gradients were smaller for in-sample than for fluid calibrations. That is, if in-sample gradients were used in a fluid calibration (where inclusion, shear stress and diaphragm flexibility effects were non existent) the transducer would under predict the applied *changes* in pressure.

After analysing the results from the laboratory calibrations, it was decided that isotropic calibration corrections should be applied to the fluid calibrations for the transducers used in the model. During excavation, near the surface of the model, values of $K_o$ were greatly reduced and much of the shear stress calibration was outside the range of stress changes experienced in the centrifuge model. Figures 4.16 and 4.17 show that hysteresis loops that caused much of the variation from the best fit line were at the top range of $K_o$ values considered. Also, the isotropic calibrations showed less variation from the best fit line and the $r^2$ term for both transducers was smaller than for shear stress calibrations.

Each of the transducers used in the centrifuge tests was calibrated at least once in-sample. Prior to each subsequent test, it was necessary to recalibrate all transducers used in the model: this was carried out in fluid. Table 4.5 shows that the Kyowa transducer required a smaller percentage correction than the Entran transducer (5.2% as apposed to 9.5%). Kyowa transducer fluid calibrations corrected by 5% were found to be close to in sample calibration results, although occasionally transducers required an additional in-sample calibration after the centrifuge test was

complete if changes recorded during the centrifuge test were different from expected values.

Also, the Kyowa transducer represented by far the cheaper alternative costing only £100 to £200 per transducer instead of £1000 for the Entran transducers. Therefore, despite the involved silicon dipping technique, Kyowa transducers were adopted throughout the centrifuge modelling programme.

## *4.10 Conclusions*

The finite element analyses were used principally as a guide to the redistribution of stresses around a relatively stiff inclusion in a less stiff medium, for stresses that were applied normal to the face of the transducer. To show the redistribution that occurred over a range of values the results were presented as a percentage variation of stress in sample at different distances from the diaphragm face. As indicated in figures 4.7 and 4.8, the stress in the sample above the face of the diaphragm was greater than the datum stress (i.e. over-read) at distances of up to three cell diameters on either side of the transducer by between +5 and +7.5%. However, the analyses presented did not take account of the effects of diaphragm flexibility or shear stresses applied across the face of the diaphragm.

Tory and Sparrow (1967) presented a chart for the estimation of the cell action factor (shown in figure 4.10), and the two transducers discussed in this chapter have been assessed using this method. Their method adopts a flexibility factor that depends on the ratio of the soil stiffness to transducer stiffness, the aspect ratio of the transducer and the geometry of the diaphragm. A summary of results is presented in table 4.6 which shows a wide range of percentage corrections for cells at different positions within the centrifuge model when calculated using this method.

| Tory and Sparrow method % correction | | |
|---|---|---|
| $E_{soil}$ | **Entran** | **Kyowa** |
| 8753.7 | -11 | +13 |
| 25695.3 | -48 | -12 |
| 30916.3 | -56 | -18 |
| 35758.5 | -61 | -22 |

Table 4.6 *Cell corrections from theoretical method*

The Tory and Sparrow (1967) flexibility factor was considered to be inappropriate, and the very wide range of proposed corrections (+13% to -22% for the Kyowa cell and -11% to -61% to the Entran cell) would be unacceptable. It was felt that the method was more suitable for larger transducers made from a softer material, with thicker diaphragms than the miniature total stress transducers used in the centrifuge.

Neither the finite element method nor the Tory and Sparrow (1967) method took the effect of transverse stresses into account. This was shown by Collins et al (1977) to have a considerable effect on the readings of the cell in certain limited circumstances. However, it was felt that when diaphragms were very thin and transducers were flat, shear effects would not substantially affect the recorded results.

A series of laboratory tests was carried out to give calibration constants that could be used in the centrifuge tests. Comparing the results obtained by calibrating the transducers in sample with those obtained from fluid calibrations suggests that the transducers will under-read the applied stress changes. The degree of under-read was different for the two transducer types, and depended on the in-sample calibration method adopted (i.e. shear stress or isotropic).

Due to the nature of centrifuge testing, installation effects were found to have a considerable effect on the recorded stresses. The use of a slurry with a high moisture content to back-fill behind and around the transducer would have caused a degree of stress relief around the cell, resulting in a variable offset, and so this dissertation is only concerned with changes in lateral stress.

As shown in table 4.5, the calibration scale factor was reduced by 5% and then compared with the isotropic in-sample calibration. After fluid calibrations had been corrected the measured changes in lateral stress were found to be repeatable to within ±15%, and showed close correlation between results from individual centrifuge tests.

Considerable further work is possible on the subject of total stress transducers. In particular, it would be desirable to develop a total stress transducer that could be used in a centrifuge model with a minimum of disturbance to the surrounding strata during installation, a minimum requirement for in-sample calibration, and the ability to measure absolute values of stress, rather than only stress changes.

# *Chapter 5*

# *Centrifuge results*

## *5.1 Introduction*

A programme of centrifuge tests was carried out to investigate the effects of diaphragm wall installation on the surrounding soil for different initial in situ stress conditions. The same basic apparatus was used for each test with slight modifications to enable different in situ conditions to be modelled. The testing apparatus was described in chapter 3.

### *5.1.1 Overview*

The results presented in this chapter are concerned primarily with:

a) The effect of different boundary conditions at the remote end of the strongbox. Both stress and strain controlled boundaries were used and a comparison is made between the two boundary conditions to investigate any possible re-establishment of pre-excavation conditions in the long term after wall installation;

b) The effect of different initial in situ lateral stress conditions on the ground movements and stress changes during wall installation;

c) The different levels of stress that remain in the model after wall installation if concrete mixes of different densities are used.

Also discussed at the end of this chapter are the effects of using a quarter width panel and the shear strength of the kaolin sample at the top of the trench.

### *5.1.2 The centrifuge tests*

In all tests presented, it was intended that the ground water level should be maintained at the surface of the model by means of a standpipe, an overflow at the ground surface level and a drip-feed top up.

Seven tests were performed and these are outlined in table 5.1. 'Additional bag height' refers to the height of fluid in the rubber bag above the soil surface, during the initial pore water pressure equilibration stage. The density of the fluid in the rubber bag was chosen in combination with the additional bag height to model a particular earth pressure coefficient profile. The total vertical stress at the bottom of the trench was in all cases approximately equal to the total vertical stress in the adjacent soil.

'Boundary control' refers to the end of the strongbox furthest from the trench. For tests 1 to 4, this boundary was strain controlled. In tests 5, 6 and 7 a stress controlled boundary was imposed by installing a second, fluid-filled rubber bag at the end of strongbox furthest from the trench. Plane strain conditions were adopted, with the

trench running the full width of the strongbox in all but test 4 where a quarter width bag was used.

In test 5, the rubber bag was overfilled with water and passive failure occurred in the soil adjacent to the trench prior to excavation and concreting. The results obtained from test 5 gave an indication of the levels of stress imposed by the rubber bag on the surrounding strata that would cause failure and are presented in section 5.7 at the end of chapter 5.

| TEST No. | Additional bag height (m) | Fluid density ($kg/m^3$) | Boundary control | Other information |
|---|---|---|---|---|
| 1 | 9 | 1.172 | strain | |
| 2 | 18 | 1.000 | strain | |
| 3 | 14 | 1.040 | strain | |
| 4 | 9 | 1.172 | strain | 1/4width |
| 5 | 18 | 1.000 | stress | failed |
| 6 | 18 | 1.000 | stress | |
| 7 | 14 | 1.040 | stress | light mix |

Table 5.1 *Test characteristics*

Pore pressure and total stress transducers were placed at four depths adjacent to the trench and at four positions back from the trench. The configuration of the transducers is shown in figure 5.1. This configuration was maintained for all of the tests but the results presented do not give pore pressure readings and total stress readings for all positions in all tests. Transducers often failed during a test or (when in short supply) were not installed in all positions.

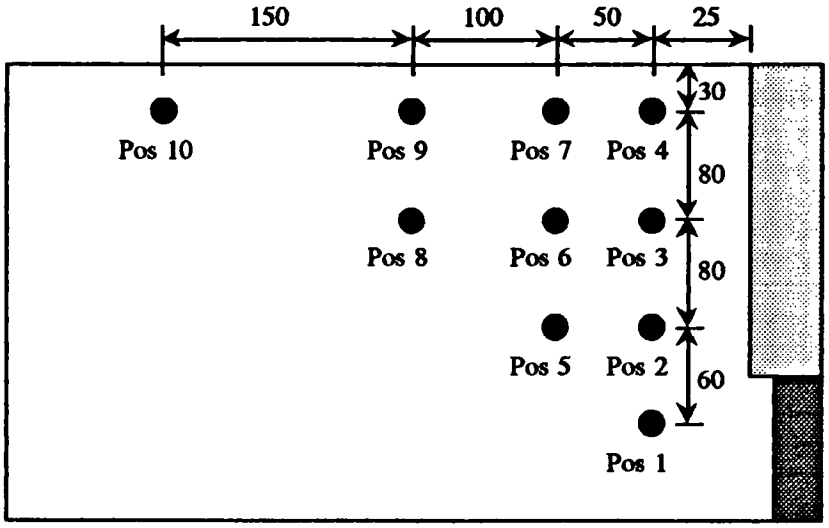


Figure 5.1 *Transducer layout (dimensions are shown in mm at model scale)*

The total stress transducer in position 1 is referred to as TST 1 and the pore water pressure transducer at position 1 as PPT 1 and so forth. The 'shallowest depth transducers' refer to positions 4, 7, 9 and 10; 'mid trench' refers to positions 3, 6 and 8; 'at' or 'around the toe' are positions 2 and 5; and 'deepest' or 'beneath the toe' refers to position 1.

### *5.1.3 Presentation of results*

The results in this chapter are presented in 5 main sections. The first section is concerned with the 'standard' case, test 3. The standard case is used to highlight the trends and stress change patterns exhibited by all tests, so that other results may be easily compared. The next two sections cover the effects of different in situ and boundary stress conditions on the surrounding soil, as mentioned previously. The fourth section looks at the effect of using concretes of different densities during installation. The last section details the results from tests 4 and 5 and discusses the effects of a quarter width trench and the levels of lateral pressure in the rubber bag that cause passive failure at the top of the trench.

Test results are presented at prototype scale with model dimensions multiplied by 100 and elapsed times by $100^2$. Other scaling factors were discussed in chapter 3.

## *5.2 The standard case - Test 3*

### *5.2.1 Introduction*

Test 3 was performed under conditions of plane strain with a strain controlled (ie. fixed) boundary at the remote end of the strongbox. A neoprene rubber bag was filled to a height of 32.5m (14m above ground level) with a weak saline solution (unit weight 1.04 kg/m$^3$) to give an earth pressure coefficient against depth profile that was consistent with published field data. The $K_o$ against depth profile used in test 3 is given in figure 5.12, where the effects of three different profiles were considered and compared to published data.

### *5.2.2 Pore water pressure results*

The pore water pressure measured by the deepest transducer (at 25m) corresponded closely with hydrostatic levels whilst PPTs 2, 3 and 4 measured values that were slightly less than expected. During reconsolidation (prior to excavation) the sample swelled, the transducers therefore did not remain at the same depth relative to the groundwater level and recorded slightly less than expected values. The combined effects of swelling and increased temperatures whilst the centrifuge was in operation had a desiccating effect on the surface of the sample, thus slightly further reducing the groundwater level relative to the model surface.

After reconsolidation but prior to excavation, satisfactorily steady levels were recorded by pore water pressure transducers, total stress transducers and the LVDTs monitoring soil surface movements. Pore water pressures from different tests, after reconsolidation, but before excavation are shown in figure 5.2 below.

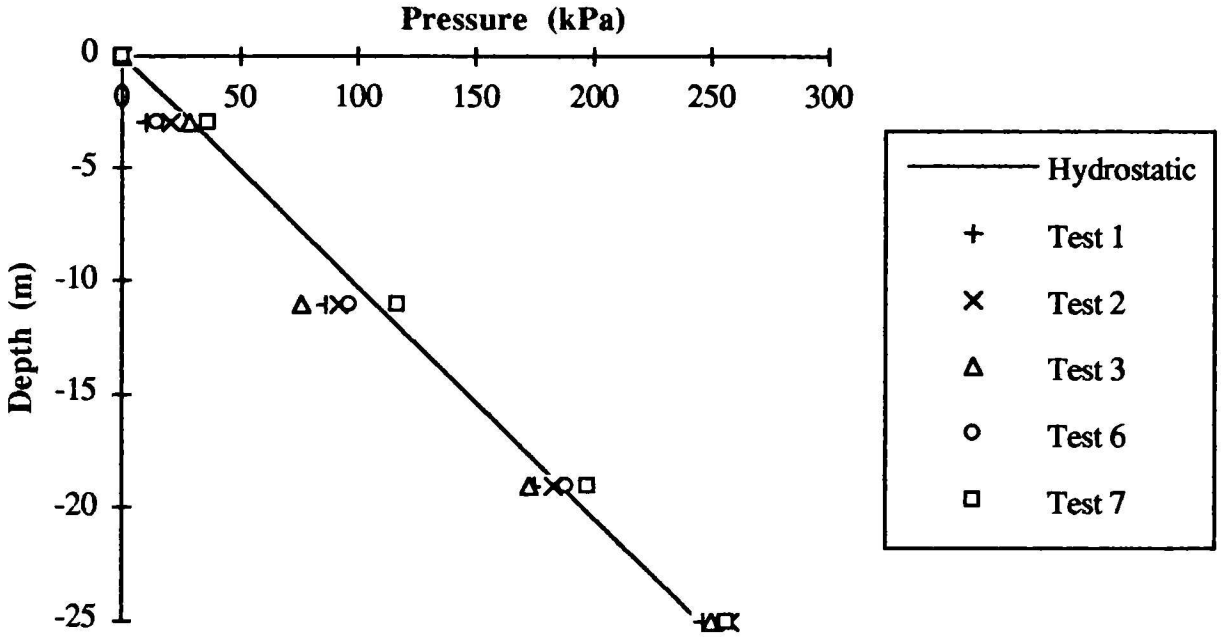


Figure 5.2 *Pore water pressures prior to excavation*

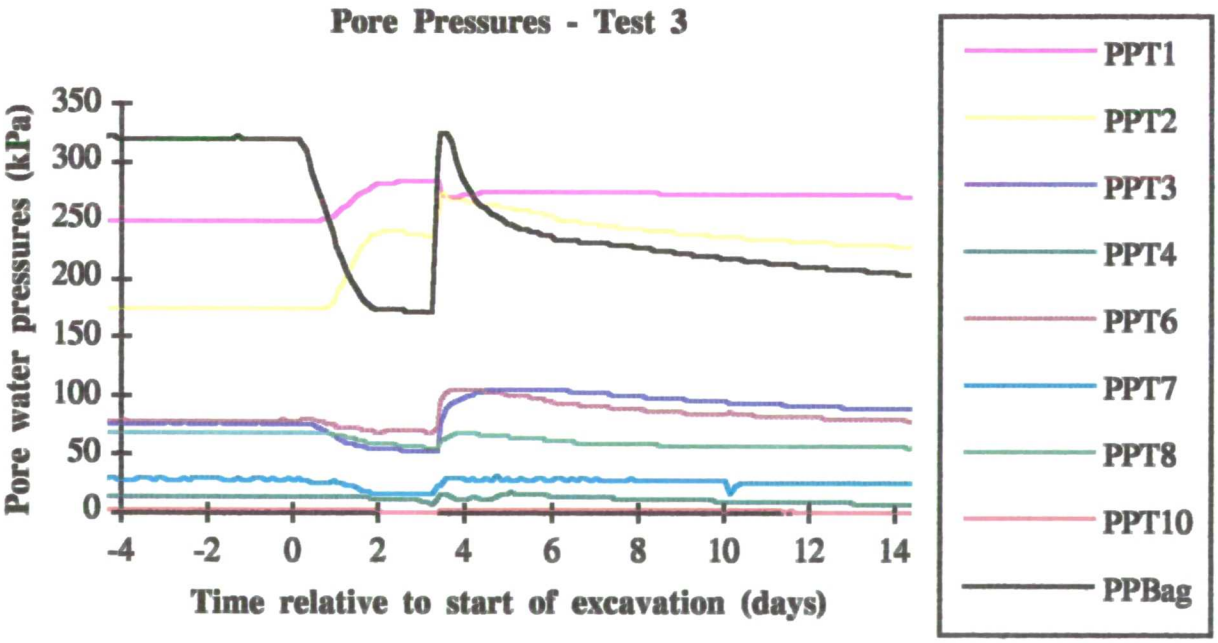


Figure 5.3 *Porewater pressure transducers - Test 3*

In figure 5.3, the time axis is presented relative to the start of excavation. The PPBag trace demonstrates the different stages of the wall installation process. The excavation stage is defined by a measured fall in bag pressure of 140 kPa; this corresponds very closely to the expected reduction in pressure during excavation of 143 kPa, due to the draining out of the excess height of fluid above ground level.

PPBag then measured a drop of 25 kPa during dilution was also close to the expected value, before measuring an increase of 163 kPa during concrete placement.

#### *5.2.2.1 Pore water pressures during excavation*

Pore water pressures at the shallowest depth (3 m) are recorded by the transducers at positions 4, 7 and 10. Results from PPTs 4 and 7 show little change in pore water pressure during excavation, but more than at position 10 (17.5 m back from the trench) where very little response was indicated.

At a depth of 11 m (mid trench) the greatest drop in pore water pressure was exhibited at position 3 (2.5 m back from the trench), with excavation having a diminishing effect at positions 6 (7.5. m back) and 8 (17.5 m back). The soil at this depth behaved in an undrained manner with significant changes in pore water pressure occurring due to changes in lateral stress in the trench.

At depths beneath and around the toe of the trench (PPT 1 and PPT 2) increases of approximately 33 kPa and over 65 kPa respectively were recorded during trench excavation. Beneath the toe of the trench, conditions of zero horizontal strain were maintained. An increase in lateral stress was recorded as a result of stress redistribution due to the vertical arching effect described by Terzaghi (1943). The increase in pore water pressure at position 2 was large and approximately double the change experienced at position 1.

In summary, during excavation horizontal total stress relief occurred at the face of the trench. Pore water pressures decreased with a semi-drained response at the shallowest depths. At all depths, transducers further back from the trench showed less response to the effects of excavation than those near the trench.

#### *5.2.2.2 Pore water pressures during concrete placement.*

As described in chapter 3, during placement the simulated concrete mixture was allowed to fall through a height of at least 10 m. The method of placement would undoubtedly have had a significant effect on the values recorded both in the trench and in the model directly after dumping. During placement the fluid in the rubber bag was displaced vertically by the powder, thus increasing the vertical stress recorded at the bottom of the trench. Much of the fluid was absorbed, with the remaining fluid draining from the bag valve into the catch tanks. This was most

prominently indicated by the PPBag response, with an initial high peak dissipating quickly directly after placement.

The measured pore water pressures at positions 3 and 4 (adjacent to the trench) increased dramatically during installation but did not reach peak recorded values immediately. This was due to the delay in transducer response as a result of blockages in the porous stones (Konig et al. 1994) and despite wall installation occuring approximately 3 days after excavation, at position 3, the peak value was not reached until nearly 6 days. Also at this position, the peak pore water pressure values dissipated more slowly than at shallower depths due to the increased length of the drainage path. Measured pore water pressures returned to hydrostatic values after the concrete hardened and the soil had consolidated.

In other positions responses were different: Near the surface of the trench, responses were smaller due to the semi-drained conditions that existed near the surface of the model: At the toe of the trench, large increases in pore water pressure were measured due to wall placement effects: Beneath the toe of the trench a slight reduction was measured immediately after placement due to stress redistribution. This reduction may best be explained as the reverse of the vertical arching effect, following the increase in imposed pressure by placing the concrete in the trench.

As expected, the effects of wall installation on the pore water pressures in the surrounding strata diminished with distance from the trench.

#### *5.2.2.3 Long term pore water pressures*

Figure 5.4 indicates that pore water pressures in the long term generally returned to near hydrostatic levels. The levels achieved at 5000 days (in all but positions 8 and 10) were within 10% of the pre-excavation values. At positions 8 and 10, the traces indicate that reconsolidation was not fully achieved prior to excavation, with pore water pressures increasing at a similar rate before and after the construction sequence, before levelling off to steady values.

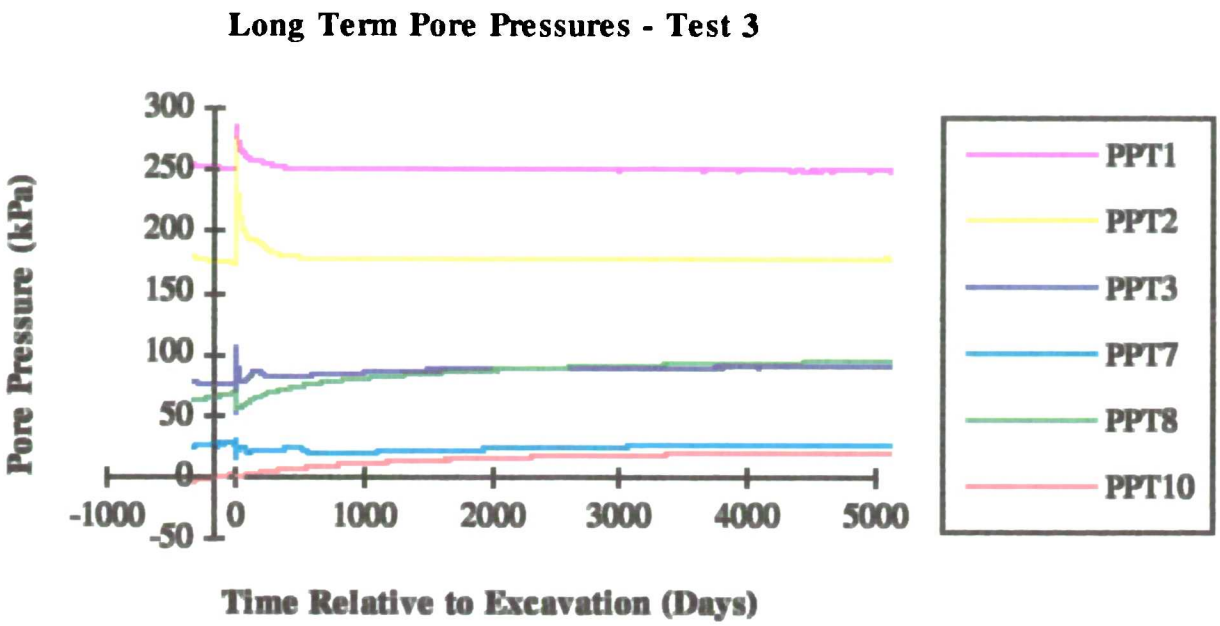


Figure 5.4 *Long term pore water pressures - Test 3*

### *5.2.3 Total stresses*

During calibration and testing, the total stress transducers exhibited consistent scale factors but a range of offsets, and hence the results presented in this chapter are used as only a measure of the changes in total stress rather than absolute values.

In figure 5.5, the pre-excavation values at positions 1, 2, 3, 6, and 8 were shifted to expected pre-excavation levels so traces from transducers at different positions could be distinguished easily. The traces at positions 4 and 7 were not adjusted as the recorded values were approximately correct.

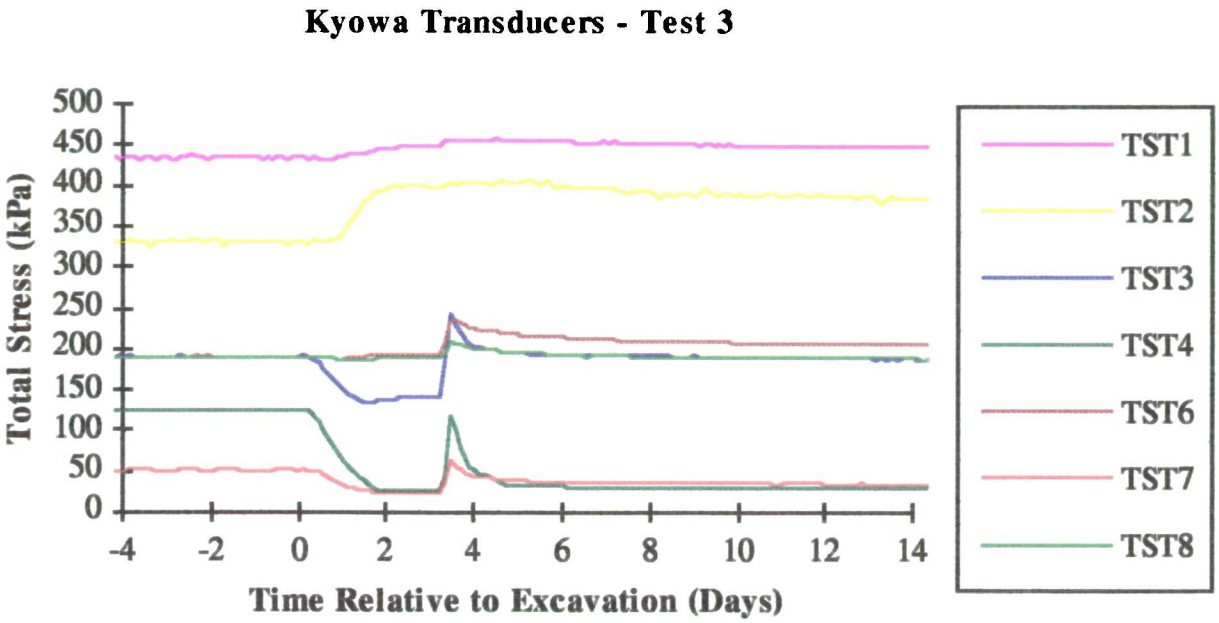


Figure 5.5 *Total stress transducers - Test 3*

### *5.2.3.1 Total stress changes during excavation.*

Throughout the depth of the trench, the lateral stress was reduced by 143 kPa as the fluid in the bag was drained to ground level. This was reflected by a total stress relief of nearly 100 kPa recorded at position 4, and 25 kPa at position 7. At position 3, where undrained conditions prevailed, a reduction in total stress of only 57 kPa was measured. At and below the toe of the trench total stresses increased due to vertical arching effects. At all depths, effects were more pronounced close to the trench than further away. The trends highlighted in test 3 were followed in other tests.

### *5.2.3.2 Total stress changes during concrete placement.*

Concrete placement resulted in an increase in total stress at all positions within the soil model. At positions 1 and 2, the changes due to concrete placement were very much less than the changes due to excavation. In contrast to the pore water pressures during placement, total stresses at these positions remained approximately constant throughout concrete placement. At the mid trench position, immediately after placement, increases in total stress diminished quickly and at 6 days after excavation

the average value recorded by the transducers was very close to pre-excavation stress levels due to the consolidation of the fresh wet mixture.

At the shallowest depths (TSTs 4 and 7), the change due to wall placement was greatest near the trench and diminished quickly, returning (in less than three days after placement) to a value that was considerably lower than the pre-excavation level and approaching the pre-concreting level.

### *5.2.3.3 Long term total stresses.*

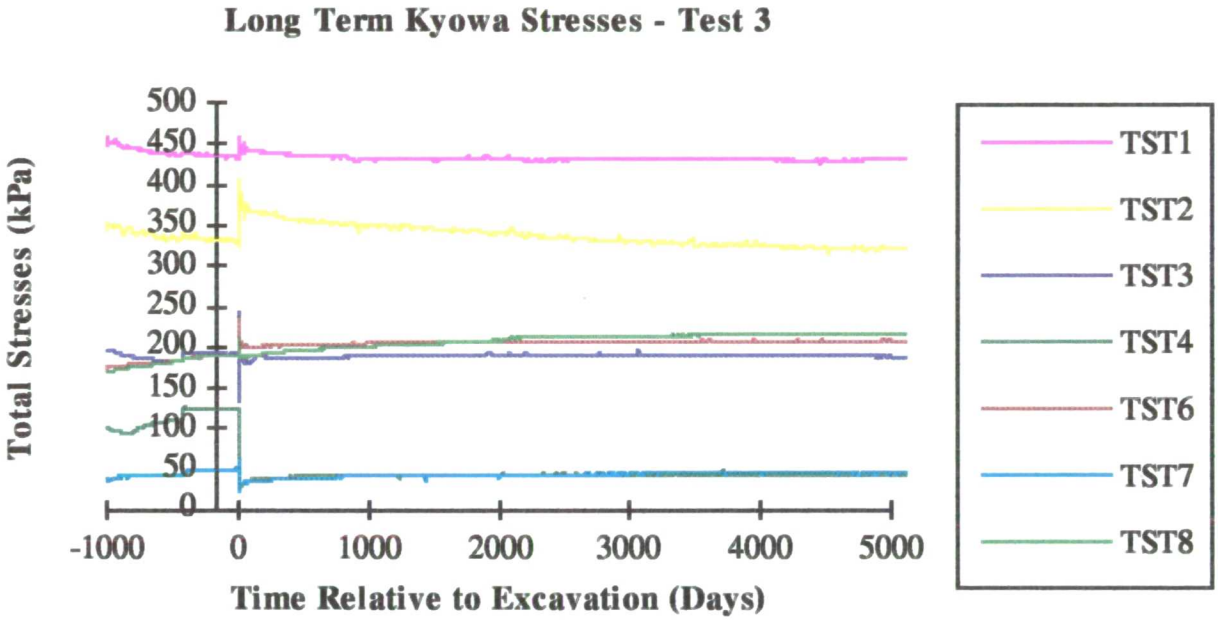


Figure 5.6 *Long term total lateral stresses*

At the toe of the trench (TSTs 1 and 2) the increase in total stress due to wall placement dissipated over a considerable period of time, eventually returning to pre-excavation levels. At mid trench, values after installation were similar to pre-excavation levels except at position 8 where re-consolidation continued to occur as demonstrated in figure 5.4 by PPT 8.

In the long term, at all but the shallowest depth, total stresses returned to close to pre-excavation values. This was partially due to concreting, where some of the reduction in stress was reapplied. Results from the transducers at positions 4 and 7 (where $K_o$ values were greatest) clearly indicated that the drop in total stress that occurred during excavation was not recovered by concrete placement. Further details of the stress relief that occurred during the wall installation process are given

in section 5.4 where the effects of different earth pressure coefficients are considered.

### *5.2.4 Settlements.*

The settlement traces are given for four different LVDT positions back from the trench. LVDT 1 is 2.5 m back; 2, 7.5 m; 3, 17.5 m and 4, 32.5 m. Results suggest that nearest the trench the measured settlement was about 900 mm with diminishing values recorded at positions further back from the trench.

Generally, an analysis carried out under conditions of plane strain will tend to over-estimate stress relief and settlements that occur in a three dimensional field situation. Conventional diaphragm wall panel installation would provide some stability to the trench with trench ends redistributing the change in total horizontal stress. Kantartzi (1994) and Ng (1993) looked at the effects of different panel widths and the results from panels of a finite length. Results from test 4 (where a quarter width trench was used) are presented in section 5.7.

Figure 5.7 below indicates settlements up to 24 days after the start of excavation. At 24 days the settlements were approaching their long term values indicating that the disturbance due to diaphragm wall installation occurs entirely in the short term.

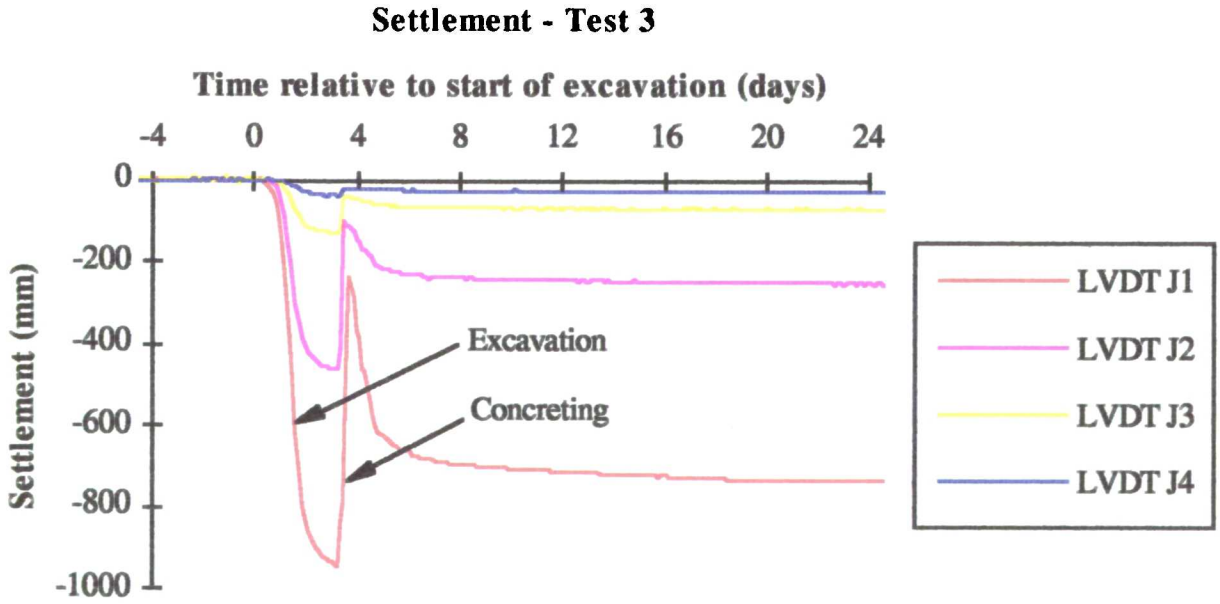


Figure 5.7 *Settlements - Test 3*

As with the changes in total stress, the excavation stage had a greater effect on the settlements than the concreting stage. The settlement traces clearly indicate that the stress reversal that occurs during wall placement has a significant effect in the short term, but, as the concrete consolidates the ground surface settles back to near pre-concreting levels.

## *5.3 The effects of a stress controlled boundary.*

### *5.3.1 Introduction.*

In test 6, a stress controlled boundary was imposed at the remote end of the strongbox. This was achieved by placing a second rubber bag at the remote end of the strongbox, 50m from the trench, and filling it with water to a height of 36.5 m (an upstand of 18 m above the soil surface). The $K_o$ condition imposed on the sample at the remote end by the second rubber bag was the same as that imposed on the sample at the trench end in tests 2 and 6 (see figure 5.12). Fluid pressure applied by the second rubber bag prevented any stress relief that might otherwise have occurred at the remote end of the strong box.

Test 2 and test 6 provided a comparison of different boundary conditions at the remote end of the strongbox by employing similar conditions at the trench end. However, due to the nature of centrifuge testing, it was very difficult to reproduce exact test conditions and two significant differences between the tests are discussed below.

Test 6 was a repeat of test 5 in which the rubber bag was over-filled and passive failure occurred in the soil adjacent to the trench. To prevent failure reoccurring, a bag support was adopted in test 6 that penetrated 1.5 m into the soil. The changes that were recorded by the transducers at position 4 were less than expected as the bag support also restrained the soil at the edge of the trench, limiting lateral movement and reducing stress relief during excavation. In test 2, the bag support plate only penetrated 0.5 m into the soil.

The results recorded at position 4 showed a smaller than expected fall in porewater pressure, total and effective stress, with greater changes experienced at position 3. The effects of the bag support could be comparable with the effects of guide walls

which are commonly used during diaphragm wall installations in clay and fine grained soils, but are in practice unlikely to offer such firm support.

The second difference between the two tests occurred during concrete placement when in test 6 the simulated concrete was not deposited into the trench in a single pour but in two stages. The pore water pressures and total stresses recorded a greater response after the first pour than after the second and it is therefore reasonable to assume that more of the mixture was dumped at four days than seven. Figures 5.9 and 5.11 show the results obtained from test 6 where the double pour effect is clearly shown. In the longer term, the two stage dumping of the concrete had only a minimal effect on the stresses.

### *5.3.2 Pore water pressure results.*

Figure 5.8 below indicates that changes in pore water pressures were close to expected values, with the model returning to hydrostatic conditions after installation. However at position 3 the measured pore pressure diminished to less than the pre-excavation values after wall installation. At 25 days after concreting, pore pressure readings showed a slight increase in hydrostatic values in all except position 3. This may be attributable to either slight upward transducer movement or recording error.

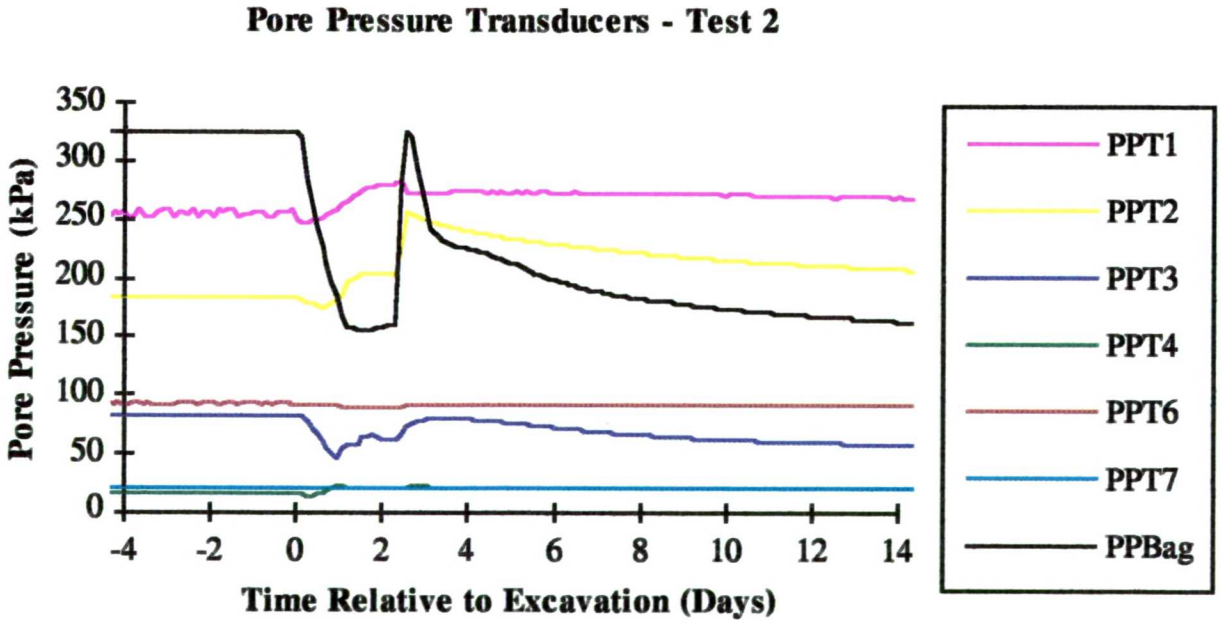


Figure 5.8 *Porewater pressure transducers - Test 2*

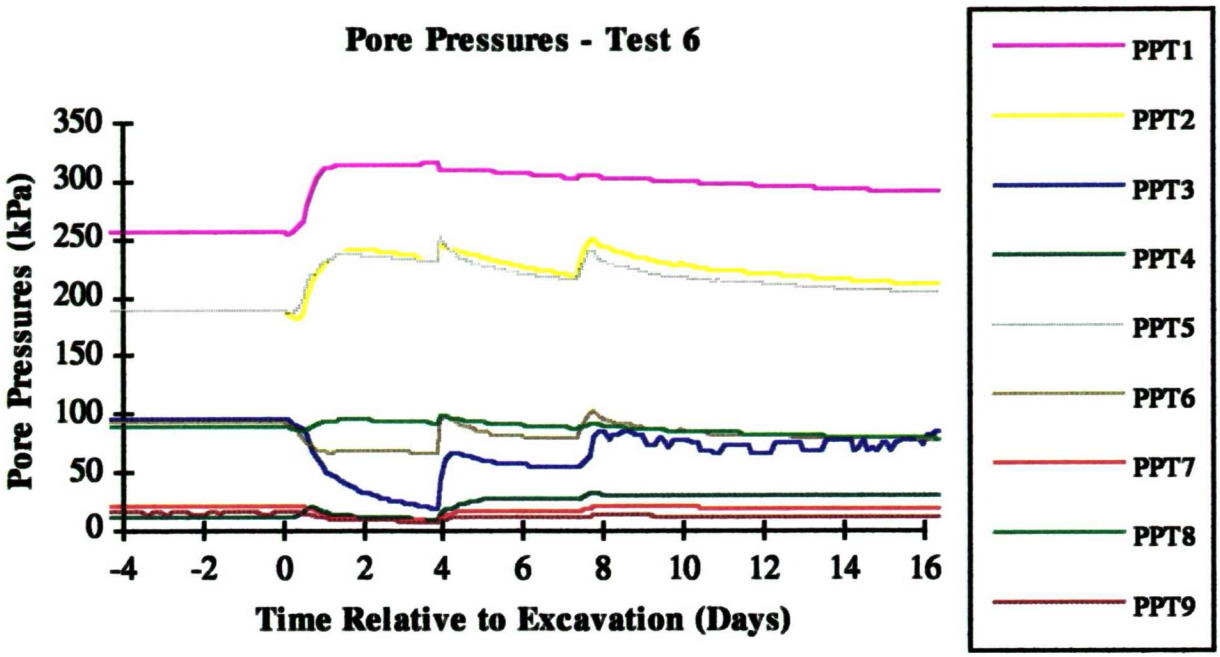


Figure 5.9 *Pore pressures - test 6*

The effect of excavation on the pore water pressures in test 6 was considerable at all but the shallowest positions. The greatest reduction was measured at position 3 with changes diminishing further back from the trench. Beneath the toe of the trench dramatic increases were measured during excavation, with smaller changes occurring during wall placement.

After both pours the initial increase in pore water pressure in the soil dissipated as the lateral stresses applied to the sides of the trench decreased due in part to concrete consolidation.

### *5.3.3 Total stress results.*

In test 2, a drop of 177 kPa was expected in the rubber bag during excavation. This was reflected by a change in hydrostatic fluid pressure of 170 kPa measured by PPBag and a change of 179 kPa in total lateral stress measured by TST 4 (these small discrepancies are within acceptable limits for transducer and system errors). The changes at shallow depths indicated a drained response, with the change in total lateral stress recorded substantially by the total stress transducer but not by the pore water transducer indicating a change in effective stress taking place during the excavation process.

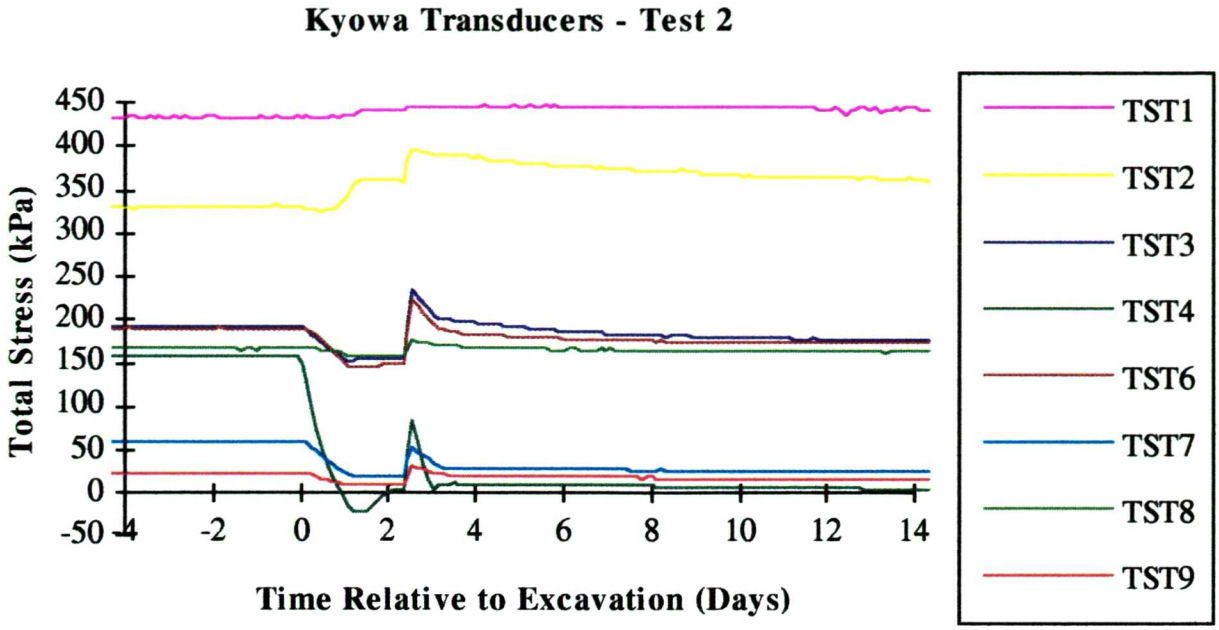


Figure 5.10 *Total stress transducers - Test 2*

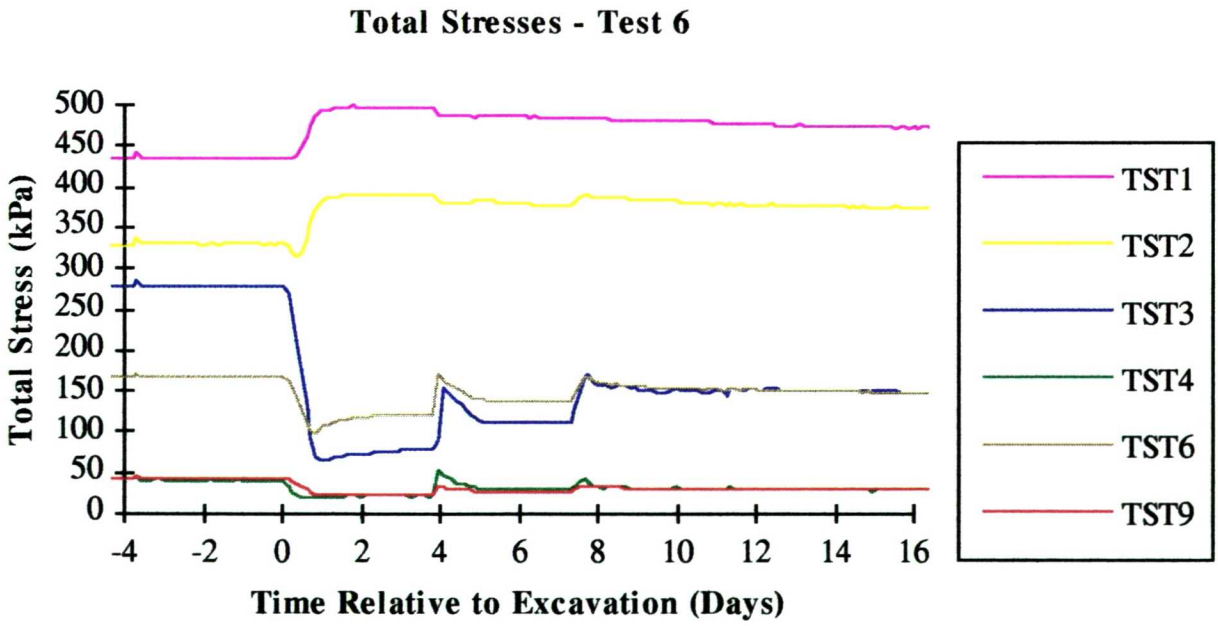


Figure 5.11 *Total stress transducers - Test 6*

In test 6, a drop of 176 kPa was measured by the transducer in the rubber bag which was reflected by a change of 208 kPa recorded at position 3. The measured total stress relief at position 3 in test 6 was much greater than at the shallowest depth

(position 4) but this is due to the effect of the bag support plate at the surface of the soil model, as mentioned above.

In summary, at position 3, greater total stress relief was experienced in test 6 than in test 2, while at position 4 greater relief was experienced in test 2 than in test 6. At and below the toe of the trench similar short term increases were recorded in both tests.

### *5.3.4 Comparison of results of different boundary conditions.*

Data presented in table 5.2 are given relative to pre-excavation levels. That is, 'imm. post conc' is the recorded difference between pre-excavation and post-concreting readings. Changes in effective stress are derived from the measured changes in total stress and measured changes in pore water pressure.

**Test 2**

| Depth | Trans | Immed. Post conc. | | | 25 days post concreting | | |
|---|---|---|---|---|---|---|---|
| (m) | number | total | pwp | effective | total | pwp | effective |
| 3 | 4 | -72.9 | 6.7 | -79.6 | -155.1 | 4.4 | -159.5 |
| 11 | 3 | 42.8 | -3.2 | 46.0 | -19.3 | -28.7 | 9.4 |
| 19 | 2 | 66.4 | 73.4 | -7.0 | 21.8 | 10.8 | 11.0 |
| 25 | 1 | 8.8 | 14.2 | -5.4 | 1.8 | 1.6 | 0.2 |

**Test 6**

| Depth | Trans | Immed. post conc. | | | 25 days post conc. | | | 5000 days post con. | | |
|---|---|---|---|---|---|---|---|---|---|---|
| (m) | number | total | pwp | effect | total | pwp | effect | total | pwp | effect |
| 3 | 4 | 12.9 | 13.1 | -0.2 | -10.7 | 16.3 | -27.0 | -12.3 | 37.3 | -49.6 |
| 11 | 3 | -121.1 | -30.2 | -90.9 | -135.1 | -6.2 | -128.9 | -96.2 | 31.6 | -127.8 |
| 19 | 2 | 50.3 | 56.1 | -5.8 | 42.0 | 11.2 | 30.8 | 52.0 | 14.2 | 37.8 |
| 25 | 1 | 53.9 | 53.9 | 0 | 33.1 | 26.0 | 7.1 | 23.2 | 11.8 | 11.4 |

Table 5.2 *Changes in pressure relative to pre-excavation levels (kPa).*

In table 5.2, the changes presented due to concreting for test 6 are between values measured immediately prior to the first pour and at different times after the second pour. The changes in total stress and pore water pressure were slightly smaller in

test 6 than test 2 due to some dissipation of the excess pore water pressures in the soil between the two pours.

In both tests, adjacent to the trench (positions 3 and 4), lateral effective stresses decreased between placement and 25 days post placement as the concrete hardened and the excess pore water pressures in the soil around the trench dissipated. In the longer term in test 6, effective stresses continued to decrease at position 4 and remained at similar values in position 3. The stress controlled boundary therefore, had no noticeable influence in re-establishing pre-excavation stresses in the long term. The influence of the stress controlled boundary is undetectable at these shallower positions and any differences that may have occurred are small compared with the differences due to the bag support.

In both tests at the two deepest positions, the effective stress changes were very much smaller. The measured increases in total stress after the wall installation processes were almost entirely due to changes in pore water pressure - this is consistent with quasi-elastic (undrained) soil behaviour. The slightly greater increases recorded at and near the base of the trench in test 6 were sufficiently small to have no implication for practice and are unlikely to have been due to the stress controlled boundary, as both positions 1 and 2 were beneath the depth of the bottom of the second rubber bag.

The overall effect of the stress controlled boundary was not obvious, especially as other discrepanices between the tests caused some significant differences in the results. It may be concluded that adjacent to the trench the effects of the stress controlled boundary were undetectable, and that differences in wall construction methods such as a double concrete pour or the presence of guide walls will have a much more significant effect on the resulting stress distribution than the boundary 50m away.

## *5.4 The effects of different initial earth pressure coefficients*

### *5.4.1 Introduction*

Tests 1, 2 and 3 investigated the effects of different pre-excavation earth pressure coefficient profiles on ground movements and stress changes during diaphragm wall installation. The different profiles are presented in figure 5.12, with a passive failure cut-off assumed at $K_o = K_p = 2.56$ (corresponding to $\phi'_{peak} = 26^\circ$ from Kantartzi, 1994). Stresses in the rubber bag at ground level in the model exceeded those at which failure of the soil would have been expected. In order to prevent failure in the soil, the rubber bag support plate was embedded 0.5m into the soil. This is discussed more fully in chapter 3.

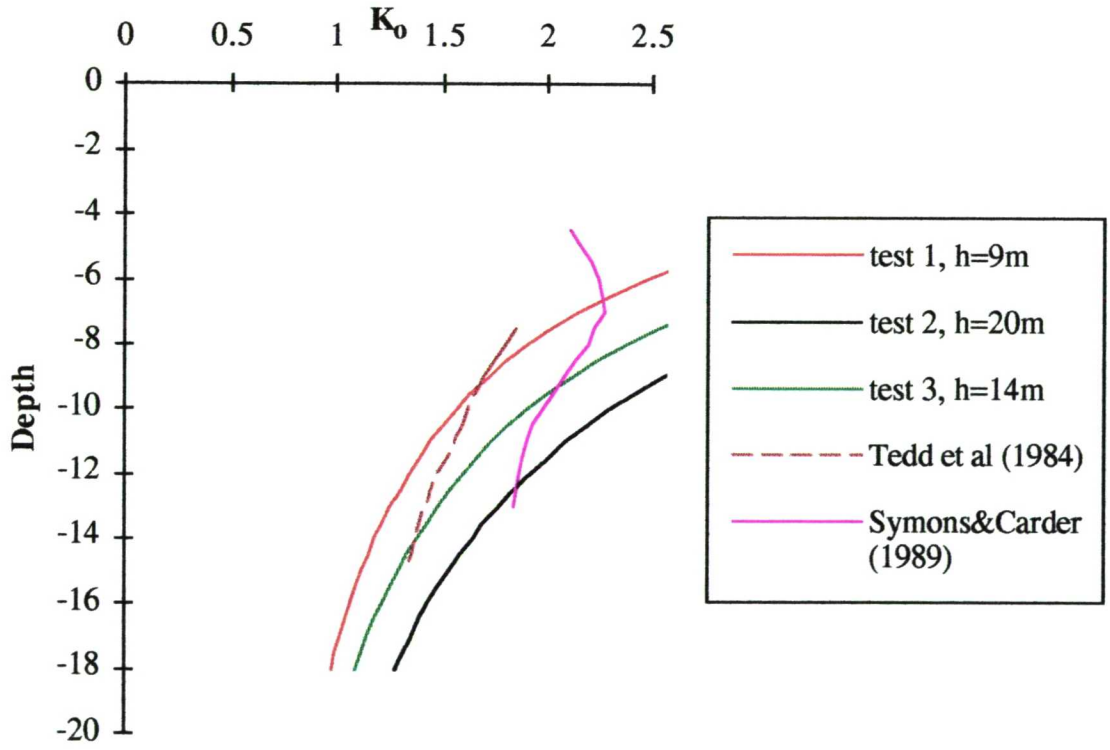


Figure 5.12 *Comparison of different earth pressure coefficients*

Figure 5.12 shows data measured by Tedd et al. (1984) and Carder and Symons (1989). The different $K_o$ against depth profiles were obtained using different levels of fluid (of different densities ranging from 1.0 kg/m$^3$ to 1.172 kg/m$^3$) in the rubber bag in the trench as described in chapter 3.

Figure 5.12 also shows values of $K_o$ well in excess of $K_p$ for depths of up to 10m. However, in the centrifuge tests failure only occurred once (in test 5) and otherwise the soil was able to tolerate these high pressures. Burland and Fourie (1985) carried out a series of triaxial tests in order to measure mobilized angles of friction during one dimensional consolidation. They concluded that under conditions of limiting passive equilibrium (passive stress relief), friction angles greater than 30° were encountered. Further, during testing on an undisturbed London Clay a maximum value of $\phi'_{mob} = 46.8°$ was measured, suggesting that values of $K_p$ may exceed those calculated by the Rankine method.

### *5.4.2 Presentation of results*

Results from test 1 are presented in figures 5.13 and 5.14 below and are compared with the results presented in figures 5.8 and 5.10 from test 2, and figures 5.3 and 5.5 from test 3.

**TEST 1**

The installation procedure for the total stress transducers adopted in test 1 (as discussed in chapter 3) caused some of the total stress transducers to rotate. Careful exhumation of the transducers indicated that only the six transducers referred to below were actually measuring lateral total stresses. Pore water pressures were recorded at most positions.

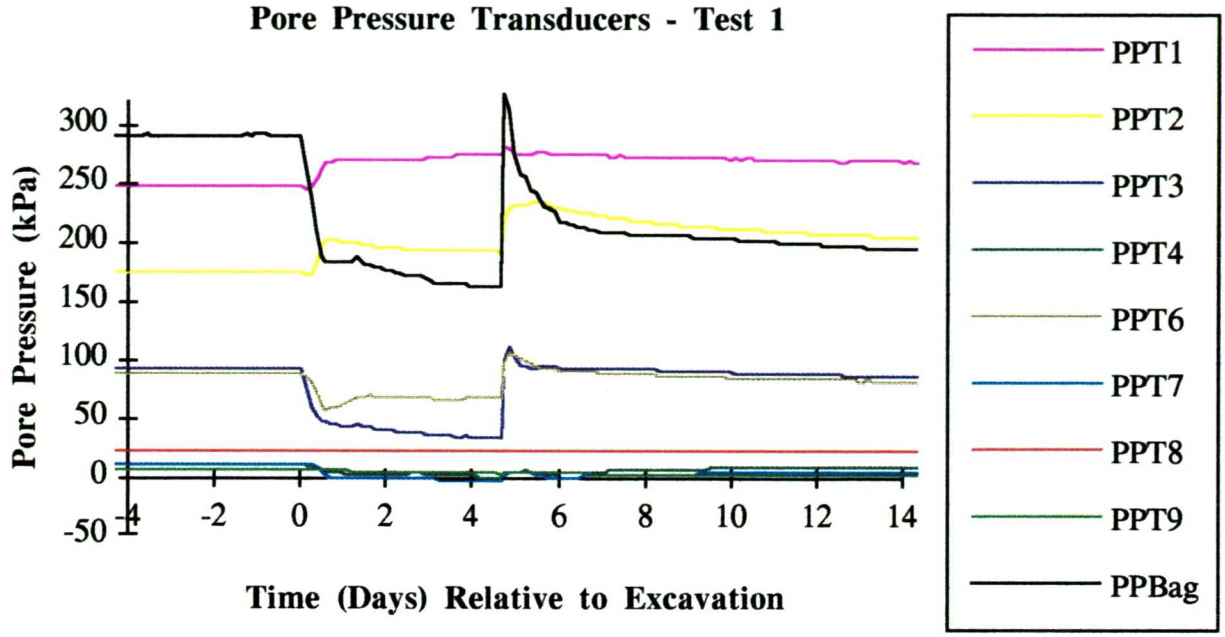


Figure 5.13 *Pore water pressure transducer results - Test 1*

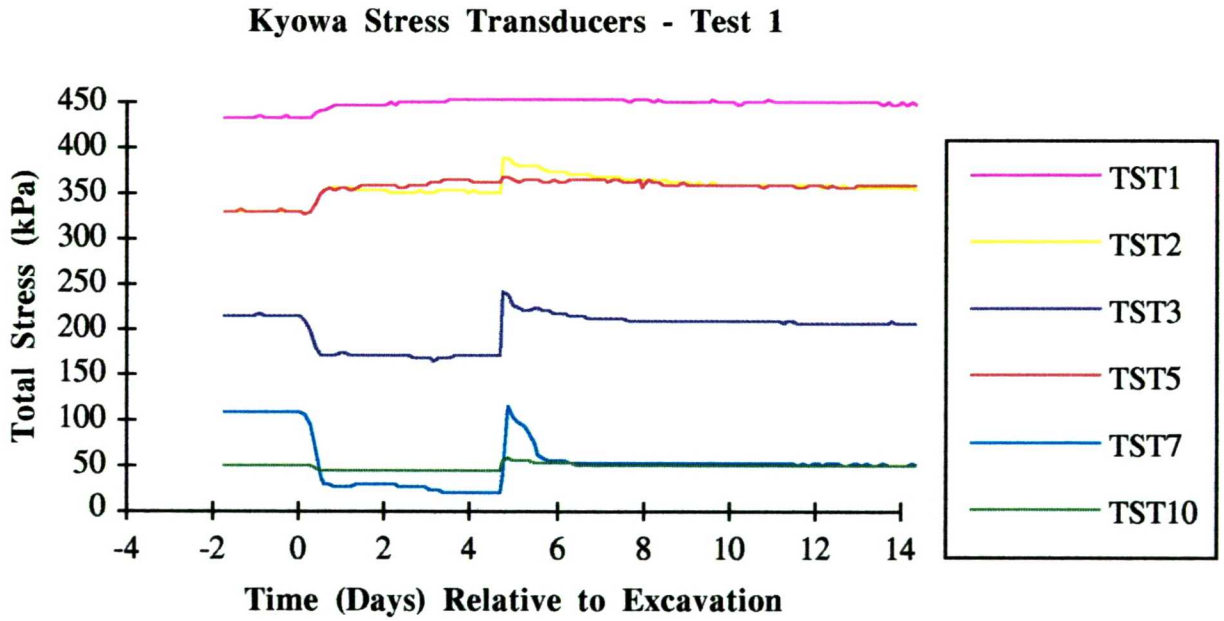


Figure 5.14 *Total stress transducer results - Test 1*

At position 7 (the shallowest position), a drop in total lateral stress of 80 kPa was recorded during excavation as the rubber bag was drained to ground level. During concrete placement a total stress of 95 kPa was reapplied. This quickly dissipated to, at 25 days, a level that was 50 kPa less than the original pre-excavation value. The changes in pore water pressure at this position were far less pronounced than

originally expected and hence the changes in effective stress are substantially the same as the changes in total stress. The values recorded at position 7 were smalller than would have been recorded closer to the trench at the same depth.

At mid depth, after wall installation, total stresses adjacent to the trench fell quickly to their pre-excavation values. By 25 days the overall change in pore water pressure due to the construction process of the diaphragm wall installation was negligible and a small overall increase in effective stress was measured. At position 2, near the toe of the trench, a larger than expected increase in pore water pressure and total stress was measured; this may have been a dynamic effect due to the depositing technique adopted.

## TEST 2

In test 2, the highest in situ earth pressure coefficient was applied, with a horizontal total stress relief of 176 kPa occurring during excavation. Semi-drained conditions were observed at a depth of 3 m, resulting in a measured change in total stress that was similar to the change experienced in the trench with only a small response in the pore water pressure transducer at the same position. A comparison of total lateral stress at position 4 prior to excavation and at 25 days after wall installation indicated an overall stress relief of 155 kPa, after pore water pressures had returned to pre-excavation values.

## TEST 3

In test 3, an intermediate earth pressure coefficient profile was applied and the reduction in lateral pressure during excavation was 147 kPa. Accordingly, the total and effective lateral stress relief at position 4 was between the values recorded in tests 1 and 2. Effective stress reductions were measured at all other levels in the model.

### *5.4.3 Comparison of results*

Values of changes in pore water pressure, lateral effective stress and lateral total stress for the different transducers are given in table 5.3. The values in the columns refer to the changes in stresses or pressures. Negative values indicate stress relief.

#### *5.4.3.1 Comparison of the effects of excavation*

As already mentioned the pore water pressure transducer response time was often longer than that of the total stress transducers due to blockages in the porous stone that protected the transducer diaphragm. The values used to mark the start and end of excavation were usually obvious for each trace; however in some circumstances, there was no pronounced 'end' of excavation and a value was taken from the results at approximately the correct time. In the longer term, the data presented were easier to collate as both transducer types had reached stable values.

'Bag Change' refers to the change in total stress due to draining the fluid down to ground level.

| Excavation | | Test 1 | | | Test 2 | | | Test 3 | | |
|---|---|---|---|---|---|---|---|---|---|---|
| Depth | Trans | Bag change = -103.5 | | | Bag change = -176.6 | | | Bag change = -142.8 | | |
| (m) | number | total | pwp | effect | total | pwp | effect | total | pwp | effect |
| 3 | 4 (7)* | -80.2 | -10.6 | -69.6 | -179.3 | 6.6 | -185.9 | -98.7 | -1.1 | -97.6 |
| 11 | 3 | -45.2 | -32.6 | -12.6 | -38.2 | -36.4 | -1.8 | -56.6 | -22.7 | -33.9 |
| 19 | 2 | 28.7 | 25.7 | 3.0 | -4.4 | -7.7 | 3.3 | 60.0 | 66.8 | -6.8 |
| 25 | 1 | 15.8 | 23.6 | -7.8 | -2.6 | -9.7 | 7.1 | 8.8 | 33.0 | -24.2 |

Table 5.3 *Effective stress changes due to excavation (* marks drained conditions) (kPa)*

In positions where undrained conditions exist and soil behaves as a quasi-elastic material one of two assumptions may be made. First, if it assumed that during wall installation shear effects are negligible then changes in vertical total stress would be zero, such that

$$s' = \frac{\sigma'_v + \sigma'_h}{2} = \frac{\sigma_v + \sigma_h}{2} - u = \text{constant.}$$

$$\Delta s' = \frac{\Delta\sigma_v + \Delta\sigma_h}{2} - \Delta u = 0 \quad \text{as there is no change in volume; hence}$$

$$\Delta u = \frac{\Delta\sigma_h}{2} \; ; \; \Delta\sigma'_h = \Delta\sigma_h - \Delta u$$

$$\Delta\sigma'_h = \Delta\sigma_h - \frac{\Delta\sigma_h}{2} = \frac{\Delta\sigma_h}{2}$$

$$\Delta\sigma'_h = \Delta u = \frac{\Delta\sigma_h}{2}$$

suggesting that changes in total lateral stress would be twice the changes in pore water pressure at the same position. Alternatively, if conditions of zero vertical strain are adopted then in order for $s'$ to remain constant

$$\Delta u = \Delta\sigma_h$$

In undrained positions, although porewater pressures generally were reduced by less than total stresses the ratio $\Delta u$:$\Delta\sigma_h$ was greater than 0.5. Therefore conditions fell between the two elastic analysis assumptions, and so some stress redistribution and some change in vertical strain may have occurred. It is also possible that in some locations, the changes in applied stress were large enough to generate additional pore water pressure changes (particularly suctions) due to shear.

Figure 5.15 demonstrates the effects of excavation, and shows that for the drained conditions at or near the surface, changes in lateral stress in the bag led rapidly to changes in lateral effective stress in the soil.

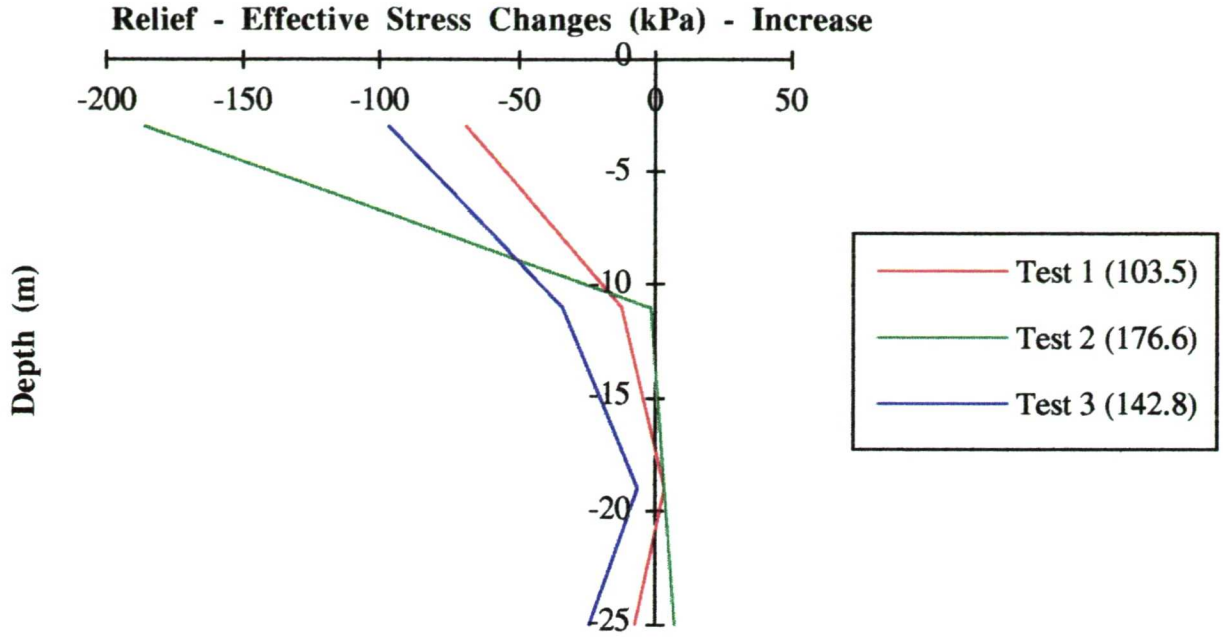


Figure 5.15 *Lateral effective stress changes due to excavation.*

The numbers in the legend given in brackets refer to the change in total stress that occurred in the trench as the bag was drained down to ground level in the model. Also, it should be noted that the results given in test 1 are from position 7 and not position 4. As figure 5.15 demonstrates, during excavation, the biggest initial earth pressure coefficient reduction in the trench occurred in test 2 and led to the biggest recorded reduction in lateral stress at position 4; this pattern was observed in tests 1 and 3.

Further down the trench, the effective stress relief was much smaller in magnitude, occurring under undrained conditions with changes in total stress generally slightly greater than the changes in pore water pressures at the same position. The changes in effective stress suggest that some reduction in vertical stress may have occurred (from shear due to vertical strain) during the excavation stage of the test. Alternatively, the suppressed tendancy of the kaolin to dilate may have led to the generation of additional negative pore water pressures with plastic strains occurring in the model. In each test, total stress changes at position 1 were of the same sign but smaller in magnitude than at position 2.

Adjacent to the trench, reductions in total stress, pore water pressure and effective stress were measured. This is most obvious in test 2 where the initial earth pressure coefficient profile was greatest.

Below the trench, in tests 1 and 3, significant increases in total stress and pore water pressure were measured as stress redistribution occurred. In all tests, where the soil behaved in a drained manner, changes in total lateral stress were very much greater than pore water pressures and effective stress changes were significant. Where undrained conditions existed, changes in lateral effective stress were very much smaller

### *5.4.3.2 Measured changes due to concrete placement*

Table 5.4 indicates the changes due to concrete placement in terms of lateral effective stress, total stress and pore water pressure. The values given are the difference between the pre excavation and state the pressures recorded at the specified time after concrete placement. Negative values represent stress relief and positive readings indicate increases.

**Test 1**

| Depth | Trans | 5 days post concreting | | | 25 days post concreting | | |
|---|---|---|---|---|---|---|---|
| (m) | number | total | pwp | effective | total | pwp | effective |
| 3 | 7 | -56.6 | -7.9 | -48.7 | -47.7 | 0.7 | -48.4 |
| 11 | 3 | -8.2 | -2.4 | -5.8 | 14.4 | 2.7 | 11.7 |
| 19 | 2 | 29.7 | 36 | -6.3 | 16.2 | -5.6 | 21.8 |
| 25 | 1 | 17.5 | 13.4 | 4.1 | 6.5 | 4.6 | 1.9 |

**Test 2**

| Depth | Trans | 5 days post concreting | | | 25 days post concreting | | |
|---|---|---|---|---|---|---|---|
| (m) | number | total | pwp | effective | total | pwp | effective |
| 3 | 4 | -150.0 | 5.0 | -155.0 | -155.1 | 4.4 | -159.5 |
| 11 | 3 | -11.5 | -20.4 | 8.9 | -19.3 | -28.7 | 9.4 |
| 19 | 2 | 37.5 | 34.0 | 3.5 | 21.8 | 10.8 | 11.0 |
| 25 | 1 | 10.5 | 14.0 | -3.5 | 1.8 | 1.6 | 0.2 |

**Test 3**

| Depth | Trans | 5 days post conc. | | | 25 days post conc. | | | 5000 days post conc. | | |
|---|---|---|---|---|---|---|---|---|---|---|
| (m) | number | total | pwp | effect | total | pwp | effect | total | pwp | effect |
| 3 | 4 | -94.8 | -3.7 | -91.1 | -95.0 | -9.1 | -85.9 | -82.1 | -8.6 | -73.5 |
| 11 | 3 | -1.3 | 18.6 | -19.9 | -6.9 | 4.5 | -11.4 | -2.9 | 14.6 | -17.5 |
| 19 | 2 | 58.2 | 62.5 | -4.3 | 46.7 | 42.4 | 4.3 | -8.0 | 4.8 | -12.8 |
| 25 | 1 | 15.8 | 22.7 | -6.9 | 9.6 | 17.6 | -8.0 | -5.6 | -0.3 | -5.3 |

Table 5.4 *Lateral effective stress changes after concrete placement (kPa)*

The kinetic effects of depositing the simulated concrete powder led to significant increases in measured values of total lateral stress. For this reason comparisons are made with values at 5, 25 and 5000 days and figure 5.16 shows changes in effective stress calculated from readings immediately prior to excavation and at various times (25 days and 5000 days) after concrete placement.

The figure also indicates that lateral stresses in heavily overconsolidated clays are not re-established after wall installation in the long term, and that higher initial $K_o$ profiles will lead to greater stress relief (particularly at shallower positions) occurring after the installation process has been completed.

Figure 5.16 also suggests that the largest changes in lateral effective stress were experienced at the shallowest depth, with the greatest 25 day stress relief experienced in test 2 and the least in test 1. This corresponds to the different earth pressure coefficient profiles and suggests that the stress relief that occurred during excavation at the shallowest depths is not re-established by the concreting process.

In test 1 by 25 days, pore water pressures had returned to levels that were close to the original hydrostatic values. At this point, the net effect of wall installation was a slight increase in effective (and total) stress at all positions except at position 4, where considerable stress relief was experienced.

In test 2 at 25 days, pore water pressures were still reaching stable conditions at positions 2 and 3. As pore water pressures approached hydrostatic values, positions 1, 2 and 3 indicated small effective stress increases, despite the greatest stress relief having occurred at position 4.

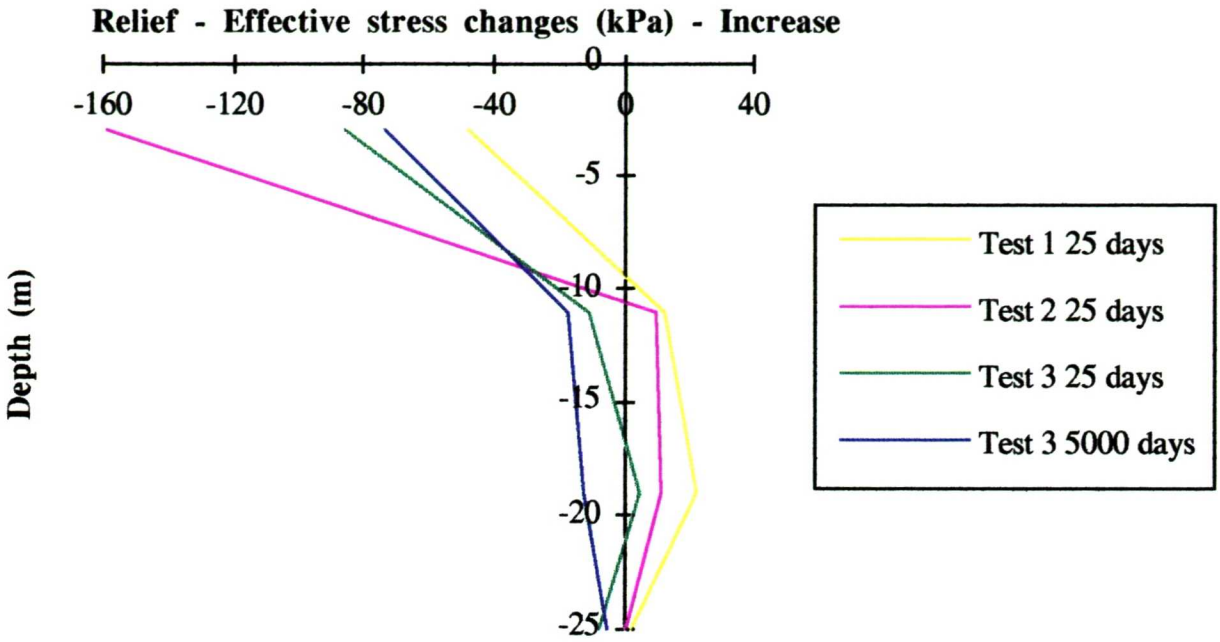


Figure 5.16 *Lateral effective stress change comparisons of pre-excavation with post installation levels.*

In test 3, the change in lateral effective stress between 25 and 5000 days was small. A 5000 day delay between installation and the main excavation in front of the wall is unrealistic in practice but serves to show that further changes in effective stress, after 25 days, are small, with only the slightest reductions occurring as pore water pressure equilibration takes place.

In summary, the effects of a high earth pressure coefficient is to cause significant relief at shallow depths with greater relief experienced for greater values of $K_o$. The changes between 25 days and 5000 days are insignificant compared with the stress relief that occurs during excavation, despite some lateral stress reapplication during concreting.

### *5.4.3.3 Results comparison with a Newmark chart analysis*

Kantartzi (1994) suggested that only a proportion of the horizontal total stress relief that occurred in the trench would be experienced in individual soil elements at the same depth at a distance away from the trench. Based on an elastic analysis (assuming no change in vertical total stress) a Newmark chart was used to calculate pore water pressure changes due to a change in total stress in the trench, and these values were compared with measured porewater pressure changes.

In table 5.5 values of measured total lateral stress change as a proportion of the reduction in fluid pressure in the trench are presented. Values calculated from a Newmark chart elastic analysis are presented in the last column.

| Depth (m) | Trans number | Measured values | | | Newmark chart |
|---|---|---|---|---|---|
| | | Excav | 5 days | 25 days | |
| 3 | 7 | 0.775 | 0.547 | 0.461 | 0.96 |
| 11 | 3 | 0.437 | 0.079 | -0.139 | 0.98 |
| 19 | 2 | -0.277 | -0.287 | -0.157 | 0.37 |
| 25 | 1 | -0.153 | -0.169 | -0.063 | 0.02 |

| Depth (m) | Trans number | Measured values | | | Newmark chart |
|---|---|---|---|---|---|
| | | Excav | 5 days | 25 days | |
| 3 | 4 | 1.015 | 0.849 | 0.835 | 1 |
| 11 | 3 | 0.216 | 0.065 | 0.109 | 0.98 |
| 19 | 2 | 0.025 | -0.212 | -0.123 | 0.37 |
| 25 | 1 | 0.015 | -0.059 | -0.010 | 0.02 |

| Depth (m) | Trans Number | Measured values | | | | Newmark chart |
|---|---|---|---|---|---|---|
| | | Excav | 5 Days | 25 Days | 5000day | |
| 3 | 4 | 0.691 | 0.664 | 0.665 | 0.575 | 1 |
| 11 | 3 | 0.396 | 0.009 | 0.048 | 0.020 | 0.98 |
| 19 | 2 | -0.420 | -0.408 | -0.327 | 0.056 | 0.37 |
| 25 | 1 | -0.062 | -0.111 | -0.067 | 0.039 | 0.02 |

Table 5.5 *Measured values for different earth pressure coefficient profiles*

Generally, the measured values are less than the those defined by the Newmark chart. The Newmark chart represents a poor predictor of undrained conditions as it takes no account of the changes due to shear effects, the kinematic restraint at the bottom of the trench or a soil stiffness/non uniform earth pressure coefficient profile. This is particularly obvious around the bottom of the trench where the measured values are predominantly of an opposite sign, where the increases due to the lateral constraint at the bottom of the trench (vertical arching) are greater than any reduction due to excavation.

### *5.4.4 The effects of earth pressure coefficients on ground movements*

Figure 5.17 below shows normalized soil surface settlement profiles for each test after excavation, immediately after concreting and 25 days after concreting (also 5000 days in the case of test 3). The settlement profiles have been normalized with respect to the depth of the trench ($H$ = 18.5m) and provide an indication of ground profiles at different stages of the installation process. $\delta$ represents displacement and $x$ represents any distance back from the trench.

The results demonstrate (to some degree) the effect of different initial in situ earth pressure coefficients. In test 1, settlements throughout the wall installation process and at 25 days were found to be smaller than in tests 2 and 3. In tests 2 and 3, after excavation and concreting the resulting settlements were similar. However, in test 2 after 25 days minor local collapse had occurred at the top of the trench, as the wall had not been cast the full height across the full width of the trench, and settlements were therefore greater.

In test 3, changes in soil surface profile between 25 and 5000 days were small, indicating only a slight further settlement as equilibrium conditions were approached. There is no reason to suppose that this would not have been the case in the other tests.

Different earth pressure coefficient profiles had a significant effect, both during excavation and in the long term. Generally, a higher in situ lateral stress leads to a higher stress reduction on excavation and increased soil settlements. The stresses applied during concreting were similar in all tests, but the recovery of the soil surface was greater in tests where movement due to excavation was greater (i.e. in test 2). This was probably due to a reduced soil stiffness with increasing strain or displacement.

At positions back from the trench, surface settlements were reduced to 1% ($\delta$/H = 0.01) at one trench depth back from the installation. This is consistent with behaviour observed by Kantartzi (1994) and her proposed zone of influence.

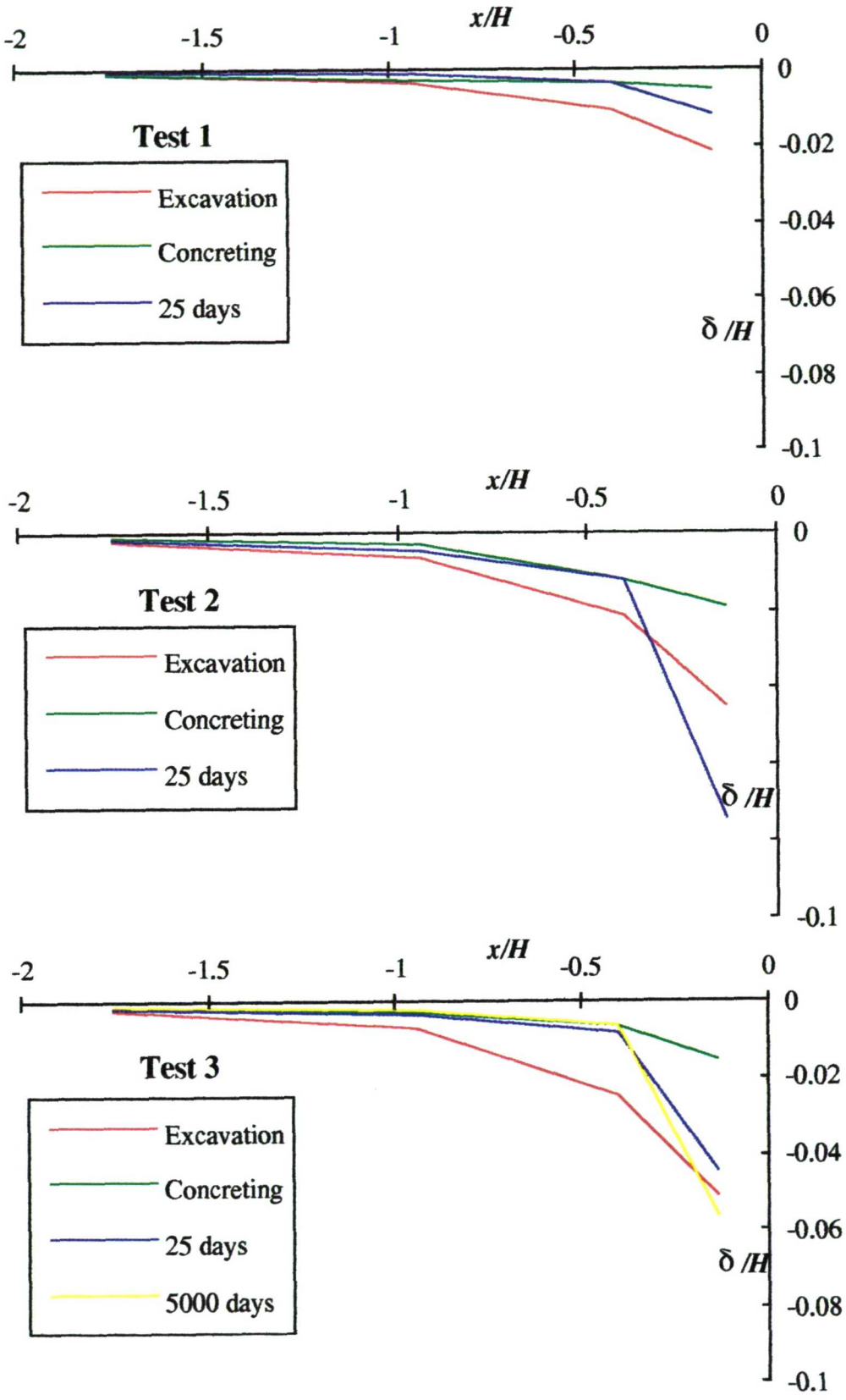


Figure 5.17 *Settlements*

## *5.5 The effects of concrete mix density*

In all tests, after initial concrete placement, pore pressures and total stresses increased dramatically, to values well in excess of the post excavation values. In test 7 an earth pressure coefficient profile similar to that adopted in test 3 was used at the trench end. At the remote end, a stress controlled boundary was employed. This, as discussed earlier, had little effect on recorded results around the trench. In test 7, a low density simulated concrete was used in order to compare the change in lateral stress due to the placement of a light mix with results from test 3, where the standard, denser mix was used. By varying the mix density in this way, it was possible to examine any re-establishment of lateral stress not due to the effects of concreting.

The apparatus employed in test 6 was slightly modified for use in test 7 by reducing the penetration depth of the bag support to 0.5 m (at prototype scale). This meant that the transducers at the shallowest level showed a greater response during concrete placement than in test 6. The comparisons are made with results obtained from test 3, which may be found in figure 5.3 and 5.5 in section 5.2.

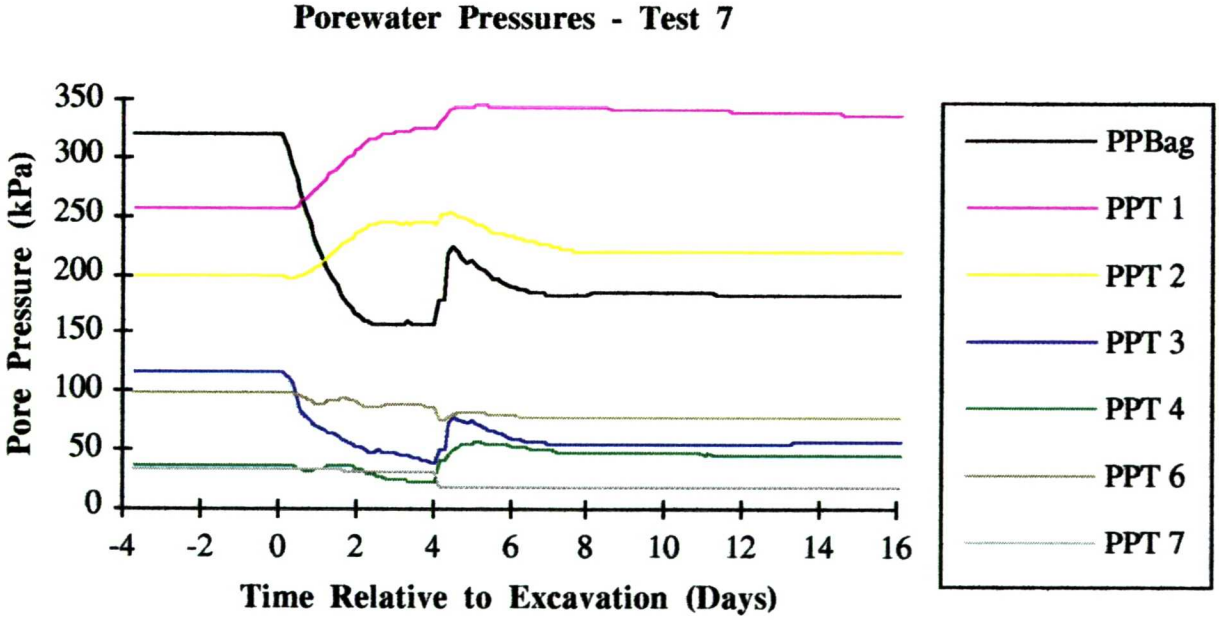


Figure 5.18 *Pore water pressures - Test 7*

The pore pressure results shown in figure 5.18 indicated that the effects of a light density mix are twofold. First, adjacent to the trench, the peak pressures that occurred during placement were much less than in the standard case. The reduced

density limits the maximum concrete hydrostatic pressures thus reducing the transient effects of placement. Second, the increased pore water pressures after placement at and below the toe appeared to be significantly greater than in the other tests. This may be due to the smaller pressures applied to the walls of the trench during concreting leading to a reduced reversal of vertical arching effects. At 5000 days pore water pressures were close to hydrostatic values at the deepest levels, and slightly less than hydrostatic at other levels.

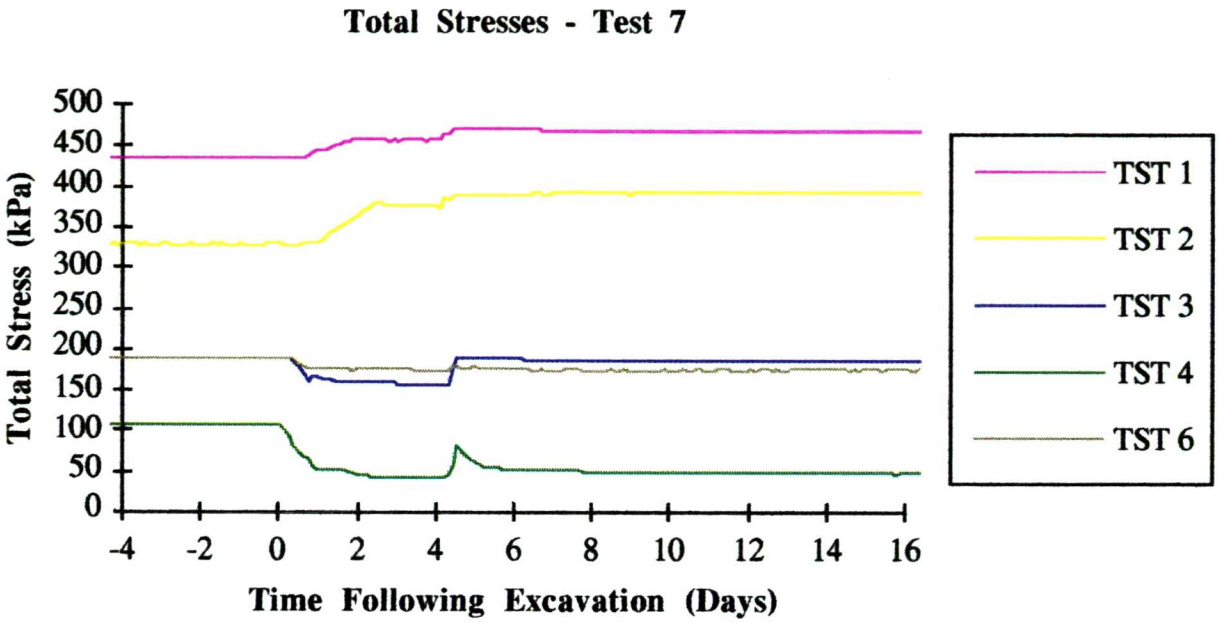


Figure 5.19 *Total stresses - Test 7*

The effect on the surrounding soil of the concrete pour in terms of changes in total stress, porewater pressure and effective stress is indicated in table 5.8. 'Due to pour' is the difference between values immediately before and immediately after concrete placement - this gives an idea of the magnitude of the stresses induced by concrete placement. The 25 day and 5000 day measurements are relative to pre-excavation levels, and give an indication of the overall stress changes that have occurred over the entire installation process.

**Test 7** (low density mix)

| Depth | Trans | Due to pour | | | 25 days post conc. | | | 5000 days post con. | | |
|---|---|---|---|---|---|---|---|---|---|---|
| (m) | number | total | pwp | effect | total | pwp | effect | total | pwp | effect |
| 3 | 4 | 38.0 | 30.4 | 7.6 | -60.6 | 8.9 | -69.5 | -59.5 | 7.5 | -67.0 |
| 11 | 3 | 31.9 | 37.9 | -6.0 | -4.5 | -56.4 | 51.9 | -4.8 | -7.6 | 2.8 |
| 19 | 2 | 14.1 | 10.2 | 3.9 | 64.1 | 20.9 | 43.2 | 72.4 | 6.8 | 65.6 |
| 25 | 1 | 14.3 | 17.0 | -2.7 | 35.4 | 70.8 | -35.4 | 35.2 | 14.4 | 20.8 |

**Test 3** (standard mix)

| Depth | Trans | Due to pour | | | 25 days post conc. | | | 5000 days post con. | | |
|---|---|---|---|---|---|---|---|---|---|---|
| (m) | number | total | pwp | effect | total | pwp | effect | total | pwp | effect |
| 3 | 4 | 91.4 | 7.3 | 84.1 | -95.0 | -9.1 | -85.9 | -82.1 | -8.6 | -73.5 |
| 11 | 3 | 101.1 | 53.0 | 48.1 | -6.9 | 4.5 | -11.4 | -2.9 | 14.6 | -17.5 |
| 19 | 2 | 10.8 | 37.6 | -26.8 | 46.7 | 42.4 | 4.3 | -8.0 | 4.8 | -12.8 |
| 25 | 1 | 5.0 | -14.1 | 19.1 | 9.6 | 17.6 | -8.0 | -5.6 | -0.3 | -5.3 |

Table 5.8 *Pore water pressure and lateral stress changes for different density mixes. (kPa)*

In test 7, measured pore water pressure changes indicated that quasi-elastic undrained conditions prevailed even at the shallowest depths. In test 3, lower measured pore water pressure changes at position 4 suggested a drained response. During placement a greater increase in total and effective stress was measured adjacent to the trench for the denser mix (test 3).

In both tests, the pore water pressures 25 days after installation suggest equilibrium conditions had not been reached. At this time the concrete mixtures should have set but pore pressure results suggest that in test 7 this may not have been the case.

By 5000 days pore water pressures had reached stable equilibrium values, making effective and total stress comparisons easier. Near the soil surface and at mid trench, there was little significant difference between the overall reductions in lateral effective stress. At positions 1 and 2, in the long term, in test 7 effective stress changes were greater where the low density mix had been deposited.

In summary, the results show that adjacent to the trench the light-weight mix has had less impact, inducing smaller stresses during placement than a normal mix. Further,

after the mix had consolidated and hardened, the changes in lateral stress indicated little significant difference that can be directly attributed to the differences in concrete density around the face of the trench. However, positions 1 and 2, the overall increase in effective stress appeared to be greater where the lighter mix was employed, perhaps due to a smaller reversal of the vertical arching effects associated with slurry trenching.

## *5.6 Test 5 - Failure*

Figure 20 shows total stress traces recorded in test 5, together with the measured pressure in the rubber bag. The pore water pressure traces (which are not presented) indicated that the pore water pressure profile was still coming into equilibration. After about 29 minutes after spin-up (model scale), during a period of 100 second logging, a drop in the rubber bag pore water pressure was noted indicating that a collapse had occurred, and one second logging was resumed as quickly as possible.

The pore water pressure transducer in the rubber bag measured a pressure of 412 kPa corresponding to a height of water of 42m. This excess height of fluid (23.5m) was used in an attempt to give a fourth, even more extreme earth pressure coefficient profile.

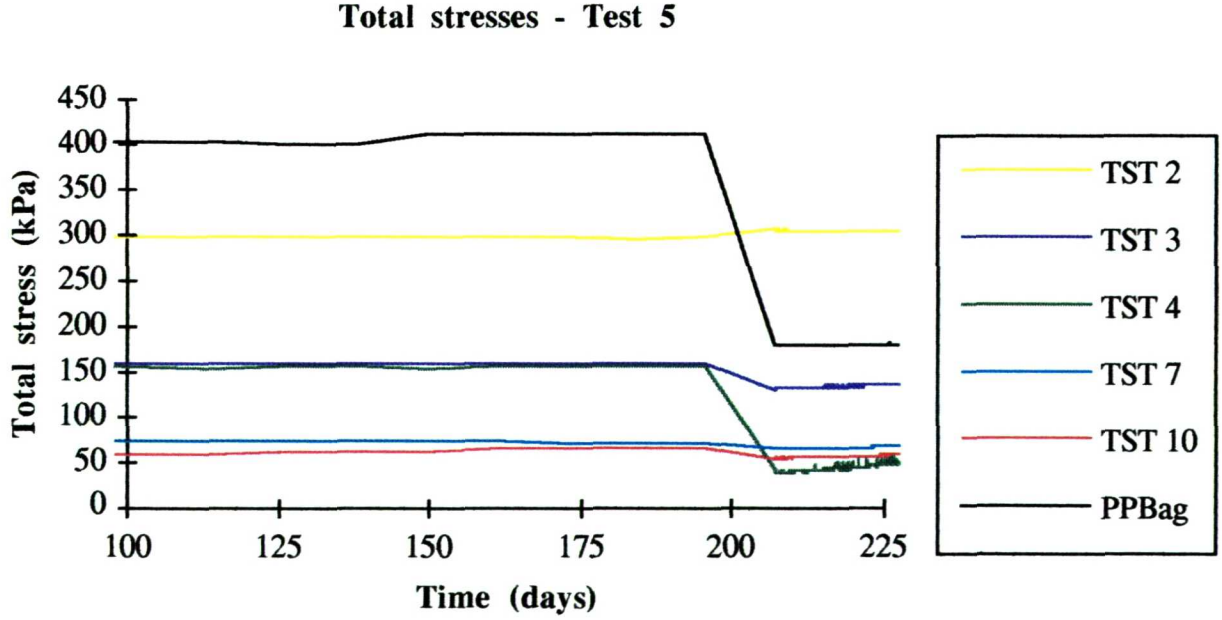


Figure 5.20 *Total stresses - Test 7*

Based on the pressure measured by PPBag, a lateral pressure of 226 kPa was applied to the soil sample at the bottom of the bag support (at a depth of 0.5m). This corresponded to a value of $K_o$ at that position of 26, which the soil is highly unlikely to be able to sustain. However, during reconsolidation, the sample had swollen by approximately 0.8m, reducing the earth pressure coefficient at the bottom of the support plate to about 10. At this depth, the sample would be experiencing unloading, having been removed from the consolidation press at 80 kPa. If at the bottom of the bag support a current vertical effective stress of approximately 10 kPa is assumed, then an over consolidation ratio of 125 is calculated based on a maximum overburden effective stress of 1250 kPa. Using (Mayne and Kulhuwy, 1982)

$$(1-\sin\phi')OCR^{\sin\phi'} = K_{unload}$$

a maximum value of $K_{unload} = 7.96$ is achieved (using $\phi' = 40°$). The failure of the sample is therefore not suprising.

After the test, further examination indicated that the rubber bag had ruptured by tearing on the bottom of the bag support, with the fluid then spilling on to the sample. The photograph presented in figure 5.21 shows the full extent of the rupture. After the rupture the trench collapsed, as shown in figure 5.22.

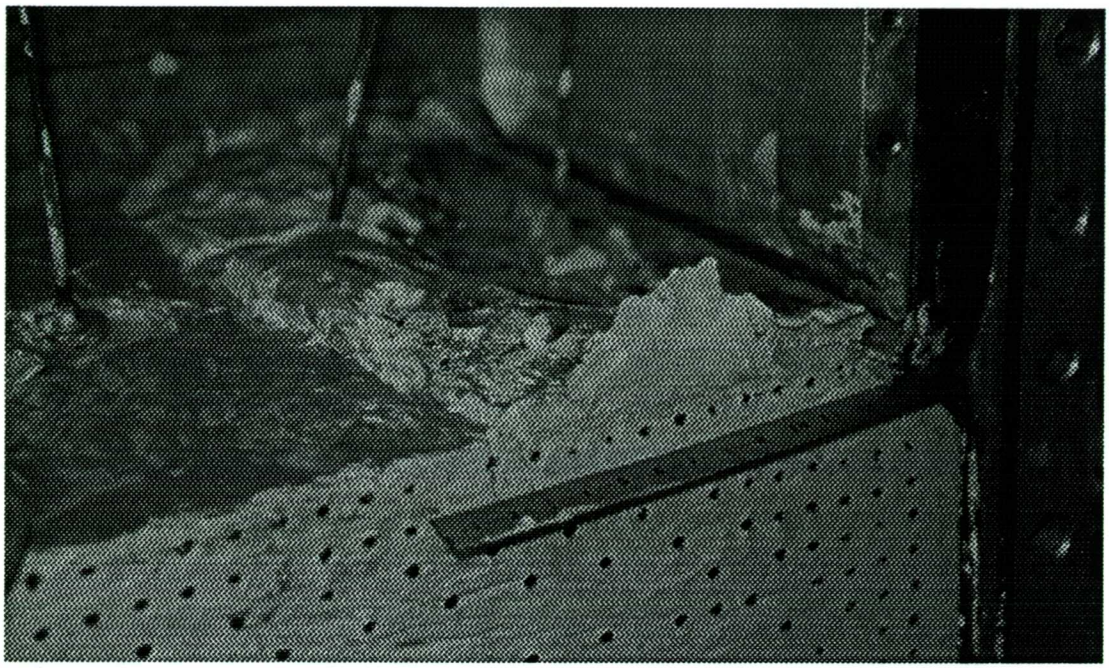

Figure 5.21 *Surface of the model after the bag rupture*

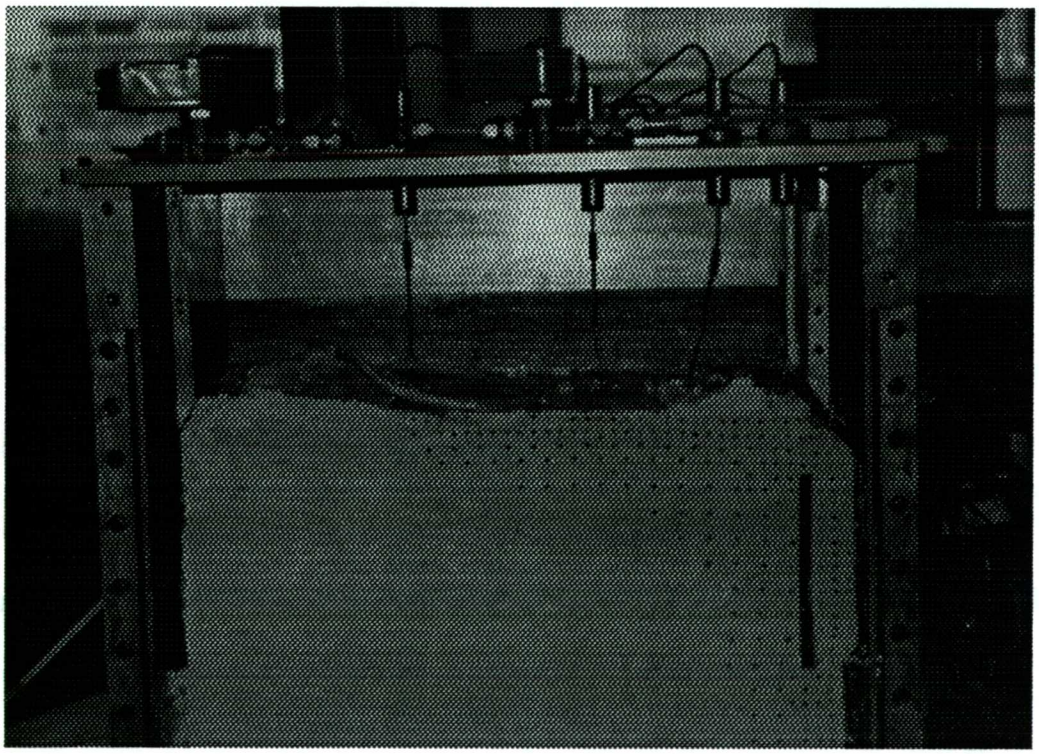

Figure 5.22 *Profile of the model showing the collapsed trench*

## *5.7 The effects of a quarter width panel - test 4.*

Pore water pressure traces are presented for test 4 in figure 5.23. In this test a quarter width panel was used, and so the changes recorded are very much smaller than in other tests. Transducers were installed in the model as described in chapter 3, on either side of the centre line of the trench, with a spacing of approximately 50mm between. This was so that the transducers would not affect each other. The panel geometry was such that the measurements were taken from each position in line with the edges of the trench. The transducers were therefore not able to record the maximum stress change that occurred during installation, but provided an indication of the stress changes at the edges of the panel.

Kantartzi (1994) noted that, when the concrete had set, the maximum soil residual centreline settlement was approximately 25% of that found where a full width trench was used. Table 5.7 below indicates the changes in lateral stress and pore water pressure at key points during the installation process, and indicates that overall the average percentage change in test 4 was 20% (on average) of that in test 1. This average is slightly less than that proposed for settlements by Kantartzi (1994) due to the positioning of the transducers at the edges of the trench. In general, the proportional stress changes are reasonably compatible with the settlement reduction factor suggested by Kantartzi (1994).

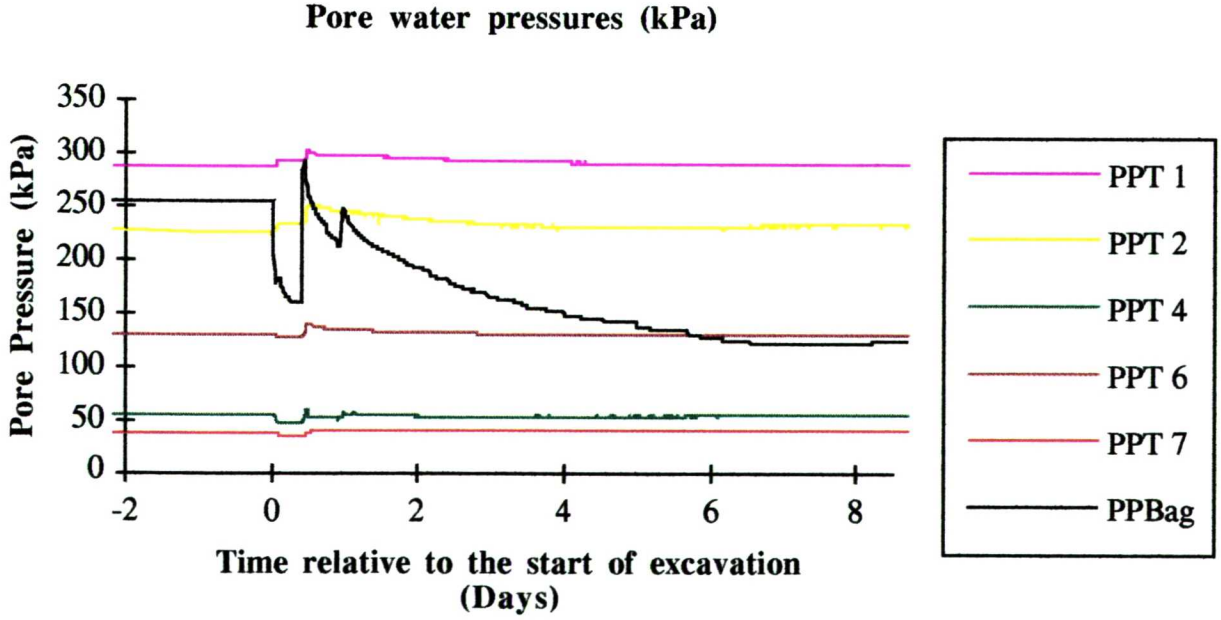


Figure 5.23 *Pore water pressures - Test 4*

**Test 4**

| Depth (m) | Trans number | Due to excavation | | | 5 days post concreting | | |
|---|---|---|---|---|---|---|---|
| | | test 4 | test 1 | % | test 4 | test 1 | % |
| 3 | 4 | -3.1 | -10.6 | 29.25 | 0.5 | -7.9 | -6.33 |
| 11 | 6/3 | -1.1 | -32.6 | 3.37 | 1.1 | 2.7 | 40.74 |
| 19 | 2 | 5.9 | 25.7 | 22.96 | 4.6 | 36.0 | 12.78 |
| 25 | 1 | 5.3 | 23.6 | 22.46 | 2.9 | 13.4 | 21.64 |

Table 5.7 *Comparisons of pore water pressures for a quarter width panel.*

Whilst results have indicated that panel construction will greatly reduce stress and pressure changes in the soil, a further factor has been highlighted that will have an effect on the changes that occur in the model (Ng, 1993). A similar effect to vertical arching occurs at the sides of the panel after the excavation stage. Finite element analyses by Ng (1993) suggested that these increases were significant, particularly where a series of panels was installed. However, this horizontal arching effect was beyond the scope of this research.

## *5.8 Conclusions*

A total of seven tests have been used to investigate three different variable factors. The results presented has provided clear evidence of the effects of testing variations and many observations have been made. Many useful observations have been made from the results.

One weakness that has been demonstrated by centrifuge testing is the effect of extraneous factors that can make comparison difficult. Computer models can be used to eliminate this variable factor and one such method is presented in chapter 6. Final conclusions are presented in chapter 7.

# *Chapter 6*

# *Finite element analyses*

## *6.1 Introduction*

The effects of diaphragm wall installation were further investigated using a finite element analysis program 'CRISP' (CRItical State Program) described by Britto and Gunn (1987). The finite element analyses were able to model the different tests without the confusion created by extraneous factors, and therefore provide a useful qualitative comparison with the centrifuge test results.

Similar (although idealised) in situ conditions to those adopted in the centrifuge tests were modelled, although some discrepancies between the centrifuge and the CRISP analyses were inevitable and these are discussed later.

Four different analyses were carried out to cover the main scope of the centrifuge model tests. Two different in situ earth pressure coefficient profiles were modelled to provide a comparison with centrifuge tests 1 and 2. A stress controlled boundary was modelled at the remote end of the finite element mesh to correspond with the conditions assumed in test 6; and a light concrete mix was simulated to correspond with conditions in test 7.

This chapter is presented in five sections. First, the geometry of the finite element mesh is described, together with the boundary conditions assumed for each of the different tests. The second section considers the soil model and the material properties that were used in the different material zones. Thirdly, a detailed summary of the sequences used to simulate the wall installation process is given. The fourth section presented discusses the results from the finite element analyses, with the final section comparing and contrasting the data from the centrifuge tests with the results of the finite element analyses.

## *6.2 The finite element mesh.*

A plane strain model was adopted as this best replicated the conditions assumed in the centrifuge model and the finite element mesh, with the prescribed boundary fixities, is shown in figure 6.1. Generally, six-noded triangular elements were used, with some eight-noded quadrilateral elements used where sufficiently small for consistency with the rest of the mesh. Consolidation elements were used throughout.

The side and base boundaries were impermeable. The pore water pressure head along the top boundary was fixed at original ground surface level throughout the test, as this was consistent with the intended ground water level in the centrifuge tests. In an attempt to replicate the centrifuge model exactly, the wooden block that was installed beneath the rubber bag was modelled as a second material zone thus reducing the effective half width of the trench to 0.5m. This is depicted on figure 6.1 by the hatched lines beneath the solid area that represents the trench.

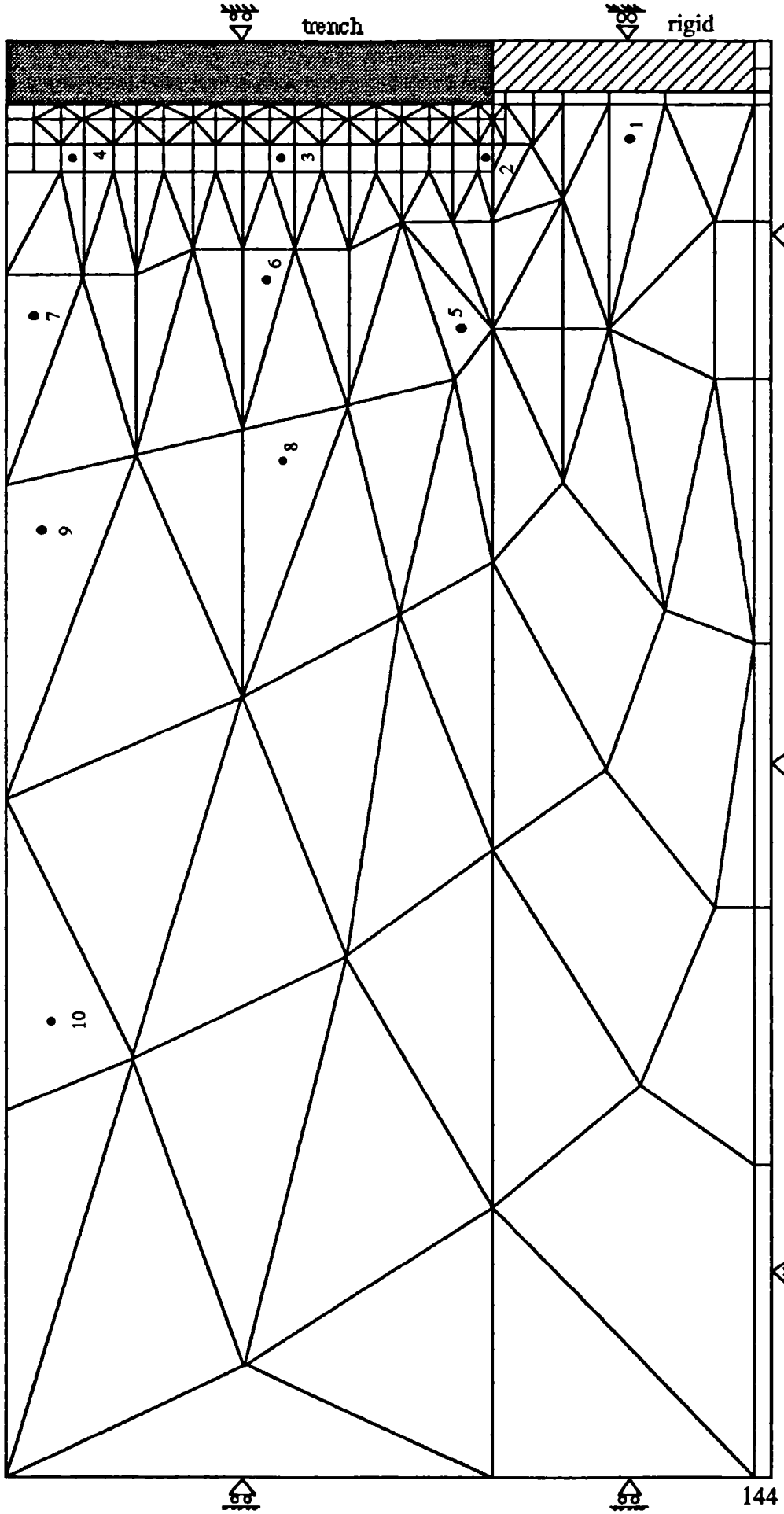


Figure 6.1. Finite element analysis mesh.

Table 6.1 compares the positions of the transducers in the centrifuge model with the positions of the integration points from which results were taken in the finite element analyses. These are also marked on the mesh in figure 6.1 above.

| Transducer | CRISP analyses | | Centrifuge model | |
|---|---|---|---|---|
| Position | x (m) | y (m) | x (m) | y (m) |
| 1 | 2.8 | 23.7 | 2.5 | 25 |
| 2 | 2 | 18.2 | 2.5 | 19 |
| 3 | 2 | 10.5 | 2.5 | 11 |
| 4 | 2 | 2.5 | 2.5 | 3 |
| 5 | 7.8 | 16.8 | 7.5 | 19 |
| 6 | 7.8 | 9.7 | 7.5 | 11 |
| 7 | 9.2 | 1 | 7.5 | 3 |
| 8 | 15.5 | 10.3 | 17.5 | 11 |
| 9 | 18.2 | 1.7 | 17.5 | 3 |
| 10 | 33.8 | 1.7 | 32.5 | 3 |

Table 6.1 *Comparison of transducer and element positions. (0,0) taken as the top of the excavation.*

The finite element analyses were performed at prototype scale. A more thorough approach might have been to model the wall installation at 1:100 scale under centrifuge conditions in an acceleration field of 100 gravities. However, considerable problems were encountered in attempting to model the spin-up and reconsolidation phases of the centrifuge tests, and so a prototype scale analysis was carried out. It was felt that the results were not significantly affected by this assumption and the effects of attempting to include the early stages could have had a detrimental effect on the later stages of the analysis.

## 6.3 Model parameters

### 6.3.1 Material properties

The soil parameters used for Speswhite kaolin (material zone 1) are presented in table 6.2.

| Speswhite kaolin | Property | Value |
|---|---|---|
| Slope of critical state in $q$-$p'$ space | M | 0.65 |
| Specific volume on critical state line at $p'$=1 kPa | $\Gamma$ | 3.48 |
| Void ratio on critical state line at $p'$=1 kPa in $v$-ln$p'$ space | $e_{cs}$ | 2.48 |
| Slope of one-dimensional compression line in $v$-ln $p'$ space | $\lambda$ | 0.25 |
| Slope of unload/reload line in $v$-ln$p'$ space | $\kappa$ | 0.05 |
| Angle of internal friction of the soil | $\phi'_{crit}$ | 22° |
| Poisson's ratio | $\nu$ | 0.33 |
| Permeability in x direction (m/s) | $K_x$ | $6.60\times10^{-10}$ |
| Permeability in y direction (m/s) | $K_y$ | $1.80\times10^{-9}$ |
| Permeability in x direction for tensile fracture region (m/s) | $K_{xt}$ | $1.00\times10^{-6}$ |
| Permeability in y direction for tensile fracture region (m/s) | $K_{yt}$ | $1.00\times10^{-6}$ |
| Bulk unit weight of soil (kN/m$^3$) | $\gamma$ | 17.34 |

Table 6.2 *Properties adopted for Speswhite kaolin. (Powrie & Li, 1991)*

In all analyses the soil behaviour was simulated using a finite element formulation of the model proposed by Schofield (1980). The Schofield model incorporates a Cam clay yield surface on the wet side, with a no-tension cut-off and Hvorslev surface on the dry side as shown in figure 6.2.

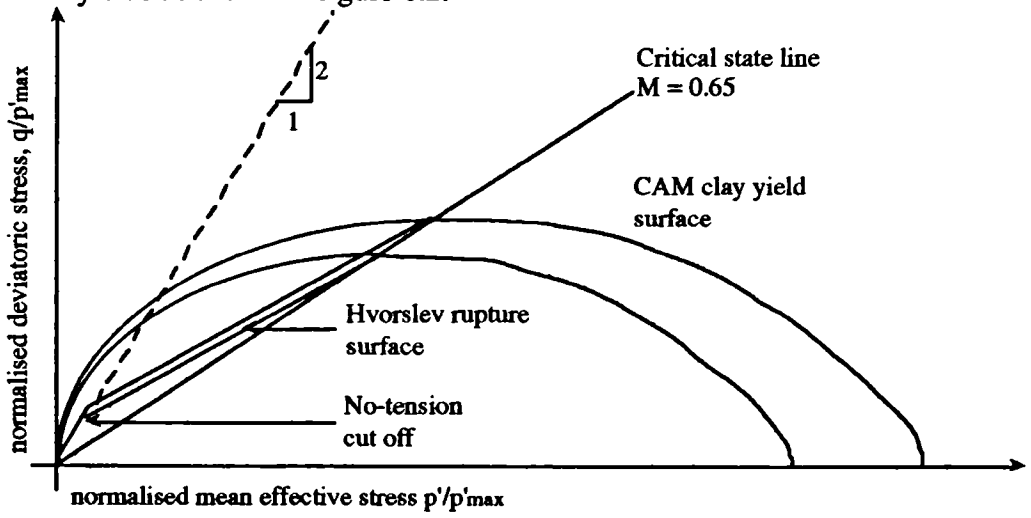


Figure 6.2. *The Schofield model.*

In drained triaxial compression starting at zero confining pressure, $\sigma'_3 = 0$. As the deviatoric stress is increased, $q = \sigma'_1$ and hence from

$$p' = \frac{1}{3}(\sigma'_1) \tag{6.1}$$

$$p' = \frac{1}{3}(q) \rightarrow \frac{q}{p'} = 3 \tag{6.2}$$

Under conditions of plane strain assuming $q = \sigma'_1 - \sigma'_3$ and $\sigma'_2 = \frac{1}{2}(\sigma'_1 + \sigma'_3)$,

$$p' = \frac{1}{2}(q) \rightarrow \frac{q}{p'} = 2 \tag{6.3}$$

This is not strictly correct, as the use of the full definition of

$$q\left( = \frac{1}{\sqrt{2}}\left((\sigma'_1 - \sigma'_2)^2 + (\sigma'_1 - \sigma'_3)^2 + (\sigma'_2 - \sigma'_3)^2\right)^{1/2}\right) \tag{6.4}$$

gives a no tension cut-off of

$$\frac{q}{p'} = \sqrt{3} \tag{6.5}$$

However, in the analyses presented, where horizontal effective stresses did not exceed theoretical passive failure limits, the no tension cut-off yield surface was not crossed. To allow for plane strain conditions $H$ and $M$ were reduced and hence the parameters used in the finite element analyses set the Hvorslev rupture surface gradient to 0.55 and the no tension cut off gradient to 2.

The kaolin used in the centrifuge tests was overconsolidated in one dimensional compression to an effective overburden of 1250 kPa. The over consolidation ratio (*OCR*) varies throughout the depth of the model from approximately 72 at a depth of 1m to 2.5 at the bottom of the mesh (29m).

A linear-elastic model was used in the second material zone to simulate a block of laminated wood and the properties adopted are presented in table 6.3. However, a reduced Young's modulus was adopted due to incompatibility errors that resulted if adjacent material zones were of vastly different stiffnesses. Similarly, the bulk unit

weight of the wooden block was modelled to be the same as the kaolin as vertical equilibrium errors result if materials of different unit weights were used in adjacent vertical zones of the mesh.

| Laminated wood | Property | Value |
|---|---|---|
| Stiffness, x direction (kPa) | $E_x$ | $1.5 \times 10^7$ |
| Stiffness, y direction (kPa) | $E_y$ | $1.5 \times 10^7$ |
| Poisson's ratio | $\nu$ | 0.33 |
| Poisson's ratio | $\nu$ | 0.33 |
| Permeability in x direction (m/s) | $K_x$ | $1.0 \times 10^{-9}$ |
| Permeability in y direction (m/s) | $K_y$ | $1.0 \times 10^{-9}$ |
| Bulk unit weight of soil (kN/m$^3$) | $\gamma$ | 17.34 |

Table 6.3 *Parameters adopted in material zone 2*

### *6.3.2 In situ stress conditions*

CRISP allows the specification of in situ stresses throughout the depth of the model. This option was used to define different initial earth pressure coefficient profiles for different analyses. Figure 6.3 shows the initial in situ earth pressure coefficient profiles adopted for analyses 1 and 2 and compares them with the pre-installation earth pressure coefficients imposed on the soil in centrifuge tests 1 and 2.

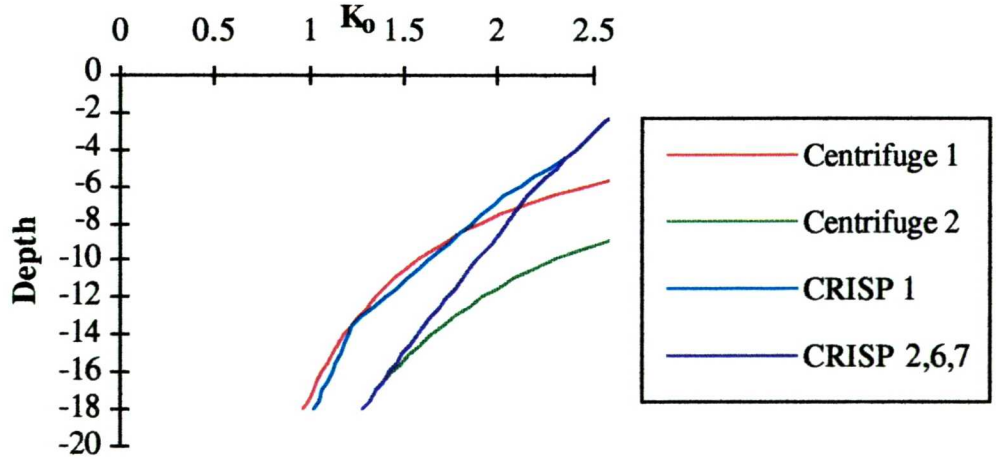


Figure 6.3 *Comparison of earth pressure coefficients*

The horizontal effective stresses defined in the finite element analyses were limited to the passive pressure limit (2.56, corresponding to a $\phi'_{peak} = 26°$) as large horizontal equilibrium errors occurred if the in situ stresses defined a position close to or outside

the yield locus. Therefore the profiles in analyses 1 and 2 were the same throughout the shallowest 2.5m depth. At the bottom of the trench the earth pressure coefficient was equal to 1.33 in analyses 2, 6, and 7 and 1 in analysis 1, corresponding to the appropriate centrifuge test profiles.

In analyses 6 and 7, a stress controlled boundary was modelled by applying horizontal compressive loads to the end of the mesh furthest from the trench. Due to the crudeness of the mesh at the remote end, it was not possible to define the compressive horizontal loading on the matrix as comprehensively as the in situ initial horizontal effective stresses. Therefore it was only possible to define the stress controlled boundary at 3 nodal points and 2 mid-side points (5 in total) where as the initial in situ stress profile was defined at a total of 10 vertical positions. This resulted in small horizontal equilibrium errors (<0.5%) occurring as finite element analyses 6 and 7 were processed.

## *6.4 Construction sequence*

The construction sequence was similar in all tests. The diaphragm wall was constructed under bentonite slurry with excavation proceeding from the top down and the concrete pressures applied from the bottom up. This was different from the construction sequence adopted in the centrifuge tests in two ways. First, during excavation in the centrifuge tests, the rubber bag was drained to ground level, reducing the pressure applied to the excavated face throughout the depth of the trench. During the finite element analyses the trench was excavated in segments, with lateral stress relief occurring only as individual segments were removed. Secondly, in the centrifuge tests, the concrete was dumped into the trench from above; in the finite element analyses the concrete pressures were applied from the bottom up.

The modelling of the construction sequence was split into three sections; excavation under bentonite slurry, concrete placement and post installation consolidation. These are discussed in turn below:

### *6.4.1 Excavation under bentonite slurry*

During excavation, the bentonite/trench interface was modelled as an impermeable boundary. For an overconsolidated clay this assumption was considered to be close to site conditions. CRISP treats all boundaries as impermeable unless otherwise

specified, and so as excavation progressed no further alterations to the elements at the sides of the trench were necessary.

The trench was excavated in six sections: the first five were 3.0m deep and the last was 3.5m deep. As each block of elements was removed a loading equivalent to the hydrostatic pressure of bentonite ($\gamma_b$ = 12 kN/m$^3$) was applied to the edges and the base of the current trench. A time of nearly 9 hours (32000 seconds) was adopted for each phase of excavation.

Prior to the excavation of each subsequent 3m block, it was necessary to remove the bentonite pressure from the base of the excavation so that the next segment could be excavated. This process added an extra approximation to the analyses. The removal of pressure was performed relatively quickly (2600 seconds) to maintain trench stability and limit effective stress relief due to consolidation in the adjacent soil. The removal of the bentonite pressures from the excavated base of the trench is shown schematically in figure 6.4.

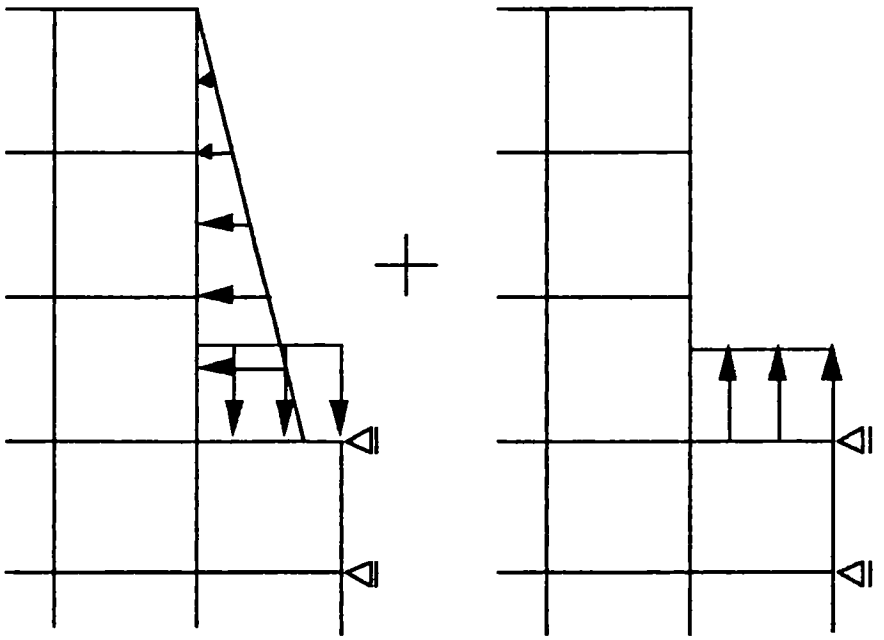

Figure 6.4 a) *application of bentonite pressure* b) *removal of bentonite pressure*

After the last section had been excavated, the bentonite surcharge was not removed from the base of the trench and so the total trench excavation time was equal to 205000 seconds (2 days 9 hours). This was similar to the length of the taken in centrifuge tests 1, 3, 4 and 7 and slightly quicker than in the other tests.

### *6.4.2 Concrete placement.*

A period of one day was allowed prior to concrete placement, which was consistent with the time delay between excavation and concreting in the centrifuge tests. Two different concrete densities were considered: 24 kN/m$^3$ in analyses 1, 2, and 6 and 16 kN/m$^3$ in analysis 7 and concrete pressures were applied by increasing the forces that simulated the bentonite pressure already applied to the excavated faces of the trench. In all analyses, the concrete pressures were applied over six increment blocks in six segments up the side of the trench and was modelled to have been tremie-piped to the bottom of the trench under the pressure of the bentonite that remained in the trench.

As shown in chapter 2 (from the analysis by Gibson, England and Hussey (1967)) a greater amount of consolidation occurs in a column of a fine-grained material that is under a great load than one under a smaller load. Hence the first segment of concrete, placed at the bottom of the trench, was modelled to consolidate more than the subsequent segments. As subsequent segments were placed, the bentonite overburden pressure was reduced and less consolidation occurred whilst that segment was placed.

During placement, the concrete was assumed to remove all of the bentonite from the excavated side and base of the trench and so throughout wall installation, the sides of the trench in contact with the concrete were modelled to act as permeable boundaries. Excess pore water pressures were specified, therefore, in the soil between the top of the concrete (at a depth $h$ below the surface) and the bottom of the trench.

The initial pressures specified were equal to the pressure applied by the fresh wet concrete, plus the overburden bentonite pressure, less the in situ pore water pressure in the soil. Throughout the installation process, excess pore water pressures were reduced as the concrete consolidated.

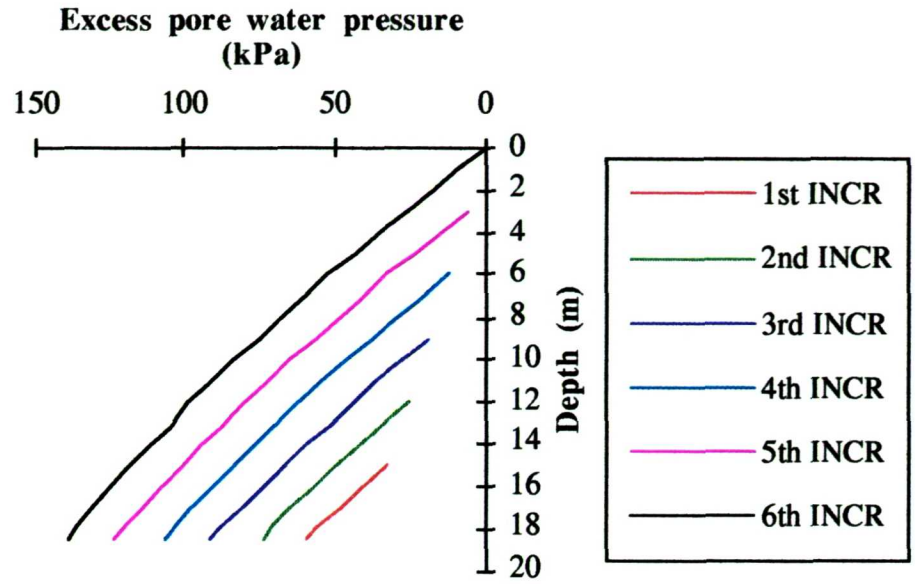


Figure 6.5 *Excess pore water pressures in the elements on the excavated face*

The initial excess pore water pressure, $\bar{u}$, at a depth $h$ (the top of the concrete segment, depth $z$) was calculated from:

$$\bar{u} = (\gamma_b - \gamma_w).h \qquad (6.6)$$

and below $h$ at any depth, $z$, from:

$$\begin{aligned} \bar{u} &= (\gamma_b - \gamma_w).h + (z-h).(K_c\gamma_c - \gamma_w) \\ &= z(K_c\gamma_c - \gamma_w) + h(\gamma_b - K_c\gamma_c) \end{aligned} \qquad (6.7)$$

where $K_c$ (<1) is a coefficient reducing the lateral stress on the sides of the trench due to partial consolidation of the concrete.

As each of the concrete segments was placed, the overburden pressure of the bentonite and concrete led to further consolidation occurring in the segments nearer the bottom of the trench, giving the excess pore water pressure profiles a curved appearance.

Similarly, the lateral stress profile applied along the excavated face during installation was built up for each time increment during placement. Initially, the upper section of the profile was equal to the lateral pressure of bentonite and the bottom section of the

line was due to the fresh wet concrete. As more concrete was placed, the bottom section extended further up the trench, until installation was complete. For analyses 1, 2 and 6 lateral total pressures are given in figure 6.6.

Also shown on the diagram is the full hydrostatic pressure of a non-consolidating concrete. Many researchers, (Higgins et al., 1989; Potts and Fourie, 1984; Kutmen 1986 etc) have applied the full pressure (often over a period of several increments) to the sides of the trench. For the purposes of this dissertation the consolidation approach was adopted as it it provides a better fit to much existing field data (Uriel and Otero, 1977; Clayton and Milititsky, 1983; Anderson et al., 1984; Ng, 1993).

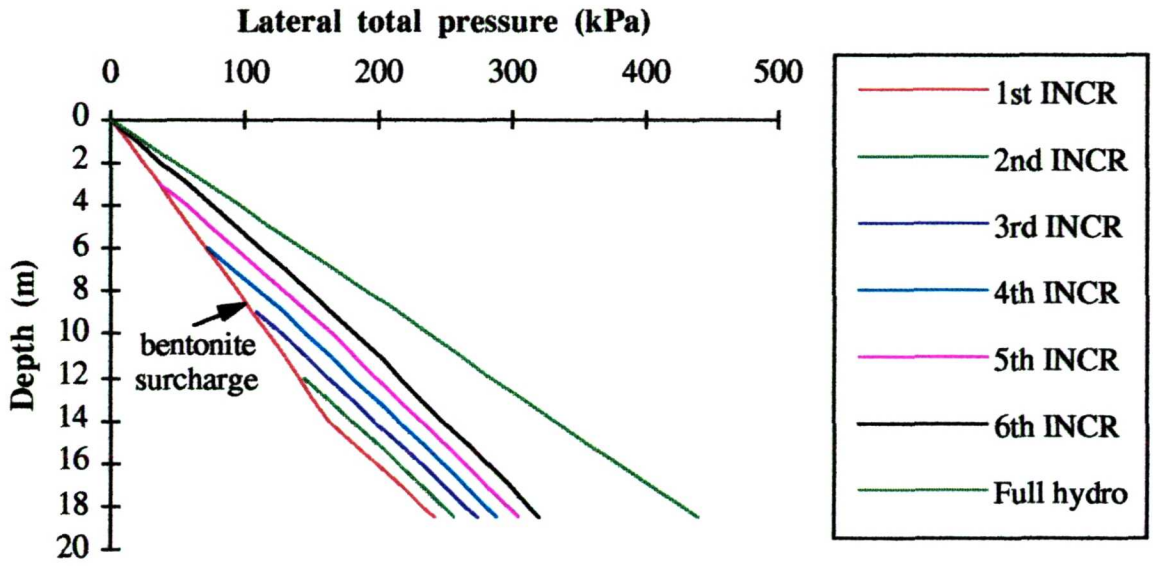


Figure 6.6 *Pressures on the sides of the trench for a 23.7 kN/m³ concrete*

The full hydrostatic pressure of a column of fresh wet concrete of $\gamma_c = 23.7$ kN/m$^3$ at a depth of 18.5m would be 438.5 kPa and therefore the reduction due to consolidation during placement was 117.5 kPa. The maximum pressure on the side at the bottom of the trench for the light density case ($\gamma_c$ = 16 kN/m$^3$) was 263 kPa, with the corresponding excess pore water pressure equal to 134 kPa.

The bilinear analysis proposed by Ng (1993), using the concrete density adopted in analyses 1, 2 and 6 gives a maximum lateral pressure of 294kPa compared with 321 kPa.

A total concrete placement time of 6 hours was adopted in the finite element analyses, which is perhaps more rapid than would be achieved in practice but corresponds closely to the centrifuge tests. If a slower placement time was adopted then the maximum lateral concrete pressure at the base of the trench would be further reduced as a greater degree of consolidation would have occurred. If the concrete had begun to set before the pour was complete, the lateral stress would have also been further reduced. Hence, the analyses presented represent an upper-bound estimation of the lateral stresses that occur in reality.

### *6.4.3 Post installation consolidation*

After wall installation, further consolidation in the concrete was modelled by further reducing the pressure applied to the sides of the trench. Similarly, the excess pore pressures were also reduced to their original in situ values. This stage of consolidation was modelled in three equal concrete pressure/excess pore water pressure reductions, with an increasing time interval for each decrement. The first third of the reduction in the concrete pressure and excess pore water pressure occurred over approximately 2¼ hours, the next over 5½ hours and the last over 11 hours.

The excess pore water pressures applied by the concrete were considered to have completely dissipated after this time (about 20 hours) as the concrete shrinks slightly away from the trench during set (Neville, 1990). Although little is known about the mechanisms of pore water behaviour in setting concrete (and it is outside the scope of this thesis), recent researchers (Holmes, 1995; Milititsky, 1983) have shown that pore pressures in fresh wet concrete started to reduce soon after placement, and for an ordinary Portland cement, suctions were found to occur within 10 hours of placement.

After this 'enforced' consolidation the concrete boundary was fixed and a further 50 days were modelled during which the soil continued to consolidate. The pore water pressure and total stress traces are shown in figures 6.7 to 6.14.

## *6.5 Results*

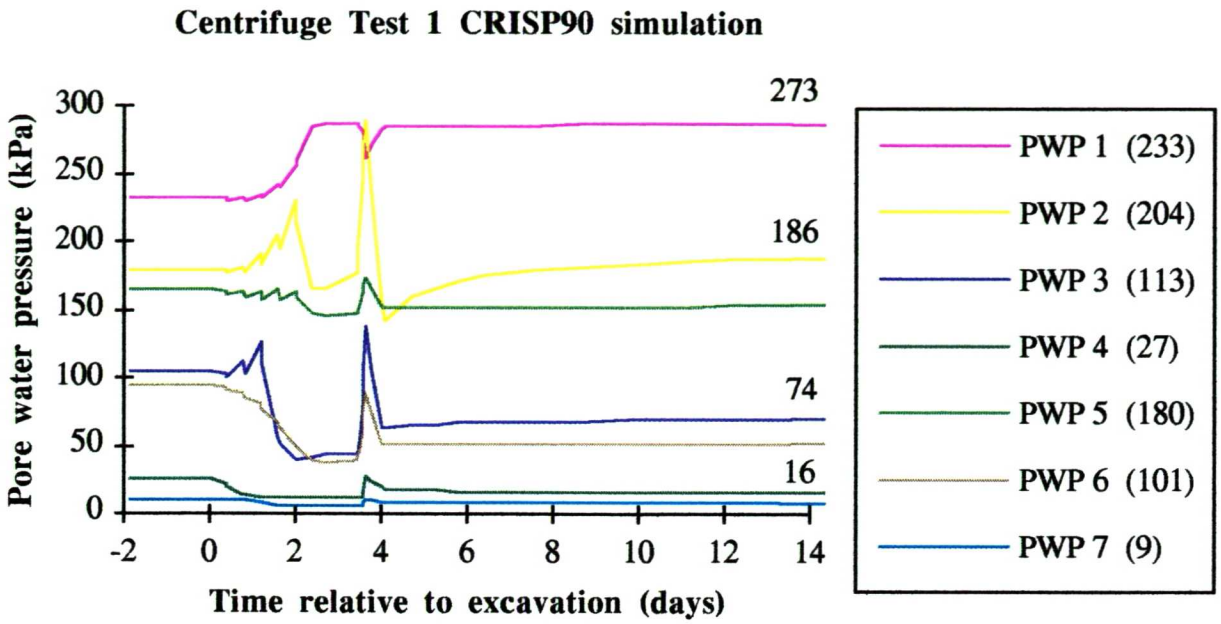


Figure 6.7 *Pore water pressures - CRISP analysis 1*

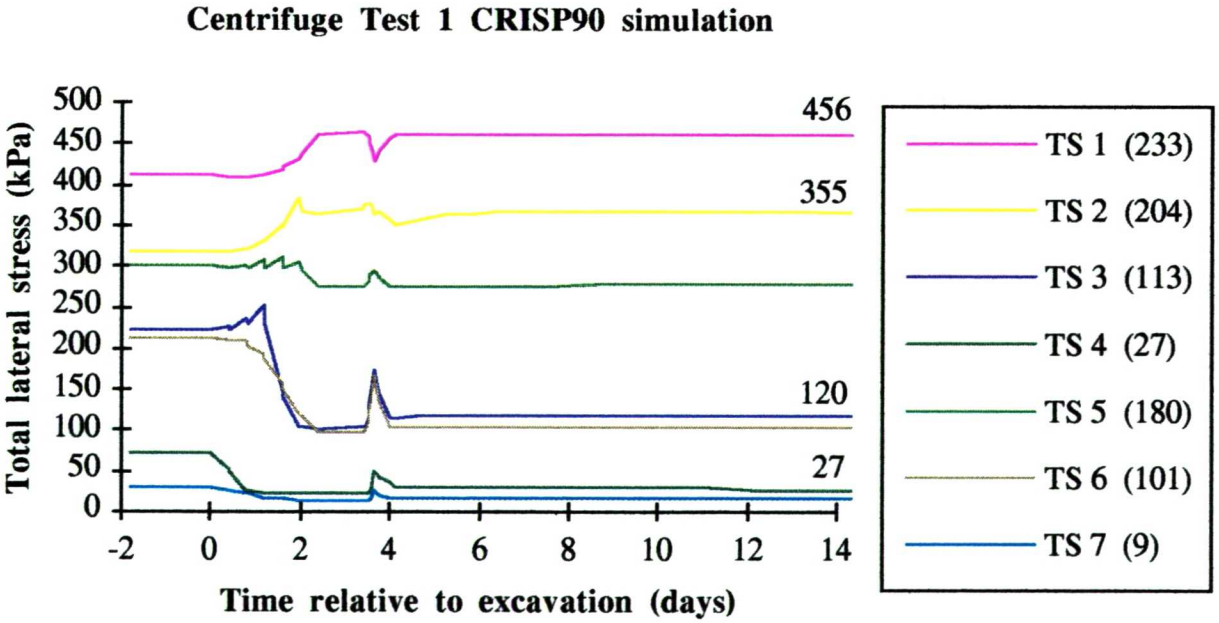


Figure 6.8 *Total stresses - CRISP analysis 1*

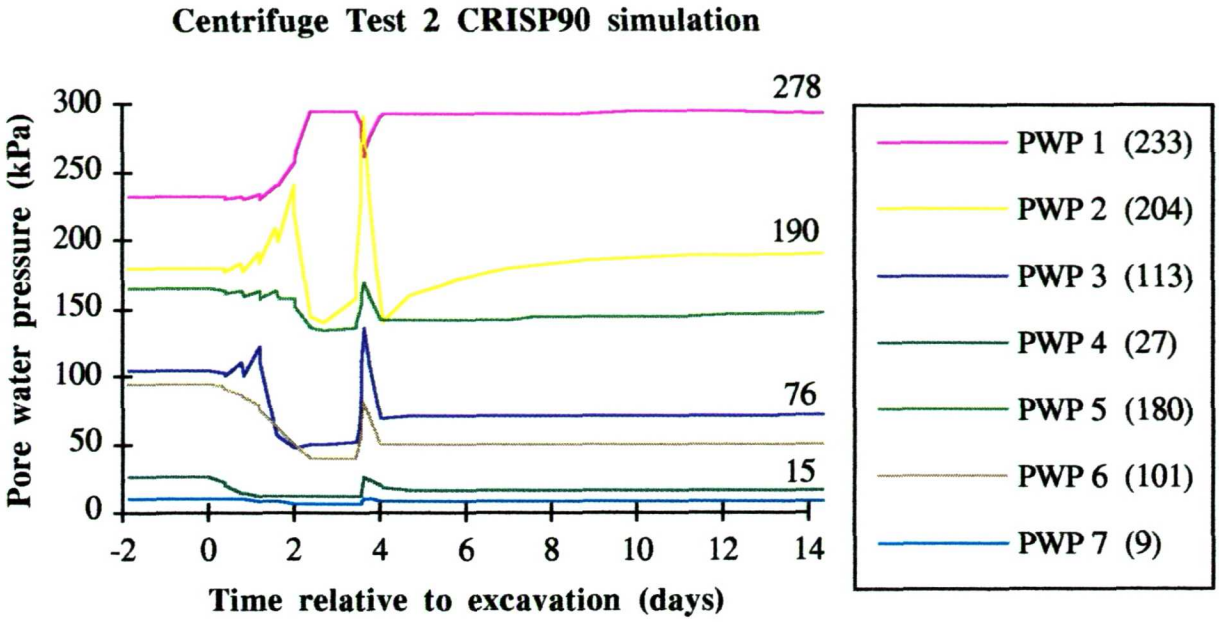


Figure 6.9 *Pore water pressures - CRISP analysis 2*

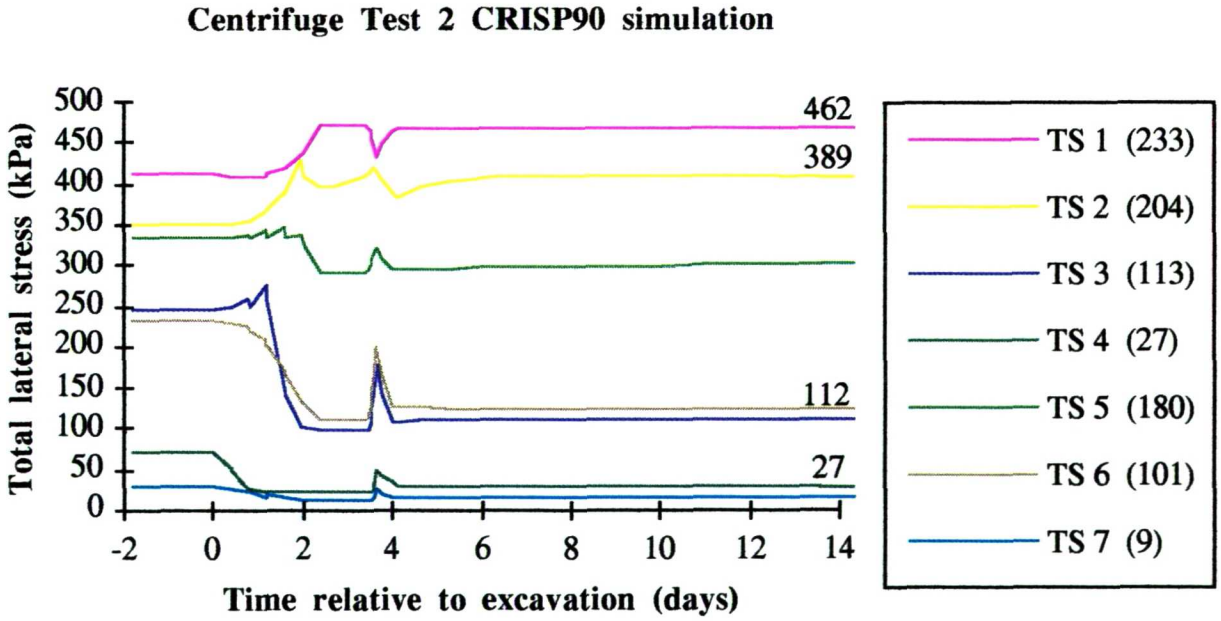


Figure 6.10 *Total stresses - CRISP analysis 2*

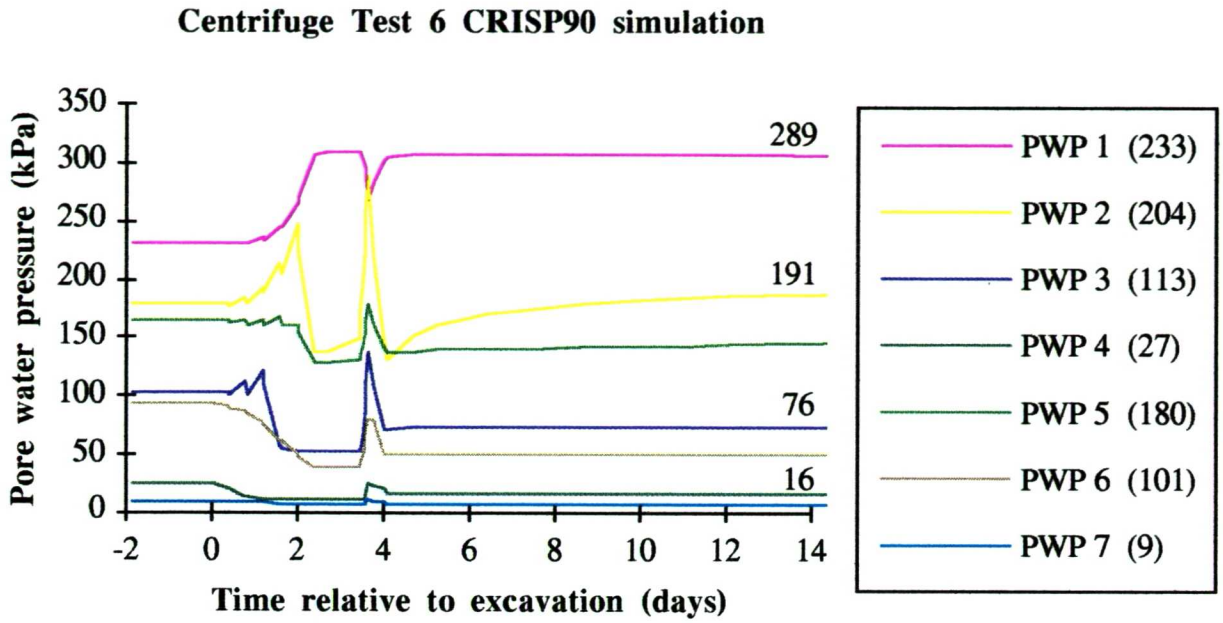


Figure 6.11 *Pore water pressures - CRISP analysis 6*

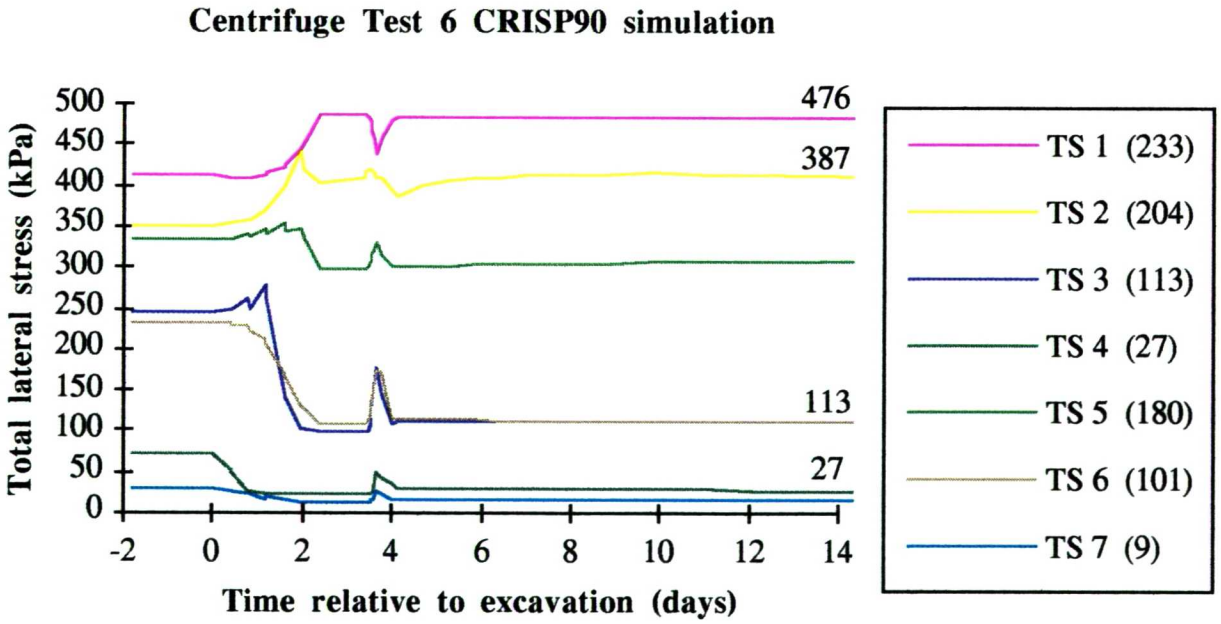


Figure 6.12 *Total stresses - CRISP analysis 6*

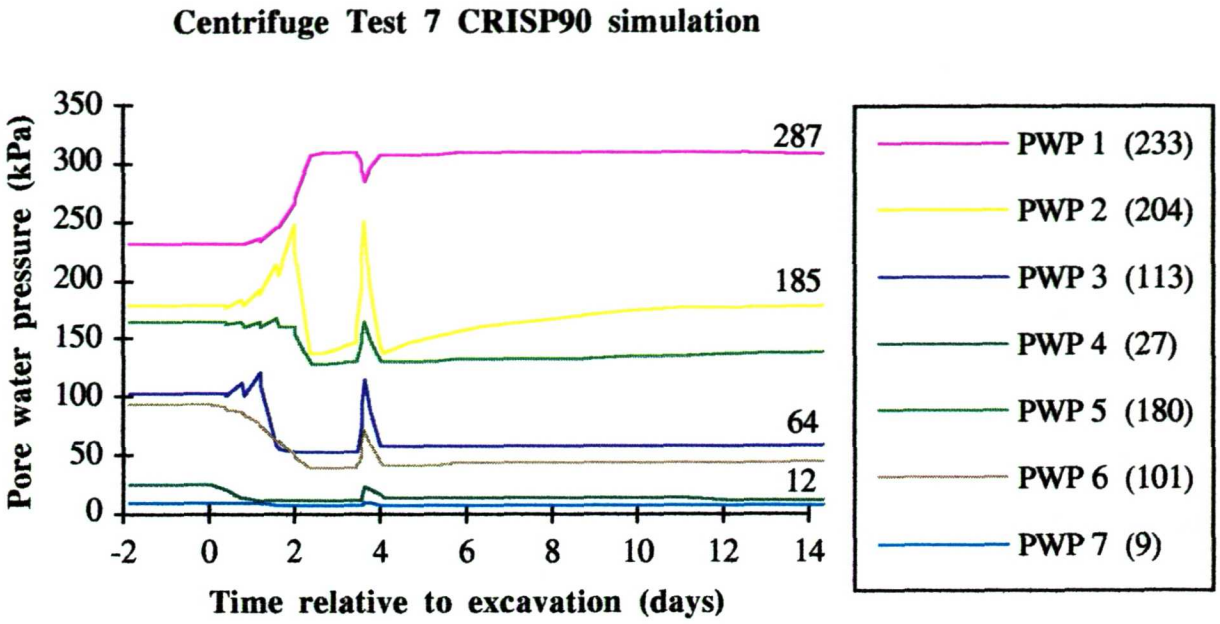


Figure 6.13 *Pore water pressure - CRISP analysis 7*

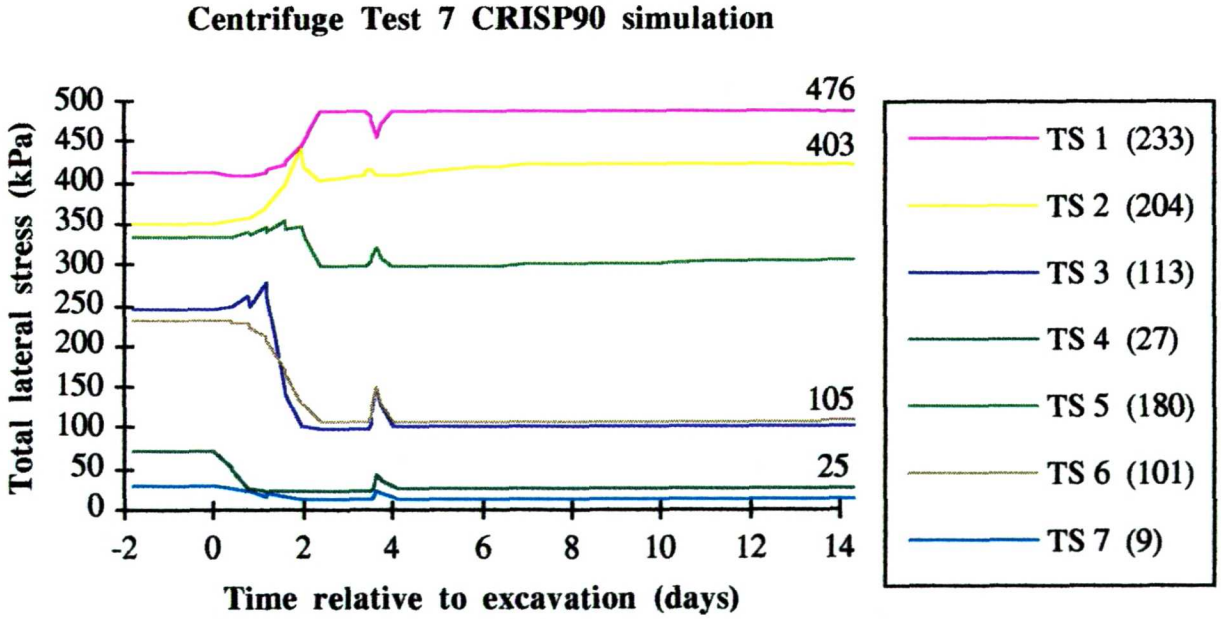


Figure 6.14 *Total stresses - CRISP analysis 7*

The common features of the finite element analyses are first discussed. The effects of a stress controlled boundary (comparing analysis 2 with analysis 6), different $K_o$ conditions (analyses 1 and 2), and a light concrete mix (analyses 6 and 7) are then discussed separately.

### *6.5.1 Common test features.*

The excavation was carried out under bentonite slurry using a top down construction technique in six increment blocks. As the top group of elements was excavated, a drop in total lateral stress and pore water pressure was recorded at positions 4 and 7 whilst at the other positions (ie. below current excavated trench base level), slight increases were recorded. At positions 1, 2 and 3, therefore, whilst the first segment was excavated, total stresses and pore water pressures increased. After excavation had been completed, at positions 2, 3 and 4 a net stress relief occurred. However, at position 1 (5.2 m beneath the final toe of the trench) total stresses and pore water pressures did not decrease at any time during the excavation simulation.

Also, during excavation, a sawtooth effect was to some extent apparent. This was most prominent at positions 2 and 5 and was due to the removal of the bentonite surcharge from the base of the excavated trench.

During concrete placement, total stresses and pore water pressures increased at all but position 1. After placement, the excess pore water pressure applied to the element faces at the soil/trench boundary were gradually reduced to zero as concrete pressures were reduced to $\sigma_h = K_a(\gamma_c - \gamma_w)z + \gamma_w z$. Results from all except position 1 indicated values of pore water pressure and total stress fell to near pre-concreting values soon after installation and consolidation. At position 1, pore water pressures and total stresses fell during concreting, returning to and remaining at their pre-concreting levels after the concrete had consolidated and set.

### *6.5.2 The effects of a stress controlled boundary.*

The total stress traces from CRISP analyses 2 (CA2) and CA6 show very little discernible difference at positions 3 and 4. At positions 1 and 2, very slightly greater increases in pore water pressure and total stress were calculated during excavation in CA6, where the stress controlled boundary was modelled. After the installation procedure was completed, the 50 day pore water pressure at position 1 was 11 kPa (4%) higher in CA6 than in CA2. At all other positions, the differences were considerably smaller.

The effects of the stress controlled boundary were most prominent during excavation and at the greater depths in the model. However, these effects were extremely small, and there was no significant difference in the long term.

### *6.5.3 The effects of different initial $K_o$ conditions.*

CRISP analyses 1 and 2 provided a comparison between the two extremes of earth pressure coefficient considered in the finite element analyses. Near identical conditions were observed in pore water pressures prior to and after installation.

The total stress traces in figures 6.8 and 6.10 show differences between the two analyses were most pronounced at mid trench (positions 3, 6 and 8) and at the toe of the trench (positions 2 and 5) - where initial in situ horizontal stresses were approximately 25 kPa greater in CA2 than in CA1. At the shallowest depths, the total stress traces were similar where a passive limit, $K_p$, was adopted in both tests.

Figures 6.15 and 6.16, show traces of $K_o$ at different positions in the soil model against time. Changes in $K_o$ diminish at positions back from the trench and this is best shown at the shallowest (3m) depth where the initial, in situ $K_o$ value was the same in both tests, as was the change due to wall installation. At position 10 (32.7m back from the excavated face) a drop of 0.3 from the initial value was calculated. At position 9 a greater drop was experienced, increasing further at position 7. At position 4 (2.5m back from the excavated face) a drop in $K_o$ of over 2 was calculated.

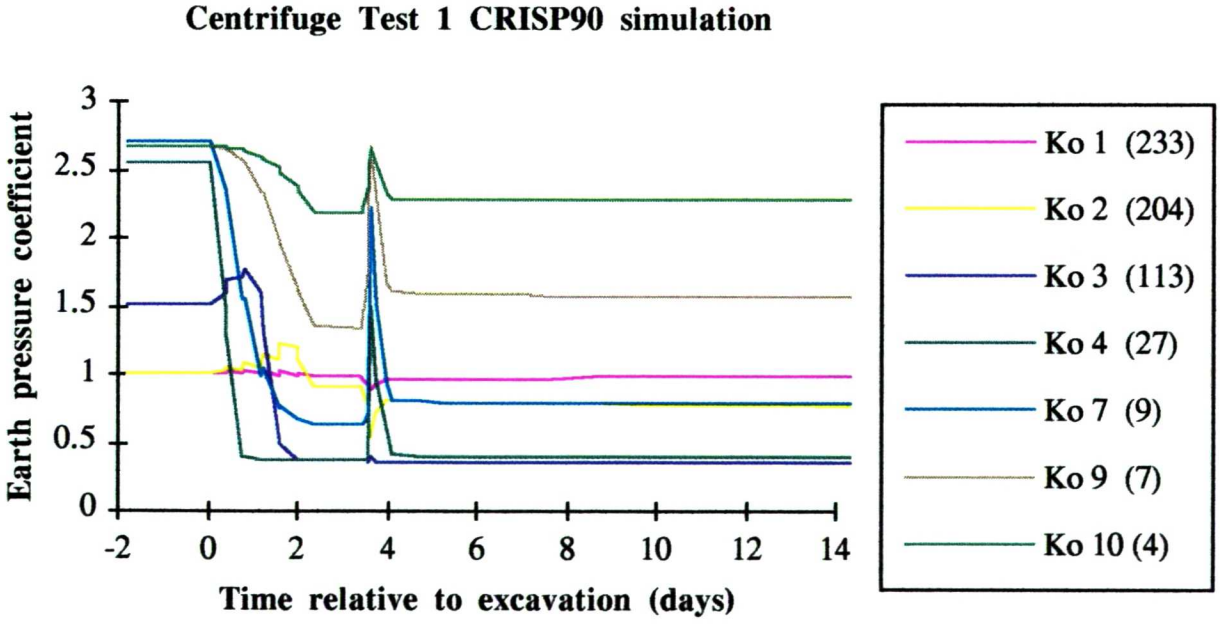


Figure 6.15 *$K_o$ against depth profiles - CRISP analysis 1*

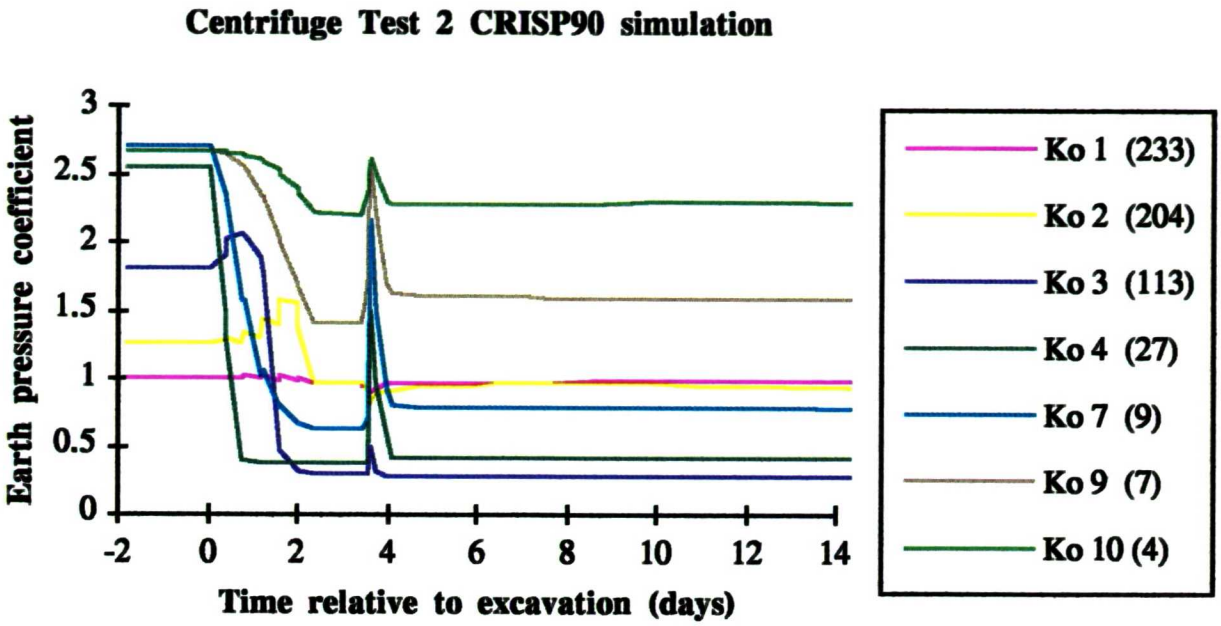


Figure 6.16 *$K_o$ against depth profiles - CRISP analysis 2*

In CA1 and CA2 the differences in values of earth pressure coefficient after the wall installation process were far smaller than the differences in initial in situ lateral stresses prior to excavation with values of earth pressure coefficient after installation tending towards similar values regardless of the initial in situ conditions.

Where different $K_o$ profiles were specified prior to excavation, the greatest drop was experienced where the greatest initial in situ values were adopted. Regardless of initial values, the long term values of $K_o$ were similar in both analyses. These effects were greatest near to the trench and diminished further back. The long term results (at 50 days after installation) showed little or no difference from the short term results (at 5 days after installation), indicating that the re-establishment of initial high lateral stresses does not occur.

### *6.5.4 The effects of different density mixes.*

Figures 6.11 to 6.14 show results calculated in analyses CA6 and CA7. The tests give a comparison between concretes of different densities, with unit weights of 23.7 kN/m$^3$ in test 6 and 16 kN/m$^3$ in test 7. The most obvious differences are the different peak total lateral stresses and pore water pressures that were recorded directly after wall installation.

Peak values in CA7 were, on average, 16% less than the corresponding values at positions 1, 2, 3 and 4 (2.5m back from the trench) in test 6. The peak value diminished to a 10% difference at 7.5m back, 6% at 17.5m back and no indicated difference 32.5m back. The results are a clear indication that concretes of different densities will have some effect on the peak stresses recorded during placement, although the percentage difference is much less than the percentage difference in mix density.

The results also indicate that the influence of lateral stress reduction diminishes at distances further back from the trench following wall installation. However, as in the centrifuge tests (discussed in chapter 5) at position 1, larger total lateral stress increases were calculated after 50 days where the light mix was used (CA7). This is due to the smaller reversal in the arching effects that occurred as the lighter mix was placed. At positions back from the trench, the 50 day values were greater in CA6. However, overall the differences were small, and were never greater than about 4%.

## *6.6 Comparison of CRISP results with centrifuge results.*

### *6.6.1 Introduction.*

Comparing CRISP analyses results with centrifuge test results highlighted two practical differences that had a significant effect. First, during excavation in the centrifuge tests, total lateral stresses were reduced at the edge of the trench by the same amount throughout the depth of the 'excavated' surface. In the CRISP analyses, individual elements were removed in stages, thus inducing lateral stress increases below the level of each new 'toe', prior to subsequent excavation stages. The total lateral stress increases measured at positions 1 and 2 were much greater in the CRISP analyses than in the centrifuge tests.

Second, the pore water pressures at the surface of the model were easier to control in the CRISP analysis than in the centrifuge tests. In the finite element analyses, the phreatic surface was maintained at the top of the mesh; however, in the centrifuge model, where swelling and desiccation occurred at the surface of the model the ground water level was found to fluctuate relative to the surface. In the centrifuge model, a quasi-drained response was noted which did not occur in the CRISP analyses.

This section attempts to draw conclusions from, and underline trends common to, both sets of data. It is split into two sub-sections, looking first at the excavation stage, and then at the concreting stage, including the longer term effects.

Table 6.4 below presents a summary of the data from the CRISP analyses. The positions were chosen to give a close comparison with the transducers used in the centrifuge model tests, where results were presented in tables 5.4 to 5.8. The depths are given relative to the surface of the kaolin sample, and the effective stress changes are presented relative to pre-excavation values. The 'Excav' column refers to the change due to excavation, '5 days', '25 days' and '50 days' refer to changes in lateral effective stress up to that period of time after concreting. Values are negative to indicate lateral stress relief and positive to indicate increases. The 'total stress' column on the right hand side of the table is calculated from

$$\Delta\sigma_h = K_o\gamma_s z - \gamma_b z \qquad (6.8)$$

where $\Delta\sigma_h$ is equal to the change in total stress that occurred in the trench during excavation in the CRISP analyses.

| CA 1 Position | Depth (m) | EPC $K_o$ | Lateral effective stress changes | | | | Total stress |
|---|---|---|---|---|---|---|---|
| | | | Excav | 5 days | 25 days | 50 days | |
| 4 | 2.5 | 1 | -35.69 | -36.32 | -36.65 | -37.05 | -81 |
| 3 | 10.5 | 1.02 | -59.07 | -68.51 | -71.01 | -72.60 | -160.0 |
| 2 | 18.2 | 1.57 | 57.56 | 47.24 | 32.13 | 29.89 | -103.5 |
| 1 | 23.7 | 2.56 | -1.70 | -2.84 | 0.48 | 4.16 | - |

| CA 2 Position | Depth (m) | EPC $K_o$ | Lateral effective stress changes | | | | Total stress |
|---|---|---|---|---|---|---|---|
| | | | Excav | 5 days | 25 days | 50 days | |
| 4 | 2.5 | 1 | -35.66 | -35.85 | -36.11 | -36.18 | -81 |
| 3 | 10.5 | 1.28 | -95.43 | -103.55 | -104.52 | -106.04 | -209 |
| 2 | 18.2 | 1.84 | 78.29 | 54.34 | 29.09 | 26.73 | -185.6 |
| 1 | 23.7 | 2.56 | -1.94 | -3.31 | 0.34 | 6.31 | - |

| CA 6 Position | Depth (m) | EPC $K_o$ | Lateral effective stress changes | | | | Total stress |
|---|---|---|---|---|---|---|---|
| | | | Excav | 5 days | 25 days | 50 days | |
| 4 | 2.5 | 1 | -35.652 | -35.932 | -36.28 | -36.72 | -81 |
| 3 | 10.5 | 1.28 | -96.58 | -104.43 | -105.14 | -105.86 | -209 |
| 2 | 18.2 | 1.84 | 93.04 | 63.36 | 32.53 | 23.73 | -185.6 |
| 1 | 23.7 | 2.56 | 0.7 | -1.39 | 3.26 | 8.30 | - |

| CA 7 Position | Depth (m) | EPC $K_o$ | Lateral effective stress changes | | | | Total stress |
|---|---|---|---|---|---|---|---|
| | | | Excav | 5 days | 25 days | 50 days | |
| 4 | 2.5 | 1 | -35.70 | -35.00 | -35.40 | -36.00 | -81 |
| 3 | 10.5 | 1.28 | -96.10 | -97.90 | -99.10 | -100.60 | -209 |
| 2 | 18.2 | 1.84 | 95.00 | 80.00 | 53.00 | 45.00 | -185.6 |
| 1 | 23.7 | 2.56 | 1.00 | 1.00 | 6.00 | 11.00 | - |

Table 6.4 *Effective stress changes in the CRISP analyses (kPa)*

### *6.6.2 Excavation*

The results presented in table 6.4 are in terms of effective lateral stress change. In a plane strain, undrained elastic analysis, the change in pore water pressure will be equal to half the imposed change in total lateral stress (assuming changes in vertical stress and boundary shear stresses are negligible). During excavation, changes in lateral effective stress on the trench face should therefore also be equal to half of the change in total lateral stress. This was found to be the case at positions 3 and 4.

During excavation at position 2 large increases in lateral effective stress were recorded due to the effects of vertical arching, with very much smaller increases measured at position 1. The increases that occurred in the CRISP analyses at position 2 are approximately equal to the relief that occurred at position 3.

In the CRISP analyses during excavation, lateral effective stress changes at positions 3 and 4 were approximately half of the change in total lateral stress in the trench. However, in the centrifuge tests, the drained response at position 4 led to very much greater changes in lateral effective stress occurring during excavation, whilst at position 3 lateral effective stress changes were considerably smaller.

Around the toe of the trench during excavation in the CRISP analyses, the effective stress increases were approximately half of the decrease in total stress in the trench. In the centrifuge tests, increases were typically less than 5% of the total stress changes as the rubber bag was drained down to the ground surface of the model.

Overall, both investigative methods indicated that during excavation, pore water pressures and total lateral stresses, increased at and below the toe of the trench, and decreased adjacent to the trench. Also, the excavation stage of the installation process induced the biggest changes in lateral effective stress and pore water pressure.

### *6.6.3 Concreting and longer term comparisons.*

During concrete placement both sets of data indicated a peak as the concrete was poured. However, greater peak stresses and pore water pressures were measured in the centrifuge tests - perhaps due to the placement method adopted.

Adjacent to the trench (positions 3 and 4), in the CRISP analyses at 5 days post installation the effects of concrete placement were negligible. At the same positions in both CRISP analyses and the centrifuge tests, the effective stress changes at 50 days were very similar to the changes that occurred at 5 days. Clearly, using either method, adjacent to the trench, excavation causes considerable effective lateral stress relief that diminishes with distance from the trench. Initial pre excavation values are not re-established after the concrete has consolidated in either the short or long term after the installation process was complete.

At the toe of the trench (position 2) in the CRISP analyses, the increases in total lateral stress that occurred during excavation were greatly reduced over time as pore water pressures returned to pre-excavation levels and total stresses were redistributed. The increases in lateral effective stress at 50 days were between a quarter and a half of the increase that occurred during excavation. Beneath the toe of the trench, initial lateral effective stresses increases were small, increasing as pore water pressures (which had increased dramatically during excavation) returned to hydrostatic values. Both methods indicated that the changes at position 1 were approximately half of the values recorded at position 2.

Generally, in both the centrifuge tests and the CRISP analyses, the changes in lateral stress were much greater due to excavation than due to concreting. A difference in the initial in situ conditions had only a small effect on the stress relief that occurred during excavation. Specifically, adjacent to the trench different initial earth pressure coeffient profiles were reduced to similar values after the excavation stage of the test and the analyses, and were not re-established in the long term after wall installation regardless of the density of the concrete used (ie. regardless of the lateral pressures reapplied during concreting). At the toe of the trench, initial increases in lateral effective stress, due to vertical arching were transient, as increases were redistributed after the wall had been installed. At greater depths, lateral effectire stresses increased as pore water pressures dissipated and the effects of verical arching at the toe of the trench were redistributed.

# Chapter 7

# Conclusions

## 7.1 Introduction

A programme of centrifuge tests and finite element analyses has been carried out to investigate the effects on the surrounding soil of the installation of a diaphragm wall in stiff overconsolidated clay. The main conclusions from the results given in previous chapters are presented below.

## *7.2 The centrifuge tests*

A new technique for the measurement of total stresses in the centrifuge was developed, using miniature total stress cells dipped in silicone rubber. Existing methods for predicting under-read and over-read by total stress cells were found to be inapplicable to the miniature cells and take little or no account of the changing soil stiffness and cell installation effects.

The disturbance to the soil caused by the inclusion of a stiff cell were investigated using finite element analyses which indicated normally applied stresses increase around a stiff inclusion. However, the true measure of the disturbance was found by calibrating the cell whilst embedded in a triaxial cell sample and results indicated that free-field stresses were reduced around the transducer. From in sample calibrations of the Kyowa transducer the likely margin of error from the best fit line was 15%.

In the centrifuge tests, pore water pressures, soil settlements and total stresses were recorded at 10 different positions in the soil model. Prior to the simulation of wall installation, the kaolin sample was reconsolidated until a steady regime of hydrostatic pore water pressures, lateral stresses and surface settlements was established. Excavation was then modelled by draining fluid from a neoprene rubber bag to the soil surface level before wall placement was simulated by depositing a synthetic concrete mix into the remaining water in the neoprene bag.

First, a standard case was presented to examine the changes that occurred during the diaphragm wall installation process. The centrifuge model was then adapted to examine the effects of a stress controlled boundary, a range of earth pressure coefficients and different density concrete mixtures.

Results showed that at all depths, the change in pore water pressure, total lateral stress and surface settlements diminished with distance away from the trench. During the centrifuge tests near the surface of the model, the soil behaved in a drained manner, with changes in lateral stress in the trench leading rapidly to changes in lateral effective stress in the adjacent soil. At greater depths larger short term changes in pore water pressure were measured, indicating undrained conditions.

Around the toe of the trench during excavation, lateral stress and pore water pressure increases were measured due to vertical arching effects, despite the considerable stress relief that was experienced further up the trench. After concreting, the increases in lateral stress and pore water pressure were found to be transient, returning to close to the pre-excavation levels in the long term.

The stress controlled boundary at the remote end of the strongbox was found to have had little effect, indicating that where a trench was excavated in an overconsolidated soil, the high initial lateral stresses were not re-established, at least if the soil does not display significant creep. Any overall increases in measured lateral stress in the long term after installation were negligible, and even slight differences in construction method were shown to have a greater effect than the different remote end boundaries.

Three different initial lateral earth pressure coefficient profiles were imposed on the centrifuge sample in different tests. These different initial $K_o$ profiles were demonstrated to have a significant impact in the reduction in lateral stress that occurred during excavation. After the installation process the greatest stress relief was experienced where earth pressure coefficients were initially highest, with the largest measured reductions in lateral effective stress occurring near the surface of the model where the soil behaved in a drained manner. At deeper positions, where initial $K_o$ values approached 1, the changes in lateral effective stress were all similar. The initial in situ earth pressure coefficients had little effect on the long term values in pore water pressure with values returning to approximately pre-excavation levels.

The concrete placement process was also examined in some detail. It was proposed that the concrete, before hydration, would consolidate in the trench, and this was found to be entirely consistent with observed behaviour. During (and directly after) placement, the concrete in the trench partially consolidated and so did not apply the full hydrostatic pressure to the sides of the trench. The degree of consolidation that occurred over time (and hence the lateral pressure exerted on the sides of the trench) was found to depend on the permeability of the cement paste and the time before the cement started to set. The peak stress level occurred during placement, and was affected significantly by the density of the concrete mixture and the rate at which the mixture was deposited. During placement, bleed water collected on the surface of the panel as the aggregate and concrete particles settled. The bleed water was then adsorbed as part of the normal hydration process.

## *7.3 The finite element analyses*

The finite element analyses were carried out under conditions of plane strain in order to simulate the centrifuge tests. Results confirmed that the stress controlled boundary had very little overall effect. Results also indicated that different initial $K_o$ profiles were reduced to similar levels during excavation and reductions were greatest near the surface of the model, diminishing further back from the trench. After the installation process was complete, the high initial lateral stresses were not re-established in the long term.

In all tests, at all positions, it was found that the changes in lateral stress, ground movement and pore water pressures that had occurred 25 days after wall installation changed little thereafter - changes at 5000 days were similar to the changes that had occurred at 25 days.

## *7.4 Significance to designers*

Kantartzi's (1994) proposed zone for settlements is consistent with the area in which lateral stresses were significantly affected. Within this zone (a 45° wedge from the toe of the trench to the surface of the model) total lateral stresses and pore water pressures showed a substantial reaction to the installation processes. Results have indicated that at the face of the trench, during excavation, lateral pressures were reduced to bentonite stresses (assuming excavation was carried out under bentonite). Smaller reductions were experienced further back from the trench, within this zone.

The tests presented showed that lateral pressures were partly reapplied during concrete placement, but quickly fell to near pre-concreting values soon afterwards. The consolidation model proposed Gibson, England and Hussey (1967) was used to predict lateral stresses imposed in the sides of the trench and after concreting and gave excellent correlation with existing field data. By treating the placement of the concrete as a consolidation problem an accurate assessment of applied lateral pressure, at any time after installation, can be made.

Most significantly, where a wide diaphragm wall panel is installed in a stiff overconsolidated clay, providing a period of 25 days is allowed post concreting, a value of $K_o$=1 down the full height of the trench would be an appropriate upperbound limiting value for the retained soil to proceed to the main excavation in front of the wall.

## *7.5 Suggestions for further work.*

There are three principal areas in which this work may be extended:

First, the total stress transducers could be adapted to give measurements of absolute values in the centrifuge tests. Probably the best method, to avoid the errors associated with installation, would be to calibrate the cells vertically in situ in the centrifuge apparatus after a period of reconsolidation.

Second, having made an attempt to understand the mechanisms involved in the consolidation of fresh wet concrete, further research is needed to measure the lateral pressures that are applied by fresh wet concrete. The consolidation model is dependent on the rate of placement, the changing permeability, the overburden pressure and the void ratio of the concrete, all of which could individually be entire research projects.

Third, the centrifuge tests provide a guide to the resulting distribution of stresses and porewater pressures that are found in the soil after the installation of a wide diaphragm wall panel. This work could now be extended to look at the installation of secant and contiguous pile walls and diaphragm walls in panels and measure the changes (and even absolute values) in total lateral stress that occur in the surrounding soil. This research could also provide a valuable insight in to the effects of horizontal and vertical arching.

**Al-Tabbaa, A.** (1987). Permeability and stress-strain response of speswhite kaolin. Ph.D thesis, University of Cambridge.

**Anderson, W.F. Yong, K.Y. and Sulaiman, J.A.**(1984). Laboratory testing of bored and cast in-situ microconcrete piles in clay to study shaft adhesion. Procs. Joint Inst. Structural Engineers and BRE Seminar, 1984, pp. 268-276.

**Arthur, J.R.F. and Roscoe, K.H.** (1961). An earth pressure cell for the measurement of normal and shear stresses. Civil Engineers and Public Works Review, Vol.56, No.659, June 1961, pp. 765-770.

**Askgaard,** (1961). Pressure redistributions around stiff bodies. Acta Polytechnica Scandinavica, Civil Engineering and Building Construction Series, No. 11. Copenhagen: Technical University of Denmark.

**Atkinson, J.H. and Stallebrass, S.E.** (1990). Modelling the effect of recent stress history on the deformation of overconsolidated clays. Procs. of 25th Annual Conf. of Engineering Geotechnical Group, Leeds. British Geology Society, pp. 353-365

**Blackledge, G.F.** (1975). Concrete practice, British Cement Association

**Bolton, M.D.** (1979). A Guide to Soil Mechanics. Macmillan Education Ltd, 1979, (Reprinted by M.D. and K. Bolton, Cambridge, 1991).

**Bolton, M.D. and Powrie, W.** (1987). The collapse of diaphragm walls retaining clay. Géotechnique 37, No.3, pp. 335-353.

**Bolton, M.D. and Powrie, W.** (1988). Behaviour of diaphragm walls in clays prior to collapse. Géotechnique 38, No.2, pp. 167-189

**Bolton, M.D., Britto, A.M., Dasari, G.R.** (1994). Effect of stiffness and recent stress history on diaphragm wall analysis. Centrifuge '94, Singapore, pp. 423-433.

**Bolton, M.D., Britto, A.M., Powrie, W. and White, T.P.** (1989). Finite element analysis of a centrifuge model of a retaining wall in a heavily overconsolidated clay. Computers and Geotechnics, Vol. 7, pp. 189-318.

**Boyes, R.G.H.** (1975). Structural and cut-off diaphragm walls. Applied Science Publishers Ltd., London.

**Britto, A.M. and Gunn, M.J.** (1987). Critical state soil mechanics via finite elements. Ellis Horwood.

**Brooker, E.W. and Ireland, H.O.** (1965). Earth pressures at rest related to stress history. Canadian Geotechnical Journal, Ottawa, Ontario, 2, No 1, pp. 1-15

**Brown, S.F.** (1977). State-of-the-art report on field instrumentation for pavement experiments. Record No. 640, Transport Research Board, Washington, D.C., 1977, pp. 13-28.

**Burland, J.B. and Fourie, A.** (1985). The testing of soils under conditions of passive stress relief. Géotechnique 35, No 2, pp. 193-198.

**Burland, J.B. and Hancock, R.J.R.** (1977). Underground car park at the House of Commons: Geotechnical aspect. Structural Eng., Vol. 55, pp. 87-100

**Burland, J.B. and Maswoswe, J.** (1982). In situ measurement of horizontal stress in over-consolidated clay using spade shaped pressure cells. Géotechnique 32, No. 2, pp. 285-286.

**Burland, J.B., Simpson, B. and St. John, H.D.** (1979). Movements around excavations in London clays. Procs. 7th Eur. Conf. Soil Mech., Brighton, pp. 13-29.

**Carder, D.R. and Symons, I.F.** (1989). Long-term performance of an embedded cantilever retaining wall in stiff clay. Géotechnique 39, No 1, pp. 55-75.

**Clarke, B.G. and Wroth, C.P.** (1984). Analysis of Dunton Green retaining wall based on results of pressuremeter tests. Géotechnique 34, No. 4, pp. 549-561.

**Clayton, C.R.I. and Bica, A.V.D.** (1993). The design of diaphragm-type total stress cells. Géotechnique 43, No.4, pp. 523-535.

**Clayton, C.R.I. and Milititsky, J.** (1983). Installation effects and the performance of bored piles in stiff clays. Ground Engineering, Vol 16, No.3, pp. 17-22.

**Clough, G.W. and O'Rourke, T.D.** (1990). Construction induced movements of in situ walls. Procs. ASCE Conf. on design and performance of earth retaining structures, Cornell University. Geot. Special Publication, 25, pp. 439-470.

**Cole, K.W. and Burland, J.B.** (1972). Observation of retaining wall movements associated with a large excavation. Procs. 5th Eur. Conf. Soil Mech., Madrid, Vol. 1, pp. 445-453.

**Collins, R., Lee, K.J., Lilly, G.P. and Westmann, R.A.** (1977). Mechanics of pressure cells. Experimental Mechanics, Nov. 1977, pp. 514-519.

**Cook, M.** (1994) Private communication, Ready Mix Concrete, Wapping, London, E1.

**Craig, R.F. and Schofield, A.N.** (1973). Centrifuges in Soil Mechanics. McGraw-Hill.

**De Moor, E.K.** (1994) An analysis of bored pile/diaphragm wall installation effects. Géotechnique 44, No. 2, pp. 341-347.

**Dibiagio, E. and Bjerrum, L.** (1957). Earth pressure measurement in a trench in stiff marine clay. Procs. 4th Int. conf. Soil Mech. Fdn Engng, London, Vol. 2, pp. 196-202.

**Dibiagio, E. and Roti, J.A.** (1972). Earth Pressure measurement on a braced slurry-trench wall in soft clay. Procs. 5th Int. conf. Soil Mech., Madrid, Vol. 1, pp. 473-482.

**Flemming, W.G.K and Sliwinski, Z.,** (1977). The use and influence of bentonite in bored pile construction. DoE/CIRIA Development Group, Report PG3.

**Fossberg, P.E.,** (1970) Load deformation characteristics of three layer pavements containing cement-stabilised base. Ph.D thesis. University of California.

**Fourie, A.B. and Potts, D.M.** (1989) Comparison of finite element and limiting equilibrium analyses for an embedded cantilever retaining wall. Géotechnique 39, No. 2, pp. 175-188.

**Gardner, N.J. and Ho, P.T.-J.** (1979) Lateral pressure of fresh concrete. ACI Journal, July 1979, pp. 809-820.

**Gibson, R.E., England, G.L. and Hussey, M.J.L.** (1967). The theory of one-dimensional consolidation of saturated clays. Géotechnique 17, pp. 261-273.

**Grim, R.** (1962). Applied clay minerology. McGraw-Hill Book Co. Inc.

**Gunn, M.J. and Clayton, C.R.I.** (1987). Installation Effects and their importance in the design of earth retaining structures. Technical Note, Géotechnique 42, No. 1, pp. 137-141.

**Hanna, T.H.** (1973 repr.1985). Earth Pressure Measurement; Foundation Instrumentation. Series on Rock and Soil Mechanics, Trans Tech Publications.

**Harrison, T.A.** (1983). Pressures on vertical formwork when concrete is placed in wide sections. Cement and Concrete Association. Research report No. 22.

**Harrison, T.A. and Clear, C.A.,** (1985). Concrete pressures on formwork. CIRIA Report 108.

**Higgins, K.G., Potts, D.M. and Symons, I.F.** (1989). Comparison of predicted and measured performance of the retaining walls of the Bell Common tunnel. TRRL Contractor report 124.

**Holmes, G.** (1995). Early age volume change and pore pressure development in cement pastes. Ph.D thesis. Queen Mary and Westfield College, University of London.

**Jáky, J.** (1944). The coefficient of earth pressure at rest. Journal for the Society of Hungarian Architects and Engineers, Budapest, Hungary, pp. 355-358.

**Jardine, R.J., Symes, M.J. and Burland, J.B.** (1984) The measurement of soil stiffness in the triaxial apparatus. Géotechnique 34, No. 3, pp. 323-340.

**Jefferis, S.A.,** (1972). The use of bentonite slurry. Ph.D Thesis, King's College, London University.

**Jefferis, S.A.,** (1992). Lecture Notes. 2 day course on Contaminated Land, Queen Mary and Westfield College, University of London.

**Kantartzi, C.** (1991) Transfer report. Queen Mary and Westfield College, University of London. M.Phil to PhD.

**Kantartzi, C.** (1994) Ground movements during diaphragm wall installation in clays. Ph.D thesis, Queen Mary and Westfield College, London University.

**Kaye and Laby** (1985). Tables of Physical and Chemical Constants. 15th Edition, Wiley, New York.

**Kim, H.M.** (1988) The use of bentonites in slurry trench walling. Ph.D Thesis, King's College, London University.

**Konig D., Jessberger H.L., Bolton M.D., Phillips R., Bagge G., Renzi R. and Garnier J.** (1994) Pore pressure measurement during centrifuge model tests: Experience of five laboratories. Centrifuge '94, Singapore, pp. 101-108.

**Kutmen, G.** (1986) The influence of the construction Procsess on bored piles and diaphragm walls: A numerical study. M.Phil Thesis, University of Surrey.

**Lings, M.L., Ng, C.W.W. and Nash, D.F.T.** (1993a) The lateral pressure of wet concrete in diaphragm wall panels cast under bentonite. Procs. of the ICE, Geotec. Eng. 107(3), July, pp. 163-172.

**Lings, M.L., Ng, C.W.W. and Nash, D.F.T.** (1993b) Reliability of earth pressure measurements adjacent to a multi-propped diaphragm wall. Retaining Structures, Edited by C.R.I. Clayton, published by T.T.L, London, pp. 258-269

**Lings, M.L., Ng, C.W.W., Nash, D.F.T. and Boyce, C.E.**(1991) Observed behaviour of a deep excavation in Gault clay: A preliminary appraisal. Procs. 10th Eur. Conf. Soil Mech., Florence, Vol. 2, pp. 467-470.

**Mayne, P.W. and Kulhawy, F.H.** (1982) $K_O$-OCE relationships in soil. Geotechnical Engineering Division, Procs. of ASCE, 108, No GT6, June 1982.

**Milititsky, J.** (1983) Installation of bored piles in stiff clays : An experimental study of local changes in soil conditions. Ph.D Thesis, University of Surrey.

**Neville, A.M.** (1990) Properties of concrete. Pitman (London).

**Ng, C.W.W.** (1993) An evaluation of soil-structure interaction associated with a multi-propped excavation. PhD thesis, Bristol University.

**Olsen, R.H., Salek, F. and Peck, C.F.** (1974). Lateral pressures on concrete formwork. Procs. American Concrete Institute. Vol. 71, July, pp. 358-361.

**Oveson** (1990) The use of physical models in design. Technical Series, Wiley, New York.

**Pantelidou, H.** (1994) Changes in soil stiffness associated with diaphragm walling. Ph.D thesis, Queen Mary and Westfield College, University of London.

**Peattie, K.R. and Sparrow, R.W.,** (1954) The fundamental action of earth pressure cells. Journal of Mechanics and Physics of Solids, Vol. 2, pp. 141-145

**Petley, D.J.** (1966) The shear strength of soils at large strains. Ph.D Thesis. Imperial College of Science and Technology, University of London.

**Potts, D.M. and Fourie, A.B.** (1984) The behaviour of a propped retaining wall: results of a numerical experiment. Géotechnique 34, No. 3, pp. 383-404.

**Potts, D.M. and Fourie, A.B.** (1985) The effect of wall stiffness on the behaviour of a propped retaining wall. Géotechnique 35, No.3, pp. 347-352.

**Powell, J.J.M.** (1990) A comparison of four different pressuremeters and their methods of interpretation in a stiff heavily overconsolidated clay. Procs. 3rd Int. Symp. on pressuremeter testing, Oxford, 2-6 April 1990, pp. 287-298.

**Powrie, W.** (1986). The behaviour of diaphragm walls in clay. Ph.D Thesis, Cambridge University.

**Powrie, W. and Kantartzi, C.** (1993) Installation effects of diaphragm walls in clay. Géotechnique 43, No. 2, pp. 238-251.

**Powrie, W. and Li, E.S.F.** (1991) Finite element analyses of an in situ wall propped at formation level. Géotechnique 41, No. 4, pp. 499-514.

**Roscoe, K.H.,** (1957) Discussion: Compressibility of soils, stress strain properties, pore pressure prediction. Procs. Int. Conf on Soil Mech. and Fndn Engng, Wiesbaden, pp. 199-213.

**Schmidt, B.** (1966). Discussion on: Earth pressures at rest related to stress history. Canadian Geotechnical Journal , National Research Council, Ottawa, Ontario, Canada, Vol. 3, No.4, 1966, pp. 239-242.

**Schofield, A.** (1980). Cambridge geotechnical centrifuge operations: 20th Rankine Lecture of BGS. Géotechnique 30, No. 3, pp. 227-268.

**Selig, E.T.** (1981). Soil stress gauge calibration. Geotechnial Testing Journal GTJODJ, Vol.3, No.4, Dec. 1980, pp. 153-158.

**Shad, H-S.** (1989) Design and performance of an experimental earth pressure cell. Ph.D Thesis, Queen Mary and Westfield College, University of London.

**Sills, G.C., Burland, J.B. and Czechowski, M.K.** (1977). Behaviour of an anchored diaphragm wall in stiff clay. Procs. 9th Int Conf on Soil Mech and Fdn Eng. Tokyo. Vol. 2, pp. 147-155.

**Simpson, B.** (1992). Retaining structures: displacement and design. 32nd Rankine Lecture. Géotechnique 42, No. 4, pp. 541-567.

**Simpson, B., Calabresi, G., Sommer, H. and Wallays, M.** (1979). Design Parameters for stiff clays. Procs. 7th European Conf. On Soil Mechanics, Brighton, Vol. 5, pp. 91-125.

**Skempton, A.W.** (1961). Horizontal stresses in an Over-Consolidated Eocene clay. Procs. 5th Int. Conf. Soil Mech. Fdn Engng, Paris, Vol. 1, pp. 351-357.

**Smiles, D.E. and Poulos, H.G.** (1969). The one-dimensional consolidation of columns of soil of finite length. Austrian Journal of Soil Research, 1969, 7, pp. 285-291.

**Stallebrasse, S.E.** (1990). Modelling the effects of recent stress history on the deformation of overconsolidated soils. Ph.D thesis. City University.

**Symons, I.F. and Carder, D.R.** (1989). Long term behaviour of embedded retaining walls in overconsolidated clay. Instrumentation in geotechnical engineering. Thomas Telford, London, pp. 155-179.

**Symons, I.F. and Carder, D.R.** (1992). Field Measurements on embedded retaining walls. Technical Note. Géotechnique 42, No. 1, pp. 117-126.

**Taylor, D.W.** (1947). Pressure distribution theories, earth pressure cell investigation and pressure distribution data. Soil Mechanics, U.S. Army Engineer Waterways Experiment Station, Vicksburg, Mississippi.

**Taylor, R.N.** (1987) Discussion on: Centrifuge scaling considerations for fluid particle systems by Tan, T-S and Scott, RF. Géotechnique 37, No. 1, pp. 131-133.

**Tedd, P., Chard, B.M., Charles, J.A., and Symons, I.F.** (1984). Behaviour of a propped embedded retaining wall in stiff clay at Bell Common Tunnel. Géotechnique 34, pp. 513-532.

**Tedd, P. and Charles, J.A.** (1981). In situ measurement of horizontal stress in over-consolidated clay using spade-shaped cells. Géotechnique 31, No. 4, pp. 554-558.

**Tedd, P. and Charles, J.A.** (1985). The strength of London clay in relation to the design of embedded retaining walls. Géotechnique 35, No. 2, pp. 199-204.

**Terzaghi, K.** (1943). Theoretical Soil Mechanics. John Wiley and Sons.

**Thompson, P.** (1990). A review of retaining walls. M.Sc Thesis, Unversity of Cambridge.

**Tory, A.C. and Sparrow, R.W.** (1967). The influence of diaphragm flexibility on the performance of an earth pressure cell. Journal of Scientific Instrumentation, 1967, Vol. 44, pp. 781-785

**Uff, J.F.** (1970). In situ measurement of earth pressure for a quay at Seaforth, Liverpool. Procs. of Conf. on In Situ Investigations in Soils and Rocks. BGS, London, pp. 229-239.

**Uriel, S. and Oteo, C.S.** (1977). Stress and strain besides a circular trench wall. Procs. 9th Int. Conf. of Soil Mech. and Fndn. Engng, Tokyo, Vol. 1, pp. 347-352.

**Van Olphan** (1962). An introduction to Clay Colloid Chemistry. Oxford Pergamon.

**Wroth, C.P.** (1971). Some aspects of the elastic behaviour of overconsolidated clay. Procs. Roscoe Memorial Symp. Foulis, pp. 347-361.

**Wroth, C.P.** (1972). The interpretation of in-situ soil tests. 24th Rankine Lecture. Géotechnique 34, No. 4, pp. 449-489.

**Bolton, M.D.** (1979). A Guide to Soil Mechanics. Macmillan Education Ltd, 1979, (Reprinted by M.D. and K. Bolton, Cambridge, 1991).

**Boyes, R.G.H.** (1975). Structural and cut-off diaphragm walls. Applied Science Publishers Ltd., London.

**Britto, A.M. & Gunn, M.J.** (1987). Critical state soil mechanics via finite elements. Ellis Horwood.

**Gibson, R.E.; England, G.L. & Hussey, M.J.L.** (1967). The theory of one-dimensional consolidation of saturated clays. Géotechnique 17, pp. 261-273.

**Gunn, M.J. & Clayton, C.R.I.** (1987). Installation Effects and their importance in the design of earth retaining structures. Technical Note, Géotechnique 42, No. 1, pp. 137-141.

**Hanna, T.H.** (1973 repr.1985). Earth Pressure Measurement; Foundation Instrumentation. Series on Rock and Soil Mechanics, Trans Tech Publications.

**Kantartzi, C.** (1994) Ground Movements during diaphragm wall installation in clays. Ph.D thesis, Queen Mary and Westfield College, London University.

**Kutmen, G.** (1986) The influence of the construction process on bored piles and diaphragm walls: A numerical study. M.Phil Thesis, University of Surrey.

**Lings, M.L., Ng, C.W.W., Nash, D.F.T.** (1993) The lateral pressure of wet concrete in diaphragm wall panels cast under bentonite. Procs. of the ICE, Geotec. Eng. 107(3), July, pp. 163-172.

**Terzaghi, K.** (1943). Theoretical Soil Mechanics. John Wiley & Sons.